Planta Medica Thieme

Five new diarylbutyrolactones and sesquilignans from Saussurea medusa and their inhibitory effects on LPS-induced NO production

Journal:	*Planta Medica*
Manuscript ID	PLAMED-2022-05-0378-OP.R4
Manuscript Type:	Original Papers
Date Submitted by the Author:	03-Oct-2022
Complete List of Authors:	Cao, JingYa; Northwest Institute of Plateau Biology Chinese Academy of Sciences, Qinghai Provincial Key Laboratory of Tibetan Medicine Research; University of the Chinese Academy of Sciences Wang, Zhiyao; Henan Academy of Science Alan, J. Stewart; School of Medicine, University of St Andrews Dong, Qi; Northwest Institute of Plateau Biology Chinese Academy of Sciences, Qinghai Provincial Key Laboratory of Tibetan Medicine Research Zhao, Ye; Shanghai Institute of Materia Medica Chinese Academy of Sciences Mei, Lijuan; Northwest Institute of Plateau Biology Chinese Academy of Sciences, Qinghai Provincial Key Laboratory of Tibetan Medicine Research Tao, Yanduo; Northwest Institute of Plateau Biology Chinese Academy of Sciences, Qinghai Provincial Key Laboratory of Tibetan Medicine Research Yu, Rui Tao; Northwest Institute of Plateau Biology Chinese Academy of Sciences, Qinghai Provincial Key Laboratory of Tibetan Medicine Research
Keywords:	Preparative Chromatography < Extraction, Isolation, NMR < Natural Products Analysis, Lignans < Phenolics < Natural Products Classes

Five new diarylbutyrolactones and sesquilignans from *Saussurea medusa* and their inhibitory effects on LPS-induced NO production

Jing-Ya Cao[1,2], Zhi-Yao Wang[3], Alan J. Stewart[4], Qi Dong[1], Ye Zhao[5], Li-Juan Mei[1], Yan-duo Tao[1,*] and Rui-Tao Yu[1,*]

Affiliation

[1]Qinghai Provincial Key Laboratory of Tibetan Medicine Research; Key Laboratory of Tibetan Medicine Research, Northwest Institute of Plateau Biology, Chinese Academy of Sciences, Xining, PR China

[2]University of Chinese Academy of Sciences, Beijing, PR China

[3]Henan Academy of Science, Zhengzhou, PR China

[4]School of Medicine, University of St Andrews, United Kingdom

[5]State Key Laboratory of Drug Research, Shanghai Institute of Materia Medica, Chinese Academy of Sciences, Shanghai, PR China

Correspondence

Prof. Yan-duo Tao

Northwest Institute of Plateau Biology, Chinese Academy of Sciences, No. 23 Xinning Road, Xining 810008, PR China

Tel: +0971-6143530.

Fax: +0971-614328286.

E-mail: tyd@nwipb.cas.cn

Correspondence

Associate Prof. Rui-Tao Yu

Northwest Institute of Plateau Biology, Chinese Academy of Sciences, No. 23 Xinning Road, Xining 810008, PR China

Tel: +0971-6143530.

Fax: +0971-614328286.

E-mail: yuruitao@nwipb.cas.cn

Abstract

Five new diarylbutyrolactones and sesquilignans (**1a/1b–4**), including one pair of enantiomers (**1a/1b**), together with ~~ten~~ 10 known analogues (**5–14**), were isolated from the whole plants of *Saussurea medusa.* Compound **1** was found to possess an unusual 7,8'-diarylbutyrolactone lignan structure. Separation by chiral HPLC analysis led to the isolation of one pair of enantiomers, (+)-**1a** and (−)-**1b**. The structures of the new compounds were elucidated by extensive spectroscopic data. All compounds, except compounds **5**, **7** and **9**, were isolated from *S. medusa* for the first time. Moreover, compounds **1–4**, **8** and **10–14** had never been obtained from the genus *Saussurea* previously. Compounds (+)-**1a**, **2**, **5**, **7**, and **9–11** were found to inhibit the lipopolysaccharide (LPS)-induced release of NO by RAW264.7 cells with IC_{50} values ranging from 10.1 ± 1.8 to 41.7 ± 2.1 μM. Molecular docking and iNOS expression experiments were performed to examine the interactions between the active compounds and the iNOS enzyme.

Keywords: *Saussurea medusa*; Asteraceae; d~~D~~iarylbutyrolactone lignan; s~~S~~esquilignan; a~~A~~nti-inflammatory activity; m~~M~~olecular docking

Introduction

Saussurea medusa Maxim. is a rare subnival plant known as "snow lotus" ~~which~~ that belongs to the genus *Saussurea* of the family Asteraceae [1]. The plant is found predominantly in the Qinghai-Tibet P~~p~~lateau at heights of 3500–4500 m [2]. *S. medusa* is an important traditional Chinese medicinal herb used to treat anthrax, stroke, rheumatoid arthritis, placental retention and mountain sickness [3]. In a previous study, we found that an ethanol extract of *S. medusa* possessed potential anti-inflammatory properties [4]. The aim of the present study was to identify and characterize the anti-inflammatory compounds of *S. medusa.*

Herein, we report on the isolation and characterization of five new diarylbutyrolactones and sesquilignans, together with ~~ten~~ 10 known analogues from the whole plants of *S. medusa*. Extensive spectroscopic data~~,~~ and time-dependent density functional theory-based electronic circular dichroism (TDDFT-ECD) calculations [5] led to the identification of their chemical structures. The anti-inflammatory activities of the compounds were preliminary assessed *in vitro* by examining their abilities to inhibit the LPS-~~-~~induced NO production in RAW264.7 macrophage-like cells. The interactions between the bioactive compounds and iNOS were further explored using molecular docking and iNOS expression experiments.

Results and Discussion

The ethyl acetate fraction from the whole plants of *S. medusa* was subjected to repeated chromatographic separations to afford five new lignans (**1a**/**1b**−**4**), namely

medusarins A−D (**1a/1b−4**), see Fig. 1.

Medusarin A (**1**) was obtained as a colorless gum. Its molecular formula was determined to be $C_{20}H_{20}O_8$ based on the sodium adduct $[M + Na]^+$ at *m/z* 411.1056 in HRESIMS corresponding to 11 indices of hydrogen deficiency (IHDs). The IR spectrum of **1** displayed characteristic absorption bands of hydroxy (3359 cm^{-1}), carbonyl (1741 cm^{-1}) and C=C bond (1645 cm^{-1}) groups. The ^1H NMR spectroscopic data (Table 1) in conjunction with HSQC data revealed the presence of two aromatic rings, including an ABX coupling system at δ_H 7.08 (1H, d, J = 1.8 Hz, H-2'), 6.83 (1H, d, J = 8.3 Hz, H-5') and 7.02 (1H, dd, J = 8.3, 1.8 Hz, H-6'), assignable to a 1,3,4-trisubstituted benzene ring. Two equivalent aromatic protons at δ_H 6.58 (2H, s, H-2, 6) indicated the existence of a 1,3,4,5-tetrasubstituted aromatic ring. In addition, an oxygenated methylene at δ_H 3.93 (1H, dd, J = 15.1, 8.1, H-9a) and 3.62 (1H, dd, J = 15.1, 7.0, H-9b), one allylic hydrogen signal at δ_H 7.49 (1H, s, H-7'), two methines at δ_H 3.66 (1H, dd, J = 8.1, 7.0, H-8) including one oxygenated at δ_H 5.60 (1H, brs, H-7), and two methoxy groups at δ_H 3.82 (6H, s, H-3, 5) were also observed. The ^{13}C NMR and DEPT spectra revealed 20 carbon signals, consisting of 12 aromatic carbons, a double bond, one oxygenated methylene carbon, two methoxy groups, two methine carbons (one oxygenated) and a lactone carbonyl group signal. Two aromatic rings (A and B), a lactone carbonyl and a double bond group accounted for ~~ten~~ 10 out of 11 IHDs. The remaining IHD in the molecule implied the existence of the butyrolactone ring C in compound **1**.

The aforementioned evidence indicated that compound **1** was similar to

impecylenolide [6], a lignan previously isolated from *Imperata cylindrica*, except for the presence of a methoxy group at C-5 and the replacement of a methoxy group by a hydroxy group at C-3' in **1**. This was confirmed by analysis of the 2D NMR and was also consistent with its molecular formula.

The (*E*)-configuration of the C7'-C8' double bond in **1** was deduced from the ROESY correlations (Fig. 2) between H-2'/H-6' and H_2-9. This was also supported by a more de-shielded signal for H-7' (7.49 ppm), which was in agreement with the reported chemical shifts (7.20−7.69 ppm) for the (*E*)-configuration [7, 8]. The ROESY correlation of H-7/H_2-9 indicated the *trans* orientation of H-7 and H-8, which was supported by a small coupling constant ($J_{7,8} = 0$) [6]. Thus, the relative configuration of **1** was determined as 7*S**,8*R**.

An ECD spectrum was recorded to establish the absolute configuration of **1**, but surprisingly, there was no obvious Cotton effect (CE), which suggested the racemic nature of **1**. This prediction was confirmed by the presence of two peaks in chiral HPLC analysis. Compounds (+)-**1a** and (−)-**1b** were successfully separated in a ratio of approximately 1:1 (Figure 46S, Supporting Information), showing typical antipodal ECD curves (Fig. 3) and specific rotations of opposite sign. By comparing their calculated ECD and experimental ECD (Fig. 3), the calculated ECD curve of (7*S*,8*R*)-form matched well with the experimental ECD spectrum of (+)-**1a**, which allowed the assignment of the absolute configuration of (+)-**1a** as 7*S*,8*R*. Thus, the almost mirror-image ECD curve of (−)-**1b** was assigned to the 7*R*,8*S* configuration.

Medusarin B (**2**) possessed a molecular formula of $C_{21}H_{24}O_7$ as deduced by (+)-

HRESIMS at *m/z* 411.1424 [M + Na]$^+$. The ^{1}H and ^{13}C NMR spectra (Table 1) showed the existence of two benzene rings (one 1,3,4-trisubstituted, the other 1,2,4,5-tetrasubstituted), three methylenes (one oxygenated), two methines, three methoxy groups and a lactone carbonyl group. The ^{1}H and ^{13}C NMR spectral features indicated that compound **2** was very similar to arctigenin [9], a compound (**5**) also isolated from this plant during this study. The difference was the existence of a hydroxy group at C-2 in compound **2**. The HMBC correlations between H-6/H_2-7 and C-2, in combination with the different pattern of proton peaks in the aromatic region, supported this deduction, which was also in accordance with its molecular formula.

According to Corrie et al. [10], the relative configuration of the 8,8'-diarylbutyrolactone lignan can be determined by NMR comparison of the methylene protons at C-9. Equivalent chemical shifts of H_2-9 correspond to the *cis*-configuration, while different chemical shifts correspond to the *trans*-configuration. Thus, the configuration at C-8 and C-8' was assigned as *trans* on the basis of the unequal chemical shifts observed for H_2-9 [δ_H 4.14 (1H, dd, J = 9.0, 6.7 Hz, H-9a) and 3.93 (1H, dd, J = 9.0, 7.0 Hz, H-9b)]. This deduction was confirmed by comparing the ^{1}H and ^{13}C NMR data with those of arctigenin (**5**), an analog with the same *trans*-configuration. ECD calculations were used to determine the absolute configuration of **2**, and the calculated ECD curve of the (8*R*,8'*R*)-form matched well with the experimental ECD spectrum of **2** (Fig. 3), indicating an 8*R*,8'*R* configuration for **2**.

Medusarin C (**3**) possessed a molecular formula of $C_{31}H_{36}O_{10}$ based on the sodium adduct at *m/z* 591.2208 [M + Na]$^+$ in (+)-HRESIMS. The ^{1}H NMR spectrum data (Table

2) of compound **3** combined with HSQC revealed three sets of ABX systems. An arylglyceryloxy moiety was revealed by signals of a vicinal coupling system attributed to two oxygenated methines at δ_H 4.94 (1H, d, J = 4.7 Hz, H-7") and 4.13 (1H, m, H-8") and an oxygenated methylene at δ_H 3.89 (1H, dd, J = 12.2, 4.0 Hz, H-9"a) and 3.66 (1H, dd, J = 12.2, 3.4 Hz, H-9"b). The ^{13}C NMR and DEPT spectra showed 31 carbon signals assignable to 18 aromatic carbon signals, four methylene carbons (two oxygenated), four methine carbons (two oxygenated), four methoxy groups and a lactone carbonyl group. These data suggested that compound **3** was a sesquilignan, and its structure made up of two parts (Figure 47S, Supporting Information).

The structure of **3** was established by further examination of the 2D NMR spectra. First, five spin-coupling units were identified via the ^{1}H−^{1}H COSY spectrum as show in Figure 47S, Supporting Information. The connection of the five structural units with other functional groups was then made using the HMBC spectrum (Figure 47S, Supporting Information). In the HMBC spectrum of **3**, the long-range correlations from H-7"/C-1", C-2", C-6"; H-2"/C-4", C-6" confirmed that part I was a 3,4-disubstituted phenylglyceryl unit, and the HMBC correlations of 3"-O*Me* identified a methoxy group at C-3". The HMBC correlations of H_2-7'/C-1', C-2', C-6', C-9'; H-2'/C-4', C-6'; 3'-O*Me*/C-3'; H_2-7/C-1, C-2, C-6; H-2/C-4, C-6; 3-O*Me*/C-3; 4-O*Me*/C-4; H_2-9/C-9' indicated that part II was arctigenin (**5**), which was confirmed by comparing their 1D NMR data. Parts I and II were linked by the formation of an ether bond between C-8" and C-4', although a correlation from H-8" to C-4' was not observed in the HMBC spectrum of **3**. NOE enhancements of H-2", H-6", and H-5', observed after irradiation

of H-8" in a NOE difference experiment (Figure 25S, Supporting Information), indicated a connection between C-8" and C-4' in **3**. This deduction was also verified by the obvious downfield chemical shift of C-8" (δ_C 87.4) compared to a typical hydroxylated carbon. Thus, the planar structure of **3** was established.

The relative configuration in part II was assigned as *trans* on the basis of observed unequal chemical shifts of H_2-9 [δ_H 4.15 (1H, dd, J = 9.0, 8.0 Hz, H-9a) and 3.88 (1H, dd, J = 9.0, 7.0 Hz, H-9b)]. The absolute configuration of 8*R*,8'*R* was assigned based upon biogenetic considerations~~,~~ and also by comparison of its ^{1}H and ^{13}C NMR spectral data with those of arctigenin (**5**). The 7",8"-*erythro* configuration was deduced ~~due to~~from the observed small coupling constant ($J_{7",8"}$ = 4.7 Hz) [11]. The 7"*S* configuration was defined by a positive CE at 345 nm (the E band) in the $Rh_2(OCOCF_3)_4$-induced ECD spectrum of **3** (Fig. 4) [12, 13]. Therefore, the absolute configuration of **3** was 8*R*,8'*R*,7"*S*,8"*R* and this conclusion was further supported by the calculated ECD spectrum of (8*R*,8'*R*,7"*S*,8"*R*)-**3**, which exhibited a pattern similar to the experimental one (Fig. 3).

Medusarin D (**4**) was found to have a molecular formula of $C_{31}H_{36}O_{10}$ established by the observation of a (+)-HRESIMS ion at *m/z* 591.2211 $[M + Na]^+$. The IR and the NMR data (Table 2) of **4** highly resembled those of **3**, suggesting that they were isomers of each other. The main difference between **3** and **4** was the coupling constant of H-7" and H-8" ($J_{7",8"}$ = 7.9 Hz), which indicated a 7",8"-*threo* configuration of **4**. The 7"*R* configuration was defined by a negative CE at 342 nm (the E band) in the $Rh_2(OCOCF_3)_4$-induced ECD spectrum of **4** (Fig. 4). Therefore, the absolute

configuration of **4** was 8*R*,8'*R*,7"*R*,8"*R*, which was further verified by the ECD calculations.

Along with the new lignans, the ~~ten~~ 10 previously reported lignans, ~~including~~ namely arctigenin (**5**) [9], (−)-traxillagenin (**6**) [14], (−)-matairesinol (**7**) [15], (+)-matairesinol (**8**) [16], (−)-7(*S*)-hydroxyarctigenin (**9**) [9], (+)-7(*R*)-hydroxyarctigenin (**10**) [9], phenaxolactone 1 (**11**) [17], acutissimalignan B (**12**) [18], (+)-7,8-didehydroarctigenin (**13**) [19] and arctignan A (**14**) [20], were also obtained and identified on the basis of spectroscopic analysis and comparison with literature data.

All the isolates were screened for their inhibitory effects on NO production in LPS-stimulated RAW264.7 macrophage-like cells (Table 3). Compounds **2**, **5** and **11** exhibited marked inhibition with IC_{50} values of 13.2 ± 1.3, 10.1 ± 1.8 and 10.3 ± 1.9 μM, respectively. These values were comparable to that of the positive control quercetin (IC_{50} = 15.9 ± 1.2 μM). Compounds (+)-**1a**, **7**, **9** and **10** displayed moderate inhibitory activities with IC_{50} values ranging from 16.2 ± 2.0 to 41.7 ± 2.1 μM. Arctigenin (**5**), the major constituent in *S. medusa*, significantly inhibited the production of NO in LPS-stimulated RAW264.7 cells and might contribute to the reported anti-inflammatory effects of *S. medusa* extracts [4].

Some preliminary structure-activity relationships could be drawn. The phenolic hydroxy group (especially the 4'-OH group) was found to be essential for the observed inhibitory effects. Absence of the 4'-OH group resulted in a loss of activity as those sesquilignans ~~which~~ that lacked this (compounds **3**, **4** and **14**) displayed poor inhibition of iNOS in LPS-induced RAW264.7 cells. Secondly, the C-8' chiral environment was

also deemed to be essential, as the introduction of a C7'-C8' double -bond led to the loss of activity (compounds **12** and **13**). Also, compound **7** exhibited good activity ~~due to~~because of its stereoselectivity. Compound **6** was inactive, likely ~~due to~~because of the additional 3-OMe group on aromatic ring B. However, the presence of a 2-OH group instead (compound **2**) enabled inhibition. Furthermore, it is interesting to note that compound (+)-**1a** showed inhibitory effects, while its enantiomer (−)-**1b** was inactive.

In order to explore the mechanisms by which these compounds inhibit NO production, molecular docking and iNOS expression studies (Fig. 5) were conducted. The active compounds (+)-**1a**, **2**, **5**, **7** and~~,~~ **9**−**11** and the positive control quercetin were selected for molecular docking studies to investigate their interactions with the iNOS enzyme. The docking results are presented in Table 4. With the exception of compound **9**, the active compounds exhibited excellent docking scores (< -7.0 kcal/mol) with iNOS. Of particular interest was the fact that compound **5** showed the lowest docking score with the iNOS enzyme, consistent with its strong inhibitory effect.

To further explore the underlying mechanisms, we investigated the effect of selected compounds on iNOS expression. As reported in the literature, arctigenin (**5**) inhibits ~~the~~ iNOS expression in LPS-induced RAW264.7 cells [21, 22]. In this study, compounds **2** and **11** were selected to investigate their inhibitory effects on ~~the~~ iNOS expression. As shown in Fig. 6, ~~the~~ iNOS expression was significantly increased after LPS stimulation and both compounds **2** and **11** showed a dose-~~-~~dependent reduction in the expression of iNOS in LPS-~~-~~treated RAW264.7 cells. The results suggest that compounds **2** and **11** inhibit the production of NO by reducing ~~the~~ iNOS expression.

In conclusion, five new diarylbutyrolactones and sesquilignans, together with ten known analogues, were separated from the whole plants of *S. medusa*. Among them, compounds **1**, **2** and **5**−**13** were diarylbutyrolactone lignans, with compound **1** featuring an unusual 7,8'-diarylbutyrolactone lignan. Compounds **3**, **4** and **14** were found to be sesquilignans. Overall, these findings not only provide more data on the chemical diversity of lignans present in *S. medusa*, but also indicate that diarylbutyrolactone lignans, such as arctigenin, may serve as potential lead compounds for further anti-inflammatory drug development. This should stimulate further studies on the anti-inflammatory activities of the constituents of *S. medusa*.

Material and Methods

General experimental procedures

Optical rotations (Na lamp, 589 nm) were measured on a Rudolph Autopol VI automatic polarimeter at room temperature. UV spectra were determined on a Shimadzu UV-2550 UV-visible spectrophotometer. ECD spectra were acquired on a JASCO J-815 spectrometer using a 0.1 cm path length sample cell and a JASCO LC-J1500 consisting of a MD-4014 photo-diode array detector, an AS-4050 HPLC auto sampler, a PU-4185 binary and a CO-4060 column oven. IR spectra were recorded on a Thermo IS5 spectrometer with KBr panels. NMR experiments were performed on a Bruker Avance III 600 MHz spectrometer (Bruker Biospin AG) using TMS as the internal standard. (±)-ESIMS and (±)-HRESIMS data were obtained on a Bruker Daltonics Esquire 3000 Plus LC-MS instrument and a Waters Q-TOF Ultima mass spectrometer, respectively. Column chromatography (CC) was performed using silica

gel (200−300 and 300−400 mesh, Qingdao Haiyang Chemical Co. Ltd.), Sephadex LH-20 (GE Healthcare), MCI gel (CHP20P, 75−150 μm, Mitsubishi Chemical Industries, Ltd.) and C18 reversed-phase silica gel (150−200 mesh, Merck). Precoated silica gel GF254 plates (Qingdao Haiyang Chemical Co. Ltd.) were used for TLC detection. Semipreparative HPLC was carried out on a Waters 2695 instrument equipped with a Waters 2489 detector (210 and 254 nm) using a Waters X-Bridge Prep C18 column (250 × 10 mm, S-5 μm) or a YMC-Pack ODS-A column (250 × 10 mm, S-5 μm). A Daicel Chiralpak IG (250 × 4.6 mm, S-5 μm) column was used for chiral HPLC separation. $Rh_2(OCOCF_3)_4$ was purchased from Sigma-Aldrich. All solvents except HPLC solvents were purchased from Shanghai Chemical Reagents Co. Ltd. and were of analytical grade. Solvents used for HPLC were of HPLC grade and were obtained from J & K Scientific Ltd.

Plant material

The whole plants of *S. medusa* were collected from Yeniu Ditch (altitude 4100 m), Qilian County, Xining City, Qinghai Province in August 2018, and authenticated by Professor Lijuan Mei from Northwest Institute of Plateau Biology. The specimen was deposited in the Key Laboratory of Tibetan Medicine of the Chinese Academy of Sciences (access number: 0341202).

Extraction and isolation

The air-dried and powdered whole herbs of *S. medusa* (15.0 kg) were soaked overnight with 95% ethanol and then extracted with 95% ethanol (3 times, 75 L and 12 h) to obtain the crude extract (800 g). The extract was suspended in water (4 L) and

successively partitioned with petroleum ether (5 × 4 L), EtOAc (5 × 4 L) and *n*-butanol (5 × 4 L). The EtOAc-soluble fraction (90 g) was subjected to column chromatography on MCI gel (5 × 40 cm, 100–200 mesh) eluted with MeOH-H_2O (10% to 100%) to give fractions F1–F7 based on TLC analysis. F5 (26.4 g) was separated by a silica gel column eluted with a gradient of CH_2Cl_2/MeOH (400:1 to 10:1) to yield fractions F5a–F5g. F5d (0.98 g) was fractioned via Sephadex LH-20 (MeOH) (3 × 150 cm), followed by RP semi-preparative HPLC (41% MeOH in H_2O) to yield **2** (19 mg, t_R = 41 min). Fraction F5f (1.6 g) was separated over a Sephadex LH-20 column (3 × 150 cm) eluted with MeOH to afford subfractions F5f1–F5f7. Fraction F5f2 (343 mg) was subjected to a silica gel column eluted with CH_2Cl_2/MeOH (400:1 to 1:1) in gradient to give subfractions F5f21–F5f24. F5f23 (61 mg) was then purified by semi-preparative HPLC with 44% MeOH in H_2O as the mobile phase to afford **3** (12 mg, t_R = 43 min) and **4** (8 mg, t_R = 46 min). Fraction F4 (15.8 g) was subjected to a silica gel column eluted with CH_2Cl_2/MeOH (400:1 to 1:1) in gradient to give subfractions F4a–F4k. Separation of F4k (1.0 g) with Sephadex LH-20 (MeOH) (3 × 150 cm) yielded subfractions F4k1–F4k3. Fraction F4k2 (243 mg) was subjected to a silica gel column eluted with *n*-hexane/isopropanol (80:1 to 1:1) in gradient to give subfractions F4k21–F4k23. F4k22 (97 mg) was then purified by RP semi-preparative HPLC (32% MeOH in H_2O) to yield **1** (15 mg, t_R = 21 min). The isolation procedure of the known compounds is described in the Experimental Section, Supporting Information.

Medusarin A (**1**): colorless gum; $[\alpha]^{25}_D$ +0.7 (*c* 0.57 in MeOH); ^1H and ^{13}C NMR (CD_3OD) data, see Table 1; IR (KBr) ν_{max} 3359, 2922, 2851, 1741, 1645, 1468, 1384,

1260, 1041 cm^{-1}; UV (MeOH) λ_{max} (log ε) 237 (3.25), 340 (3.37) nm; (+)-ESIMS *m/z* 799.1 $[2M + Na]^+$; (−)-ESIMS *m/z* 387.4 $[M - H]^-$; (+)-HRESIMS *m/z* 411.1056 $[M + Na]^+$ (calcd for $C_{20}H_{20}NaO_8$, 411.1050, Δ -1.39 ppm).

1a: colorless gum; $[\alpha]^{25}_D$ +83.8 (*c* 0.1 in MeOH); ECD (MeOH) λ (Δε) 209 (−14.95), 239 (−7.47), 305 (+7.90), 336 (+9.07) nm;

1b: colorless gum; $[\alpha]^{25}_D$ −87.2 (*c* 0.1 in MeOH); ECD (MeOH) λ (Δε) 209 (+16.50), 239 (+9.68), 305 (−9.38), 336 (−10.42) nm;

Medusarin B (**2**): white amorphous solid; $[\alpha]^{25}_D$ +5.2 (*c* 0.23 in MeOH); ^1H and ^{13}C NMR ($CDCl_3$) data, see Table 1; IR (KBr) ν_{max} 3422, 2933, 1751, 1612, 1518, 1452, 1384, 1204, 1117, 1031 cm^{-1}; UV (MeOH) λ_{max} (log ε) 230 (3.44), 286 (3.18); ECD (MeOH) λ ($\Delta\varepsilon$) 211 (−8.59), 233 (−6.56), 290 (+0.85) nm; (+)-ESIMS *m/z* 406.4 $[M + NH_4]^+$; (−)-ESIMS *m/z* 387.4 $[M - H]^-$; (+)-HRESIMS *m/z* 411.1424 $[M + Na]^+$ (calcd for $C_{21}H_{24}NaO_7$, 411.1414, Δ -2.44 ppm).

Medusarin C (**3**): light yellow amorphous solid; $[\alpha]^{25}_D$ −11.8 (*c* 0.22 in MeOH); ^1H and ^{13}C NMR ($CDCl_3$) data, see Table 2; IR (KBr) ν_{max} 3447, 2936, 1763, 1591, 1514, 1463, 1421, 1265, 1235, 1123, 1028 cm^{-1}; UV (MeOH) λ_{max} (log ε) 230 (3.68), 280 (3.27); ECD (MeOH) λ ($\Delta\varepsilon$) 238 (−7.78), 282 (−2.17) nm; (+)-ESIMS *m/z* 591.6 $[M + Na]^+$; (−)-ESIMS *m/z* 567.3 $[M - H]^-$; (+)-HRESIMS *m/z* 591.2208 $[M + Na]^+$ (calcd for $C_{31}H_{36}NaO_{10}$, 591.2201, Δ -1.28 ppm).

Medusarin D (**4**): light yellow amorphous solid; $[\alpha]^{25}_D$ −26.7 (*c* 0.31 in MeOH); ^1H and ^{13}C NMR ($CDCl_3$) data, see Table 2; IR (KBr) ν_{max} 3471, 2936, 1763, 1605, 1515, 1464, 1266, 1156, 1028 cm^{-1}; UV (MeOH) λ_{max} (log ε) 230 (3.61), 278 (3.23); ECD

(MeOH) λ ($\Delta\varepsilon$) 211 (+4.97), 236 (−8.28) nm; (+)-ESIMS *m/z* 591.5 $[M + Na]^+$; (−)-ESIMS *m/z* 567.3 $[M - H]^-$; (+)-HRESIMS *m/z* 591.2211 $[M + Na]^+$ (calcd for $C_{31}H_{36}NaO_{10}$, 591.2201, Δ -1.78 ppm).

*ECD calculations for **1**−**4***

The absolute configurations of **1**−**4** were determined by TDDFT-ECD calculations. For calculation details see the Experimental Section, Supporting Information.

Determination of NO production and cell viability assay

Measurements of NO production in an activated macrophage-like cell line were performed as described previously [23]. Briefly, RAW264.7 cells (1×10^5 cells/well) were cultured in 96-well plates with a DMEM high-glucose medium supplemented with 10% fetal bovine serum (FBS), 1 mM pyruvate, 2.0 mM glutamine, 100.0 U/mL of penicillin and 10.0 μg/mL of streptomycin at 37-°C in a humidified atmosphere with 5% CO_2. The cells were treated with 1.0 μg/mL of LPS and with the test compounds for 24 h. Absorbance was measured at 540 nm after incubating the culture media (100 μL/each well) with Griess reagent (100 μL) (Sigma-Aldrich) at room temperature. The concentration of NO was calculated using a $NaNO_2$ solution standard. Cell viability was measured using the MTT-based colorimetric assay (fFor experimental details see the Experimental Section, Supporting Information).

Molecular docking study

Chemical structures of active compounds were drawn using the ChemDraw program and converted to their three-dimensional (3D) coordinates in Chem3D. Each of them was subjected to energy minimization by the MM2 method and saved in "pdb"

format. The 3D crystal structure of iNOS (PDB ID: 3E6T) was obtained from the RCSB Protein Data Bank (https://www.rcsb.org/pdb) [24] and handled in the Biovia Discovery Studio Visualizer 2020 program for checking any missing residue/atom and deleting co-crystallized molecules such as cofactors, inhibitors~~,~~ and water. The proteins and ligands were processed and converted to "pdbqt" format. A grid box with dimensions of 30, 30~~,~~ and 30 points in x, y, and z directions, respectively, were built. Molecular docking was performed using AutoDock Vina with default parameters, and the binding sites were defined within 10 Å around the co-crystallized ligands. Each docking involved nine independent runs. The docked model with the lowest docking energy was selected to represent its most favorable binding pattern.

Measurement of iNOS expression

iNOS expression was measured according to a previous report [25]. Briefly, after the treatment with LPS (1.0 μg/mL) and target compounds for 24 h, cells were washed with PBS and suspended in a lysis buffer. Cell debris were removed by centrifugation. After the protein concentration for each aliquot was determined with BCA reagent, suspensions were boiled in an SDS-PAGE loading buffer. The proteins were subjected to gel electrophoresis and electrophoretically transferred onto PVDF membranes. The membranes were blocked with blocking solution at r. t. for 2 h. After washing, the membranes were incubated with a 1:1000 dilution of monoclonal anti-iNOS antibody and a 1:5000 dilution of β-actin antibody overnight at 4 °C~~℃~~. Blots were then washed thrice with TBST and incubated with a 1:3000 dilution of secondary antibody solution for 1 h at r.~~-~~t.~~.~~ Blots were again washed thrice with TBST and then detected by using

enhanced chemiluminescence reagent and exposed to photographic films. Images were collected and the related bands were quantitated by densitometric analysis.

Supporting Information

1D and 2D NMR, IR, UV, ESIMS, and HRESIMS spectra of compounds **1**–**4**, chiral HPLC separation profile of **1a**/**1b**, ^{1}H-^{1}H COSY and key HMBC correlations of compounds **1**–**4**, data of cell viability and the inhibition of NO production, isolation procedure of known compounds and the ECD calculation method are available as Supporting Information.

Contributors' Statement

Prof. Ruitao Yu, Yanduo Tao and Lijuan Mei were responsible for the experimental design; Ms. Jingya Cao was responsible for isolation and writing the article; Mr. Zhiyao Wang contributed to the spectrometric identification; Mr. Ye Zhao performed computational calculations; Ms. Qi Dong completed the biological experiments and data analysis; and Prof. Alan J. Stewart contributed to the revision of the article and the experimental analysis of the molecular docking. All the authors reviewed and validated the present manuscript prior to submission.

Acknowledgements

The authors are thankful to Prof. Jian Min Yue at Shanghai Institute of Materia Medica, Chinese Academy of Sciences for providing the necessary facilities for this research. This work was supported by the Natural Science Foundation of Qinghai Province (No. 2022-ZJ-930), the science and innovation platform for the development and construction of special projects of Key Laboratory of Tibetan Medicine Research

of Qinghai Province (No. 2022-ZJ-Y03).

Conflict of Interest

The authors declare that they have no conflicts of interest.

References

[1] The angiosperm phylogeny group. An update of the angiosperm phylogeny group classification for the orders and families of flowering plants: APG IV. Bot J Linn Soc 2016; 181: 1−20

[2] Li HH, Qiu J, Chen FD, Lv XF, Fu CX, Zhao DX, Hua XJ, Zhao Q. Molecular characterization and expression analysis of dihydroflavonol 4-reductase (DFR) gene in *Saussurea medusa*. Mol Biol Rep 2012; 39: 2991–2999

[3] Northwest Institute of Plateau Biology. The Chinese Academy of Sciences. The Tibetan Medicine Glossary. Qinghai People's Press 1991; 222–223

[4] Yu RX, Jiang L, Mei LJ, Tao YD, Yu RT, Xia XC. Anti-inflammatory effects of alcohol extract from *Saussurea medusa* Maxim. against lipopolysaccharides-induced acute lung injury mice. Int J Clin Exp Medic Res 2019; 3: 112–118

[5] Pescitelli G, Bruhn T. Good computational practice in the assignment of absolute configurations by TDDFT calculations of ECD spectra. Chirality 2016; 28: 466–474

[6] Liu X, Zhang BF, Yang L, Chou GX, Wang ZT. Four new compounds from *Imperata cylindrica*. J Nat Med 2013; 68: 295–301

[7] Mali RS, Babu KN. Efficient synthesis of α-benzylidene-γ-methyl-γ- butyrolactones. Helv Chim Acta 2002; 85: 3525–3531

[8] Datta A, Ila H, Junjappa H. Polarized ketene dithioacetals 63. Tetrahedron 1987;

43: 5367–5374

[9] Fischer J, Reynolds AJ, Sharp LA, Sherburn MS. Radical carboxyarylation approach to lignans. Total synthesis of (-)-arctigenin, (-)-matairesinol, and related natural products. Org Lett 2004; 6: 1345–1348

[10] Corrie J, Green GH, Ritchie E, Taylor WC. The chemical constituents of Australian *Zanthoxylum* species. V. The constituents of *Z. pluviatile* Hartley; the structures of two new lignans. Aust J Chem 1970; 23: 133–145

[11] Gan ML, Zhang YL, Sheng L, Liu MT, Song WX, Zi JC, Yang YC, Fan XN, Shi JG, Hu JF, Sun JD, Chen NH. Glycosides from the root of *Iodes cirrhosa*. J Nat Prod 2008; 71: 647–654

[12] Frelek J, Szczepek WJ. [$Rh_2(OCOCF_3)_4$] as an auxiliary chromophore in chiroptical studies on steroidal alcohols. Tetrahedron Asymmetry 1999; 10: 1507–1520

[13] Frelek J, Klimek A, Ruskowska P. Dinuclear transition metal complexes as auxiliary chromophores in chiroptical studies on bioactive compounds. Curr Org Chem 2003; 7: 1081–1104

[14] Jang YP, Kim SR, Kim YC. Neuroprotective dibenzylbutyrolactone lignans of *Torreya nucifera*. Planta Med 2001; 67: 470–472

[15] Tiwari AK, Srinivas PV, Kumar SP, Rao JM. Free radical scavenging active components from *Cedrus deodara*. J Agric Food Chem 2001; 49: 4642–4645

[16] Chang H, Wang YW, Gao X, Song ZH, Awale S, Han N, Liu ZH, Yin J. Lignans from the root of *Wikstroemia indica* and their cytotoxic activity against PANC-1 human pancreatic cancer cells. Fitoterapia 2017; 31: 1–27

[17] Piccinelli AL, Mahmood N, Mora G, Poveda L, Simone FD, Rastrelli L. Anti-HIV activity of dibenzylbutyrolactone-type lignans from *Phenax* species endemic in Costa Rica. J Pharm Pharmacol 2005; 57: 1109–1115

[18] Tuchinda P, Kornsakulkarn J, Pohmakotr M, Kongsaeree P, Prabpai S, Yoosook C, Kasisit J, Napaswad C, Sophasan S, Reutrakul V. Dichapetalin-type triterpenoids and lignans from the aerial parts of *Phyllanthus acutissima*. J Nat Prod 2008; 71: 655–663

[19] Matsumoto T, Hosono-Nishiyama K, Yamada H. Antiproliferative and apoptotic effects of butyrolactone lignans from *Arctium lappa* on leukemic cells. Planta Med 2006; 72: 276–278

[20] Umehara K, Sugawa A, Kuroyanagi M, Ueno A, Taki T. Studies on differentiation-inducers from *Arctium* fructus. Chem Pharm Bull 1993; 41: 1774–1779

[21] Zhao F, Wang L, Liu K. *In vitro* anti-inflammatory effects of arctigenin, a lignan from *Arctium lappa* L., through inhibition on iNOS pathway. J Ethnopharmacol 2009; 122: 457–462

[22] Kou XJ, Qi SM, Dai WX, Luo L, Yin ZM. Arctigenin inhibits lipopolysaccharide-induced iNOS expression in RAW264.7 cells through suppressing JAK-STAT signal pathway. Int Immunopharmacol 2011; 11: 1095–1102

[23] Cuong TD, Hung TM, Kim JC, Kim EH, Woo MH, Choi JS, Lee JH, Min BS. Phenolic compounds from *Caesalpinia sappan* heartwood and their anti-inflammatory activity. J Nat Prod 2012; 75: 2069–2075

[24] Zhang Y, Liu JZ, Wang MY, Sun CJ, Li XB. Five new compounds from *Hosta*

plantaginea flowers and their anti-inflammatory activities. Bioorg Chem 2020; 95: 1–7

[25] Zhao F, Wang L, Liu K. In *vitro* anti-inflammatory effects of arctigenin, a lignan from *Arctium lappa* L., through inhibition on iNOS pathway. J Ethnopharmacol 2009; 122: 457–462

Legends for Figures

Fig. 1. Chemical structures of compounds **1**–**14**.

Fig. 2. Key ROESY correlations of compound **1**.

Fig. 3. Experimental and calculated ECD spectra of compounds **1**–**4**.

Fig. 4. $Rh_2(OCOCF_3)_4$-induced ECD spectra of compounds **3** and **4** in CH_2Cl_2.

Fig. 5. Molecular docking simulations of compounds **1a** (A), **2** (B), **5** (C), **7** (D), **9** (E), **10** (F), **11** (G) and quercetin (S) with the iNOS enzyme.

Fig. 6. Concentration-dependent inhibition of compounds **2** and **11** on iNOS expression. (A)

Typical blotting of iNOS and β-actin. (B) The bar chart shows the quantitative evaluation of iNOS bands by densitometry. Data represents the mean ± SD (n=3). *p<0.05, **p<0.01 compared with LPS.

Table 1. ^{1}H NMR Data (400 MHz) and ^{13}C NMR Data (125 MHz) for compounds **1** and **2**

	1[a]		**2**[b]	
position	δ_H (*J* in Hz)	δ_C, type	δ_H (*J* in Hz)	δ_C, type
1	—	133.0, C	—	115.5, C
2	6.58, s	103.7, CH	—	147.8, C
3	—	149.6, C	6.35, s	101.2, CH
4	—	136.8, C	—	148.6, C
5	—	149.6, C	—	143.0, C
6	6.58, s	103.7, CH	6.41, s	114.6, CH
7	5.60, brs	83.2, CH	a 2.62, dd (13.8,7.7)	32.6, CH_2
			b 2.55, dd (13.8, 8.1)	
8	3.66, dd (8.1, 7.0)	51.5, CH	2.59, m	39.8, CH
9	a 3.93, dd (15.1, 8.1)	62.5, CH_2	a 4.14, dd (9.0, 6.7)	71.8, CH_2
	b 3.62, dd (15.1, 7.0)		b 3.93, dd (9.0, 7.0)	
1'	—	126.9, C	—	129.9, C
2'	7.08, d (1.8)	117.9, CH	6.63, d (1.8)	111.9, CH
3'	—	146.9, C	—	146.7, C
4'	—	149.6, C	—	144.5, C
5'	6.83, d (8.3)	116.9, CH	6.78, d (8.0)	114.2, CH
6'	7.02, dd (8.3, 1.8)	125.0, CH	6.60, dd (8.0, 1.8)	122.4, CH
7'	7.49, s	141.0, CH	a 2.93, dd (14.1, 4.9)	34.6, CH_2
			b 2.88, dd (14.1, 6.4)	
8'	—	122.1, C	2.61, m	46.8, CH
9'	—	175.0, C	—	179.6, C
O*Me*-3/3'	3.82, s /	56.8, CH_3/	/3.80, s	/56.0, CH_3
O*Me*-4/5	/3.82, s	/56.8, CH_3	3.78, s/3.76, s	56.1, CH_3/56.8, CH_3

[a]Measured in CD_3OD. [b]Measured in $CDCl_3$.

Table 2. ^{1}H NMR Data (400 MHz) and ^{13}C NMR Data (125 MHz) for compounds **3** and **4** in $CDCl_3$

3						**4**					
position	δ_H (J in Hz)	δ_C, type	position	δ_H (J in Hz)	δ_C, type	position	δ_H (J in Hz)	δ_C, type	position	δ_H (J in Hz)	δ_C, type
1	—	130.5, C	1"	—	131.9, C	1	—	130.5, C	1"	—	131.6, C
2	6.50, d (1.9)	112.1, CH	2"	6.96, d (1.7)	108.8, CH	2	6.51, d (1.9)	112.1, CH	2"	6.96, d (1.7)	109.5, CH
3	—	149.2, C	3"	—	146.8, C	3	—	149.2, C	3"	—	146.8, C
4	—	148.1, C	4"	—	145.3, C	4	—	148.1, C	4"	—	145.8, C
5	6.76, d (8.1)	111.6, CH	5"	6.87, d (8.1)	114.4, CH	5	6.77, d (8.1)	111.6, CH	5"	6.88, d (8.1)	114.5, CH
6	6.55, dd (8.1, 1.9)	120.7, CH	6"	6.80, dd (8.1, 1.7)	119.2, CH	6	6.56, dd (8.1, 1.9)	120.8, CH	6"	6.90, dd (8.1, 1.7)	120.3, CH
7	a 2.65, dd (14.0, 6.0)	38.3, CH_2	7"	4.94, d (4.7)	73.0, CH	7	a 2.69, dd (14.2, 6.0)	38.3, CH_2	7"	4.94, d (7.9)	74.2, CH
	b 2.55, dd (14.0, 7.0)						b 2.58, dd (14.2, 7.0)				
8	2.48, m	41.3, CH	8"	4.13, m	87.4, CH	8	2.49, m	41.2, CH	8"	3.99, m	89.5, CH
9	a 4.15, dd (9.0, 8.0)	71.4, CH_2	9"	a 3.89, dd (12.2, 4.0)	61.0, CH_2	9	a 4.15, dd (9.0, 8.0)	71.4, CH_2	9"	a 3.50, dd (12.0, 4.5)	61.3, CH_2
	b 3.88, dd (9.0, 7.0)			b 3.66, dd (12.2, 3.4)			b 3.90, dd (9.0, 7.0)			b 3.61, dd (12.0, 3.7)	
1'	—	133.9, C	O*Me*-3	3.82, s	56.1, CH_3	1'	—	133.9, C	O*Me*-3	3.82, s	56.1, CH_3
2'	6.73, d (1.9)	113.3, CH	O*Me*-4	3.85, s	56.1, CH_3	2'	6.74, d (1.9)	113.3, CH	O*Me*-4	3.85, s	56.1, CH_3
3'	—	151.7, C	O*Me*-3'	3.83, s	56.1, CH_3	3'	—	151.4, C	O*Me*-3'	3.83, s	56.1, CH_3
4'	—	145.9, C	O*Me*-3"	3.87, s	56.1, CH_3	4'	—	145.8, C	O*Me*-3"	3.87, s	56.1, CH_3
5'	6.85, d (8.1)	120.8, CH				5'	7.01, d (8.1)	120.8, CH	OH-4"	5.65, s	
6'	6.64, dd (8.1, 1.9)	122.4, CH				6'	6.64, dd (8.1, 1.9)	122.5, CH			
7'	2.94, m	34.7, CH_2				7'	2.94, m	34.6, CH_2			
8'	2.60, m	46.7, CH				8'	2.60, m	46.7, CH			
9'	—	178.7, C				9'	—	178.7, C			

Table 3. Inhibition of LPS-induced NO production

compound	IC_{50} (μM) [a]	compound	IC_{50} (μM)
1a	21.7 ± 1.7	**8**	＞50
1b	＞50	**9**	34.2 ± 2.3
2	13.2 ± 1.3	**10**	41.7 ± 2.1
3	＞50	**11**	10.3 ± 1.9
4	＞50	**12**	＞50
5	10.1 ± 1.8	**13**	＞50
6	＞50	**14**	＞50
7	16.2 ± 2.0	[b]quercetin	15.9 ± 1.2

[a] Data expressed as the mean ± SD (n = 3). [b]Positive control.

Table 4. Docking results of active compounds with iNOS enzyme

compound	docking scores (kcal/mol)	hydrogen bonds	hydrophobic interaction
1a	-8.2	TYR341, GLN257, GLY365	VAL346
2	-7.3	TYR341, GLN257 , TYR367, ASP376	GLN257
5	-8.8	ARG260, ARG375	ALA276, GLN381, TRP84
7	-7.6	SER256, GLN257	
9	-6.7	ASN348, GLY365	PHE363, VAL346, TYR485, TRP457
10	-7.3	ARG382, ASP376, , GLU371	GLN257
11	-7.3	TYR341, TYR367, ASP376, ARG375	GLU371, ARG375
quercetin	-7.5	TYR341, PHE363	PRO344, VAL346

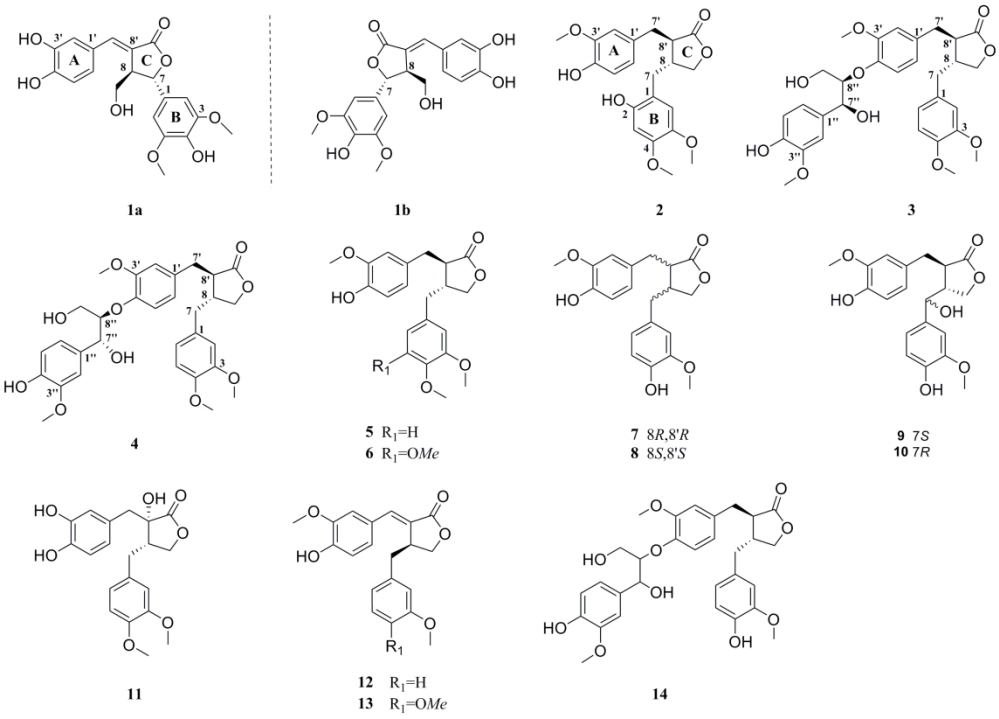

Fig. 1. Chemical structures of compounds **1**–**14**.

226x162mm (300 x 300 DPI)

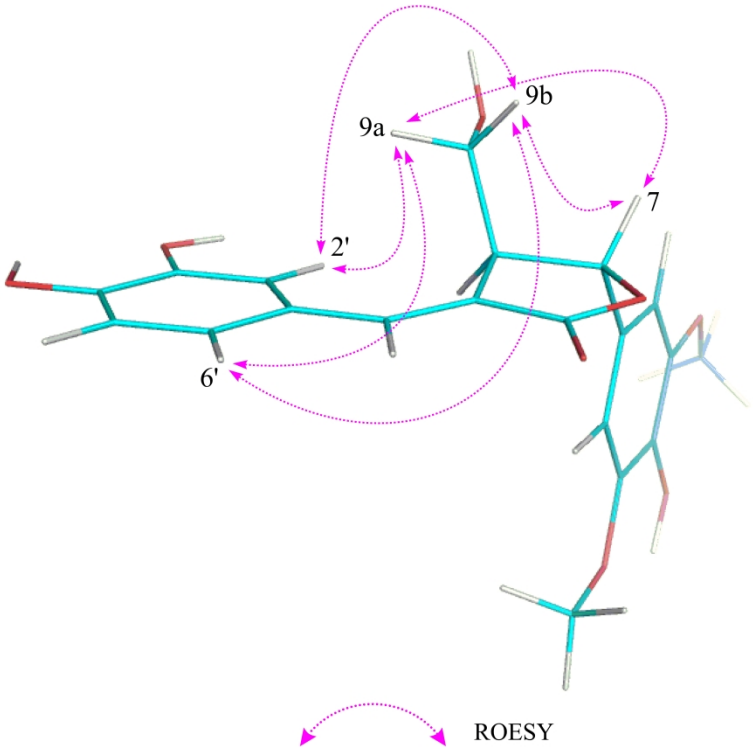

Fig. 2. Key ROESY correlations of compound **1**.

432x327mm (300 x 300 DPI)

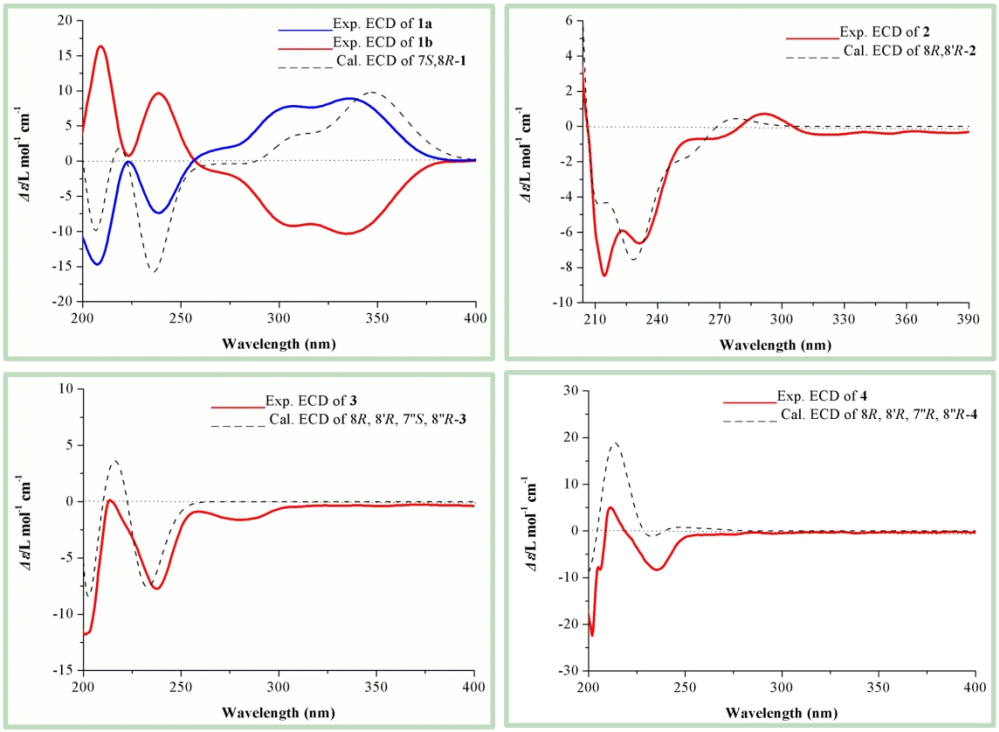

Fig. 3. Experimental and calculated ECD spectra of compounds **1**–**4**.

211x154mm (300 x 300 DPI)

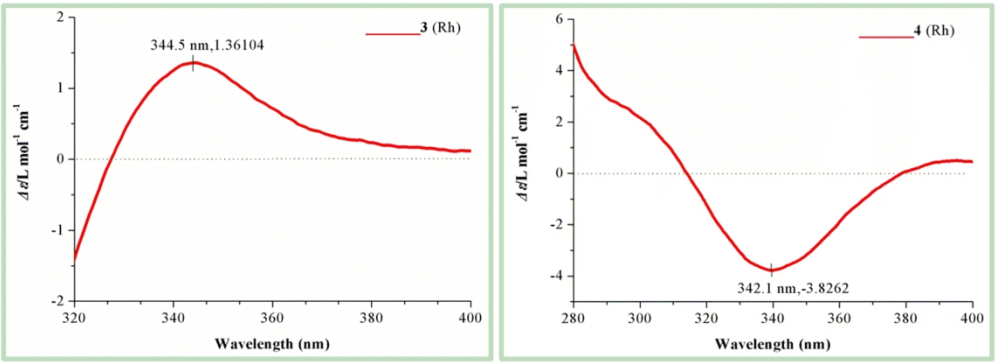

Fig. 4. The $Rh_2(OCOCF_3)_4$ induced ECD spectra of compounds **3** and **4** in CH_2Cl_2.

211x77mm (300 x 300 DPI)

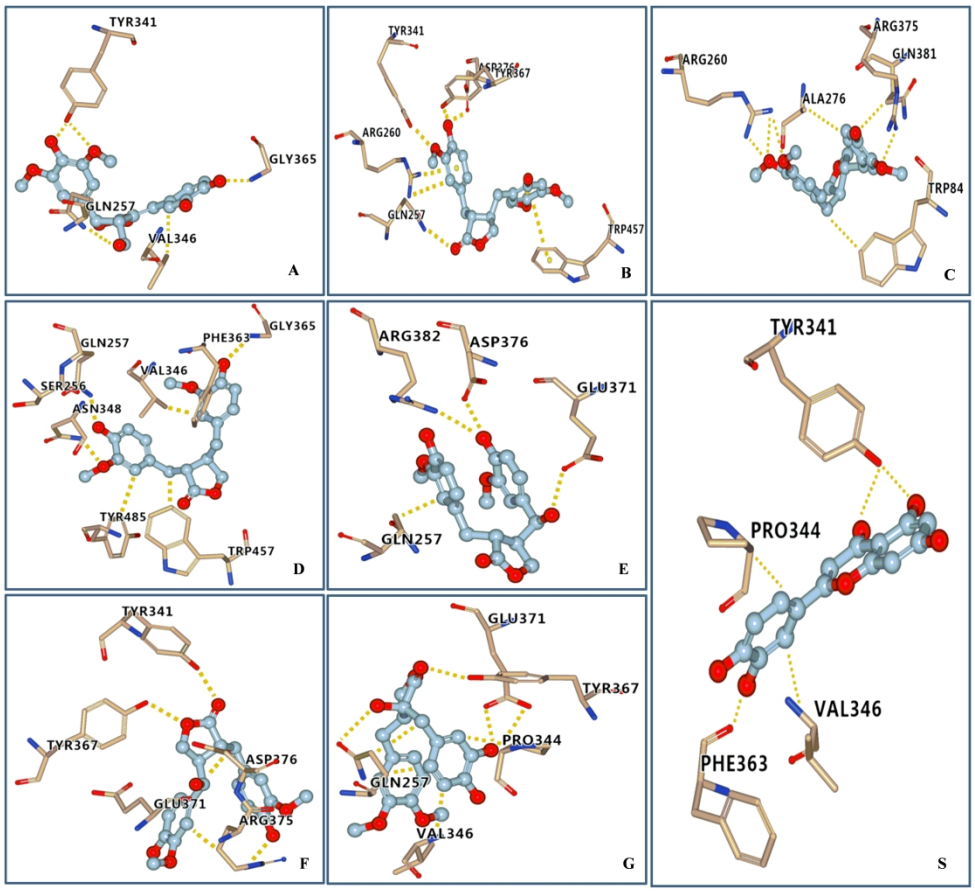

Fig. 5. Molecular docking simulations of compounds **1a** (A), **2** (B), **5** (C), **7** (D), **9** (E), **10** (F), **11** (G) and quercetin (S) with iNOS enzyme.

442x390mm (300 x 300 DPI)

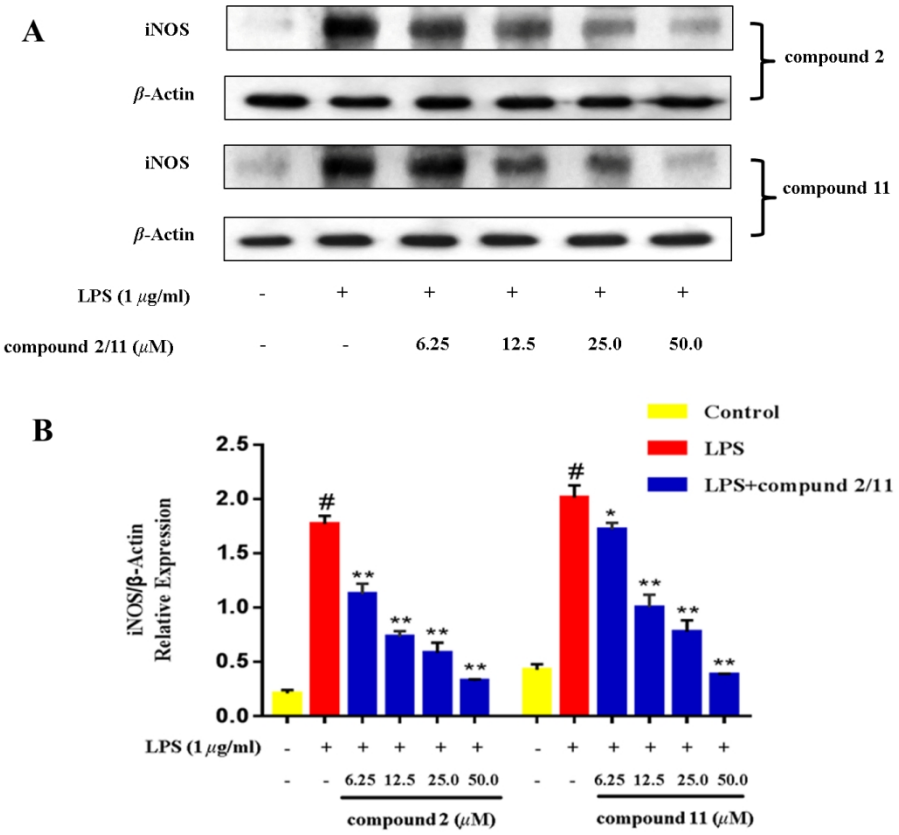

Fig. 6. Concentration dependency of the inhibitory effects of compounds **2** and **11**. (A) Typical blotting of iNOS and *β*-actin. (B) The bar chart shows the quantitative evaluation of iNOS bands by densitometry. Data represents the mean ± SD (n=3). *p<0.05, **p<0.01 compared with LPS.

258x222mm (150 x 150 DPI)

Supporting Information for

Five new diarylbutyrolactones and sesquilignans from *Saussurea medusa* and their inhibitory effects on LPS-induced NO production

Jing-Ya Cao[1,2], Zhi-Yao Wang[3], Alan J. Stewart[4], Qi Dong[1], Ye Zhao[5], Li-Juan Mei[1], Yan-duo Tao[1,*] and Rui-Tao Yu[1,*]

Affiliation

[1]Qinghai Provincial Key Laboratory of Tibetan Medicine Research; Key Laboratory of Tibetan Medicine Research, Northwest Institute of Plateau Biology, Chinese Academy of Sciences, Xining, PR China

[2]University of Chinese Academy of Sciences, Beijing, PR China

[3]Henan Academy of Science, Zhengzhou, PR China

[4]School of Medicine, University of St Andrews, United Kingdom

[5]State Key Laboratory of Drug Research, Shanghai Institute of Materia Medica, Chinese Academy of Sciences, Shanghai, PR China

Correspondence

Prof. Yan-duo Tao

Northwest Institute of Plateau Biology, Chinese Academy of Sciences, No. 23 Xinning Road, Xining 810008, PR China

Tel: +0971-6143530.

Fax: +0971-614328286.

E-mail: tyd@nwipb.cas.cn

Correspondence

Associate Prof. Rui-Tao Yu

Northwest Institute of Plateau Biology, Chinese Academy of Sciences, No. 23 Xinning Road, Xining 810008, PR China

Tel: +0971-6143530.

Fax: +0971-614328286.

E-mail: yuruitao@nwipb.cas.cn

Contents

Experimental Section

Extraction and isolation

The air-dried and powdered whole herbs of *S. medusa* (15.0 kg) were soaked overnight with 95% ethanol and then extracted with 95% ethanol (3 times, 75 L and 12 h) to obtain the crude extract (800 g). The extract was suspended in water (4L) and successively partitioned with petroleum ether (5 × 4 L), EtOAc (5 × 4 L) and *n*-butanol (5 × 4 L). The EtOAc-soluble fraction (90 g) was subjected to column chromatography on MCI gel (5 × 40 cm, 100–200 mesh) eluted with MeOH-H_2O (10% to 100%) to give fractions F1–F7 based on TLC analysis. The solid in fraction F5 (26.4 g) was filtered out and then recrystallized from MeOH to give an additional amount of **5** (10.1 g). The filtrate was further separated by a silica gel column eluted with a gradient of CH_2Cl_2/MeOH (400:1 to 10:1) to yield fractions F5a–F5g. Fraction F5a (0.67 g) was separated over a Sephadex LH-20 column (2 × 150 cm) eluted with EtOH to afford subfractions F5a1–F5a3. Fraction F5a3 (108 mg) was then purified by semi-preparative HPLC with 50% MeOH in H_2O to afford **7** (9 mg, t_R = 17 min), **8** (2 mg, t_R = 19 min) and **12** (3 mg, t_R = 21 min). Fraction F5b (1.3 g) was separated over a Sephadex LH-20 column (3 × 150 cm) eluted with MeOH to afford subfractions F5b1–F5b4. Fraction F5b2 (45 mg) was then purified by semi-preparative HPLC with 55% MeOH in H_2O as the mobile phase to afford **6** (6 mg, t_R = 16 min). Similarity, F5c (0.2 g) was separated over a Sephadex LH-20 column (2 × 150 cm) eluted with EtOH and purified by semi-preparative HPLC with 32% acetonitrile in H_2O to afford **11** (5 mg, t_R = 23 min). F5d (0.98 g) was fractioned via Sephadex LH-20 (MeOH) (3

× 150 cm) followed by RP semi-preparative HPLC (41% MeOH in H_2O) purification to yield **2** (19 mg, t_R = 41 min) and **10** (11 mg, t_R = 22 min). Fraction F5f (1.6 g) was separated over a Sephadex LH-20 column (3 × 150 cm) eluted with MeOH to afford subfractions F5f1–F5f7. Fraction F5f2 (343 mg) was subjected to a silica gel column eluted with CH_2Cl_2/MeOH (400:1 to 1:1) in gradient to give subfractions F5f21–F5f24. F5f23 (61 mg) was then purified by semi-preparative HPLC with 44% MeOH in H_2O as the mobile phase to afford **3** (12 mg, t_R = 43 min) and **4** (8 mg, t_R = 46 min). Similarly, F5f24 (72 mg) afforded **14** (3 mg, t_R = 46 min). Fraction F4 (15.8 g) was subjected to a silica gel column eluted with CH_2Cl_2/MeOH (400:1 to 1:1) in gradient to give subfractions F4a–F4k. Separation of F4k (1.0 g) with Sephadex LH-20 (MeOH) (3 × 150 cm) yielded subfractions F4k1–F4k3. Fraction F4k2 (243 mg) was subjected to a silica gel column eluted with *n*-hexane/isopropanol (80:1 to 1:1) in gradient to give subfractions F4k21–F4k23. F4k22 (97 mg) was then purified by RP semi-preparative HPLC (32% MeOH in H_2O) to yield **1** (15 mg, t_R = 21 min) and **9** (62 mg, t_R = 32 min). Similarly, F4k23 (59 mg) afforded **13** (23 mg, t_R = 11 min).

*ECD calculations for **1**−**4***

The absolute configurations of **1**−**4** were determined by quantum chemical TDDFT calculations of their theoretical ECD spectra. Using the MM2 force field in the Chem3D pro 14.0 software, the initial conformers of each compound were established. Conformational searches were conducted with the torsional sampling method (Monte Carlo Multiple Minimum, MCMM) under OPLS3 [1] force field by

Maestro 11.5 software (Maestro Technologies, Inc., Trenton, NJ, USA) in an energy window of 12.6 kJ/mol. The conformational optimization and the following TDDFT calculations for the conformers that satisfied the experiment coupling constants and NOE signals were all carried out with the Gaussian 16 program package [2] at the B3LYP/6-31G(d) level in methanol. All TDDFT calculations were computed at the PCM/ωB97XD/6-311G** level of theory in methanol. Finally, the Boltzmann-averaged ECD spectra were simulated with SpecDis 1.71 [3,4].

Cell culture

A murine macrophage cell line RAW264.7 was purchased from Procell Life Science & Technology Co. Ltd. RAW264.7 murine macrophage cells were cultured in plastic dishes containing Dulbecco's Modified Eagle Medium (DMEM) supplemented with 10% fetal bovine serum (FBS) at 37 °C in a humidified atmosphere with 5% CO_2.

Cell viability assay

RAW264.7 cells (1×10^5 cells/well) were cultured in 96-well plate for 24 h to become nearly confluent. Then cells were cultured with the test compounds for 24 h. After that, the cells were incubated with 100 μL of 0.5 mg/mL MTT for 4 h at 37 °C. The medium was then discarded and 100 μL dimethyl sulfoxide (DMSO) was added. Absorbance was measured at 570 nm after incubation for 40 min.

Supplementary References

[1] Harder E, Damm W, Maple J, Wu CJ, Reboul M, Xiang JY, Wang LL, Lupyan D, Dahlgren MK, Knight JL, Kaus JW, Cerutti D, Krilov G, Jorgensen WL, Abel R, Friesner RA. OPLS3: A force field providing broad coverage of drug-like small molecules and proteins. J Chem Theory Comput 2015; 12: 281–296

[2] Frisch MJ, Trucks GW, Schlegel HB, Scuseria GE, Robb MA, Cheeseman JR, Scalmani G, Barone V, Petersson GA, Nakatsuji H, Li X, Caricato M, Marenich AV, Bloino J, Janesko BG, Gomperts R, Mennucci B, Hratchian HP, Ortiz JV, Izmaylov AF, Sonnenberg JL, Williams-Young D, Ding F, Lipparini F, Egidi F, Goings J, Peng B, Petrone A, Henderson T, Ranasinghe D, Zakrzewski VG, Gao J, Rega N, Zheng G, Liang W, Hada M, Ehara M, Toyota K, Fukuda R, Hasegawa J, Ishida M, Nakajima T, Honda Y, Kitao O, Nakai H, Vreven T, Throssell K, Montgomery JAJ, Peralta JE, Ogliaro F, Bearpark MJ, Heyd JJ, Brothers EN, Kudin KN, Staroverov VN, Keith TA, Kobayashi R, Normand J, Raghavachari K, Rendell AP, Burant JC, Iyengar SS, Tomasi J, Cossi M, Millam JM, Klene M, Adamo C, Cammi R, Ochterski JW, Martin RL, Morokuma K, Farkas O, Foresman JB, Fox DJ. Gaussian 16, Revision B.01. GaussView 5.0. E.U.A. Wallingford, CT: Gaussian Inc. 2016

[3] Pescitelli G, Bruhn T. Good computational practice in the assignment of absolute configurations by TDDFT calculations of ECD spectra. Chirality 2016; 28: 466–474

[4] Bruhn T, Schaumlöffel A, Hemberger Y, Bringmann G. SpecDis: Quantifying the comparison of calculated and experimental electronic circular dichroism spectra. Chirality 2013; 25: 243–249

Table 1S. Re-optimized conformers, energies and proportions for 7*S*,8*R*-1

Number	Conformer	Energy (hartree)	Energy (Kcal/mol)	Proportion (%)
1	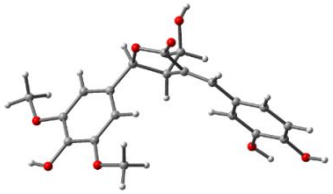	-1375.71985	-863277.1253	36.18
2	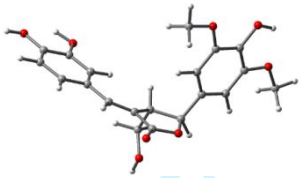	-1375.719844	-863277.1215	35.95
3	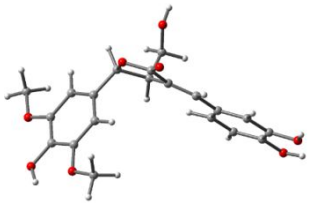	-1375.717684	-863275.7661	3.64
4	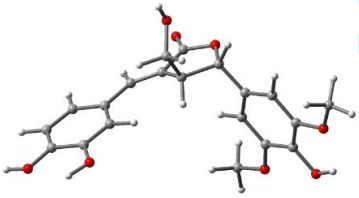	-1375.717471	-863275.6324	2.90
5	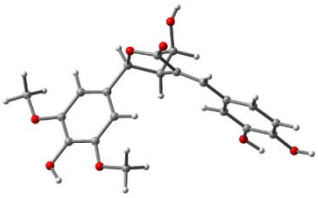	-1375.71739	-863275.5816	2.66
6	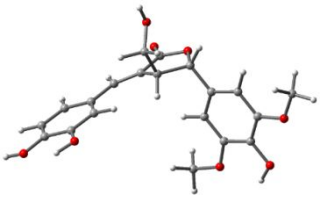	-1375.717388	-863275.5803	2.66
7	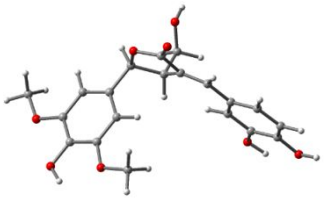	-1375.717384	-863275.5778	2.65

8	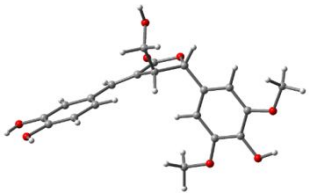	-1375.717194	-863275.4586	2.16
9	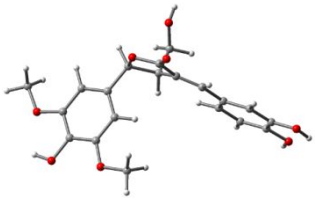	-1375.717193	-863275.458	2.16
10	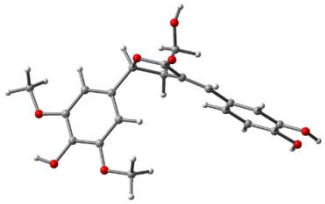	-1375.717189	-863275.4555	2.15
11	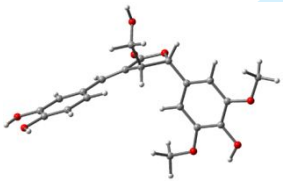	-1375.716979	-863275.3237	1.72
12	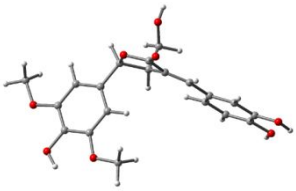	-1375.716979	-863275.3237	1.72
13	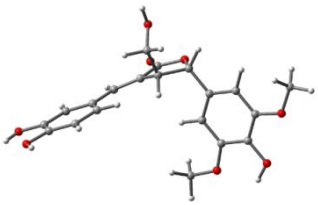	-1375.716977	-863275.3224	1.72
14	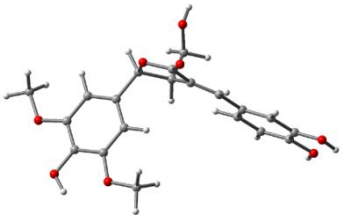	-1375.716973	-863275.3199	1.71

Table 2S. Re-optimized energies and proportions for 8*R*,8'*R*-2

Number	Energy (hartree)	Energy (Kcal/mol)	Proportion (%)	8*R*,8'*R*-**2**
1	-1341.003379	-841492.2137	38.77	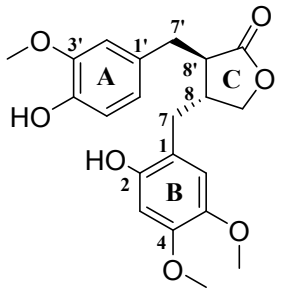
2	-1341.00325	-841492.1327	33.82	
3	-1341.002758	-841491.824	20.07	
4	-1341.001282	-841490.8978	4.20	
5	-1340.999672	-841489.8875	0.76	
6	-1340.999415	-841489.7262	0.58	
7	-1340.999275	-841489.6384	0.50	
8	-1340.998977	-841489.4514	0.36	
9	-1340.99879	-841489.334	0.30	
10	-1340.998556	-841489.1872	0.23	
11	-1340.998253	-841488.9971	0.17	
12	-1340.997841	-841488.7385	0.11	
13	-1340.997603	-841488.5892	0.08	
14	-1340.996262	-841487.7477	0.02	
15	-1340.996186	-841487.7	0.02	

Table 3S. Re-optimized energies and proportions for 8*R*,8'*R*,7''*S*,8''*R*-3

Number	Energy (hartree)	Energy (Kcal/mol)	Proportion (%)	8*R*,8'*R*,7''*S*,8''*R*-**3**
1	-1954.816281	-1226665.574	42.73	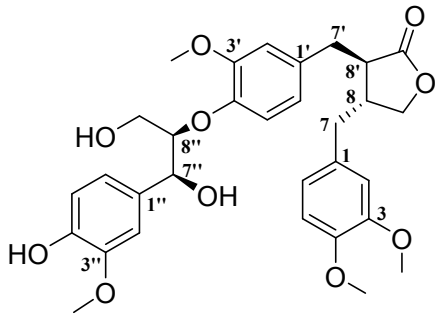
2	-1954.816248	-1226665.553	41.26	
3	-1954.81437	-1226664.375	5.63	
4	-1954.814109	-1226664.211	4.27	
5	-1954.813501	-1226663.83	2.24	
6	-1954.812759	-1226663.364	1.02	
7	-1954.812687	-1226663.319	0.95	
8	-1954.812668	-1226663.307	0.93	
9	-1954.812373	-1226663.122	0.68	
10	-1954.810822	-1226662.148	0.13	
11	-1954.810528	-1226661.964	0.10	
12	-1954.809606	-1226661.385	0.04	
13	-1954.809437	-1226661.279	0.03	
14	-1954.806349	-1226659.342	0.01	

Table 4S. Re-optimized energies and proportions for 8*R*,8'*R*,7''*R*,8''*R*-4

Number	Energy (hartree)	Energy (Kcal/mol)	Proportion (%)	8*R*,8'*R*,7''*R*,8''*R*-**4**
1	-1954.815495	-1226665.081	52.08	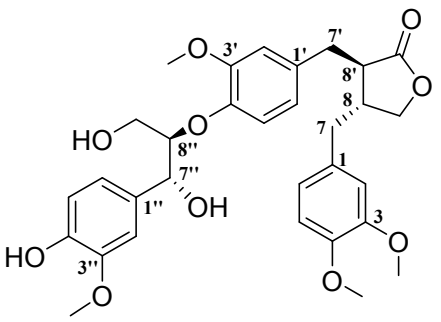
2	-1954.814334	-1226664.352	15.21	
3	-1954.814234	-1226664.289	13.68	
4	-1954.813942	-1226664.106	10.04	
5	-1954.813535	-1226663.851	6.52	
6	-1954.81198	-1226662.875	1.25	
7	-1954.811372	-1226662.494	0.66	
8	-1954.810754	-1226662.106	0.34	
9	-1954.809393	-1226661.252	0.08	
10	-1954.809381	-1226661.244	0.08	
11	-1954.808496	-1226660.689	0.03	
12	-1954.808282	-1226660.555	0.02	
13	-1954.80728	-1226659.926	0.01	
14	-1954.806887	-1226659.679	0.01	
15	-1954.805654	-1226658.905	0.01	

Table 5S. Cell viability of compounds 1-14.

Sample		Blank control	Drug treatment group					
compound **1a**	Concentration (μM)	0	3.125	6.25	12.5	25	50	100
	Cell viability (%)	99.98±2.54	97.43±1.21	94.74±2.10	87.56±1.34	84.49±1.53	85.68±0.40	80.52±1.74
compound **1b**	Concentration (μM)	0	3.125	6.25	12.5	25	50	100
	Cell viability (%)	99.98±2.72	100.58±2.10	96.91±2.20	87.92±1.71	86.70±2.49	84.07±2.41	81.23±0.39
compound **2**	Concentration (μM)	0	3.125	6.25	12.5	25	50	100
	Cell viability (%)	99.98±1.97	95.26±2.63	91.03±0.76	86.39±1.71	85.78±1.50	82.45±1.16	80.81±2.05
compound **3**	Concentration (μM)	0	3.125	6.25	12.5	25	50	100
	Cell viability (%)	100.00±1.78	102.22±1.63	103.75±1.42	95.39±2.79	88.82±2.45	85.05±0.68	83.02±1.65
compound **4**	Concentration (μM)	0	3.125	6.25	12.5	25	50	100
	Cell viability (%)	100.02±1.96	93.33±2.07	86.76±0.91	87.03±1.35	85.84±2.18	81.01±0.32	78.78±2.71
compound **5**	Concentration (μM)	0	3.125	6.25	12.5	25	50	100
	Cell viability (%)	99.98±1.39	103.32±1.71	100.92±2.65	96.31±0.71	90.13±1.93	86.90±0.94	81.16±1.16
compound **6**	Concentration (μM)	0	3.125	6.25	12.5	25	50	100
	Cell viability (%)	100.00±2.13	96.51±2.30	94.55±2.77	93.19±2.12	86.55±1.81	85.55±2.67	81.85±2.11
compound **7**	Concentration (μM)	0	3.125	6.25	12.5	25	50	100
	Cell viability (%)	100.02±2.45	102.44±2.62	100.58±1.93	94.72±1.35	94.02±2.04	87.85±2.88	84.81±0.76
compound **8**	Concentration (μM)	0	3.125	6.25	12.5	25	50	100
	Cell viability (%)	100.02±2.40	96.03±2.16	92.41±1.40	90.33±2.29	84.60±1.48	82.16±1.45	79.27±2.36
compound **9**	Concentration (μM)）	0	3.125	6.25	12.5	25	50	100
	Cell viability (%)	100.00±2.58	94.30±2.28	95.85±2.82	91.29±2.80	88.27±1.58	84.30±2.88	81.97±2.14
compound **10**	Concentration (μM)）	0	3.125	6.25	12.5	25	50	100
	Cell viability (%)	100.02±1.14	103.57±2.36	97.67±2.51	92.16±0.44	87.30±1.45	85.34±2.33	82.00±0.52
compound **11**	Concentration (μM)	0	3.125	6.25	12.5	25	50	100
	Cell viability (%)	99.98±2.39	97.48±0.79	97.25±2.54	92.15±1.87	85.52±2.45	82.67±2.30	80.13±1.24
compound **12**	Concentration (μM)	0	3.125	6.25	12.5	25	50	100
	Cell viability (%)	100.02±2.70	104.10±2.68	98.26±2.57	94.48±2.33	92.43±1.85	85.94±2.69	81.85±2.69
compound **13**	Concentration (μM)	0	3.125	6.25	12.5	25	50	100
	Cell viability (%)	99.98±1.74	95.29±1.57	93.67±0.81	87.37±2.45	82.90±1.37	81.02±1.81	75.17±2.22
compound **14**	Concentration (μM)	0	3.125	6.25	12.5	25	50	100
	Cell viability (%)	100.00±2.43	99.46±1.91	91.36±2.71	91.43±0.79	87.29±2.87	86.88±1.97	84.38±0.40

Table 6S. Inhibition of NO production in LPS-induced RAW264.7 macrophages.

compound **1a**	Concentration (μM)	3.125	6.25	12.5	25	50
	Inhibition (%)	8.37±1.07	19.09±1.77	35.10±1.41	54.86±2.59	71.67±1.96
	IC_{50} (μM)	21.7±1.7				
compound **2**	Concentration (μM)	3.125	6.25	12.5	25	50
	Inhibition (%)	9.99±1.98	23.04±3.50	48.36±3.26	74.69±2.33	85.81±1.70
	IC_{50} (μM)	13.2±1.3				
compound **5**	Concentration (μM)	3.125	6.25	12.5	25	50
	Inhibition (%)	19.45±3.95	35.95±4.17	55.14±4.20	76.20±4.13	89.48±3.86
	IC_{50} (μM)	10.1±1.8				
compound **7**	Concentration (μM)	3.125	6.25	12.5	25	50
	Inhibition (%)	10.38±3.23	20.37±3.20	42.46±2.76	65.31±2.96	80.22±2.99
	IC_{50} (μM)	16.2±2.0				
compound **9**	Concentration (μM)	3.125	6.25	12.5	25	50
	Inhibition (%)	7.70±0.94	16.02±1.96	26.07±1.85	44.50±2.38	57.92±1.15
	IC_{50} (μM)	34.2±2.3				
compound **10**	Concentration (μM)	3.125	6.25	12.5	25	50
	Inhibition (%)	6.80±0.18	13.60±2.51	22.93±0.98	36.51±1.17	55.20±1.32
	IC_{50} (μM)	41.7±2.1				
compound **11**	Concentration (μM)	3.125	6.25	12.5	25	50
	Inhibition (%)	18.90±4.19	35.50±4.39	55.63±4.42	75.79±4.27	89.29±4.46
	IC_{50} (μM)	10.3±1.9				
compound **quercetin**	Concentration (μM)	3.125	6.25	12.5	25	50
	Inhibition (%)	9.86±2.27	21.36±2.40	39.05±2.48	68.11±3.26	82.04±0.51
	IC_{50} (μM)	15.9±1.2				

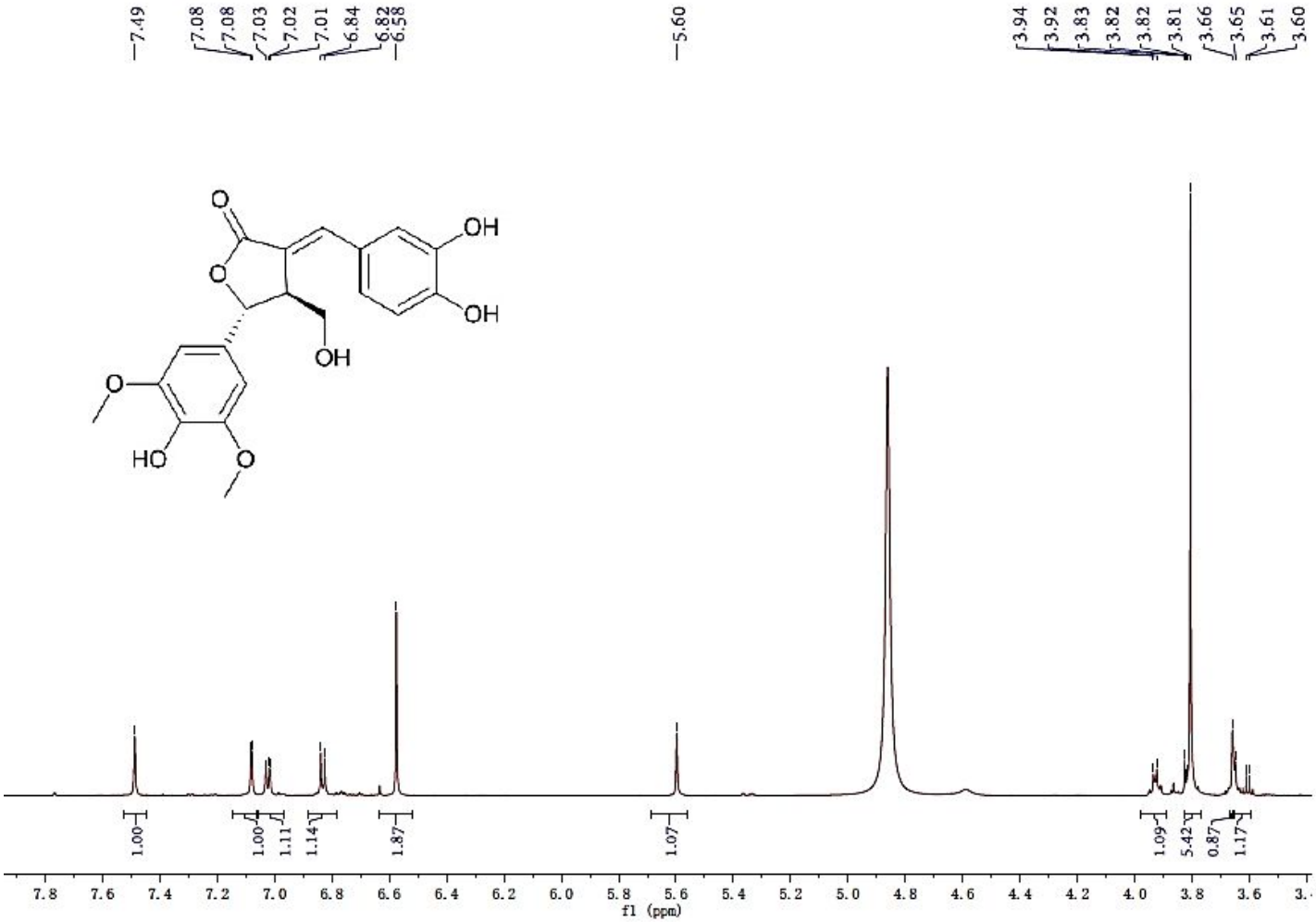

Figure 1S. ^{1}H NMR spectrum of compound 1 (1a/1b) in CD_3OD

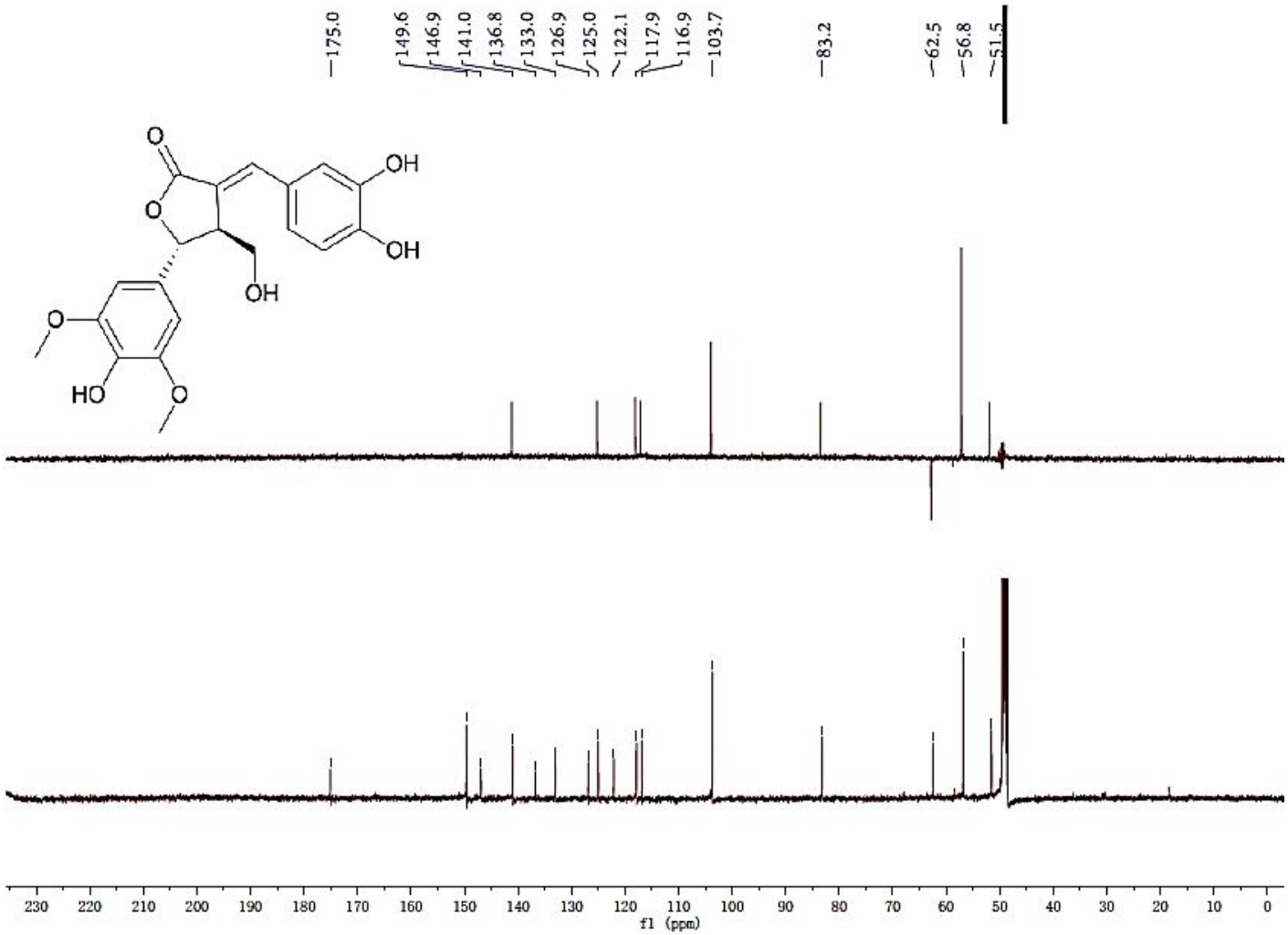

Figure 2S. ^{13}C NMR spectrum of compound 1 (1a/1b) in CD_3OD

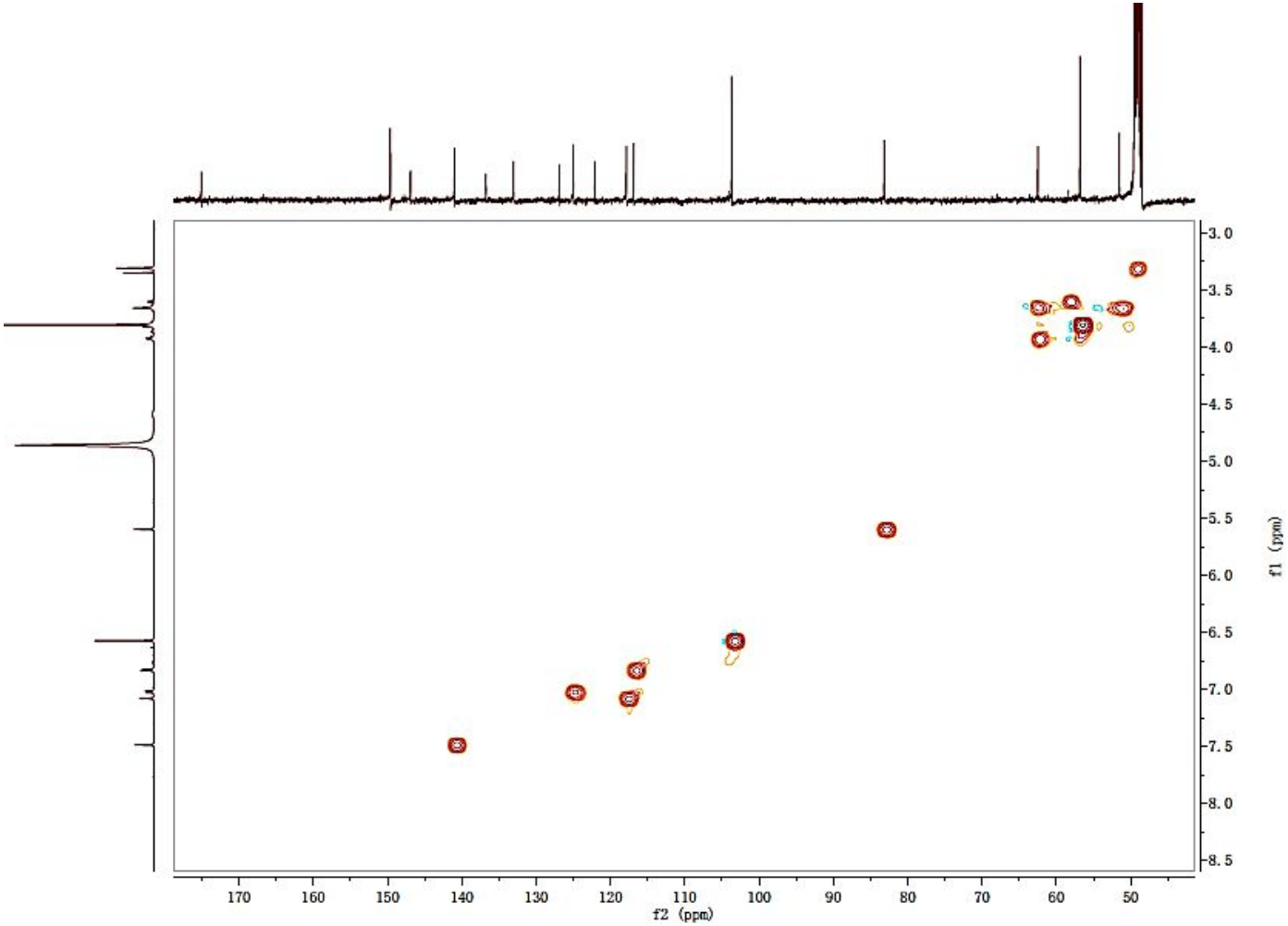

Figure 3S. HSQC spectrum of compound 1 (1a/1b) in CD_3OD

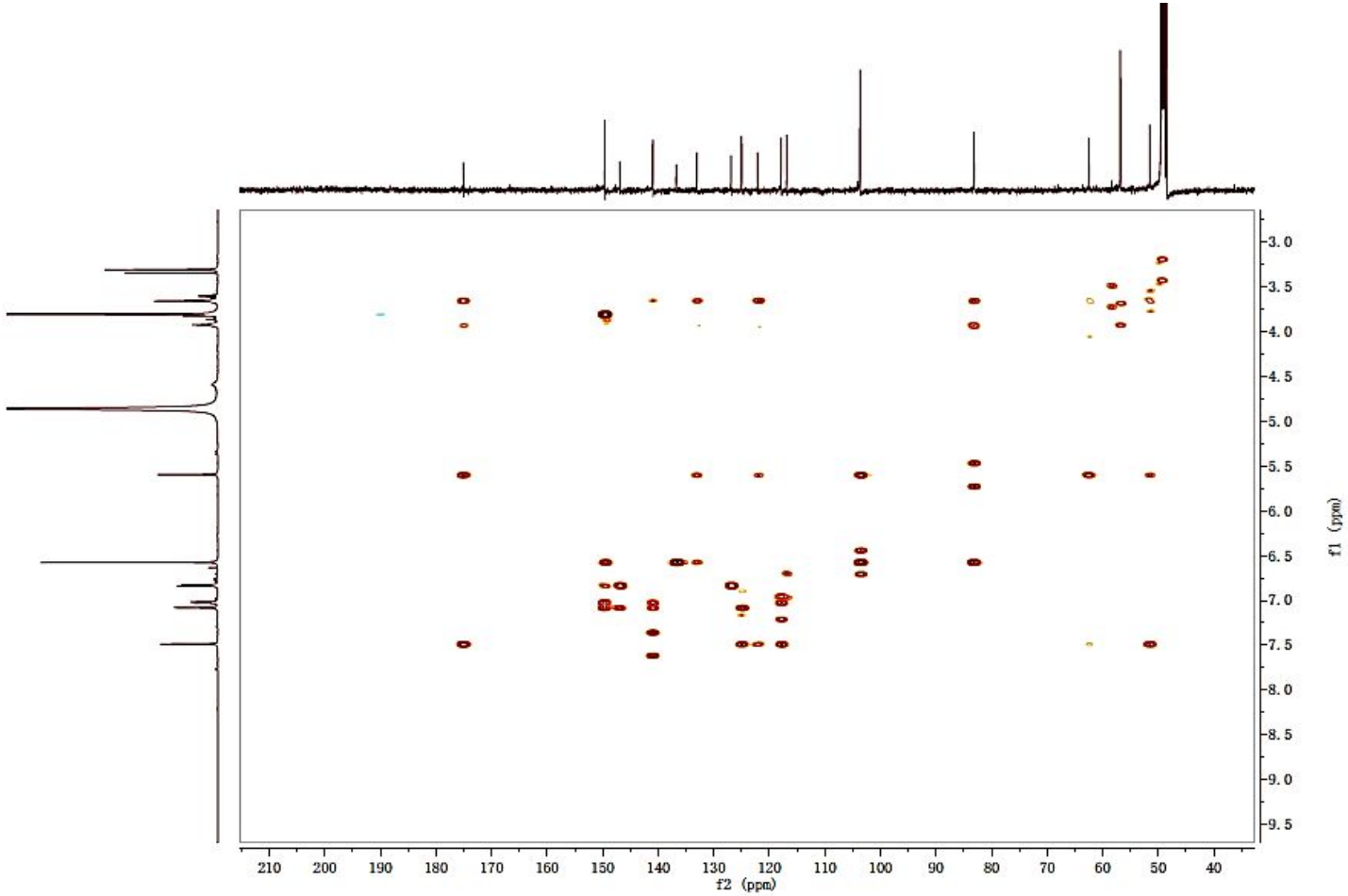

Figure 4S. HMBC spectrum of compound 1 (1a/1b) in CD_3OD

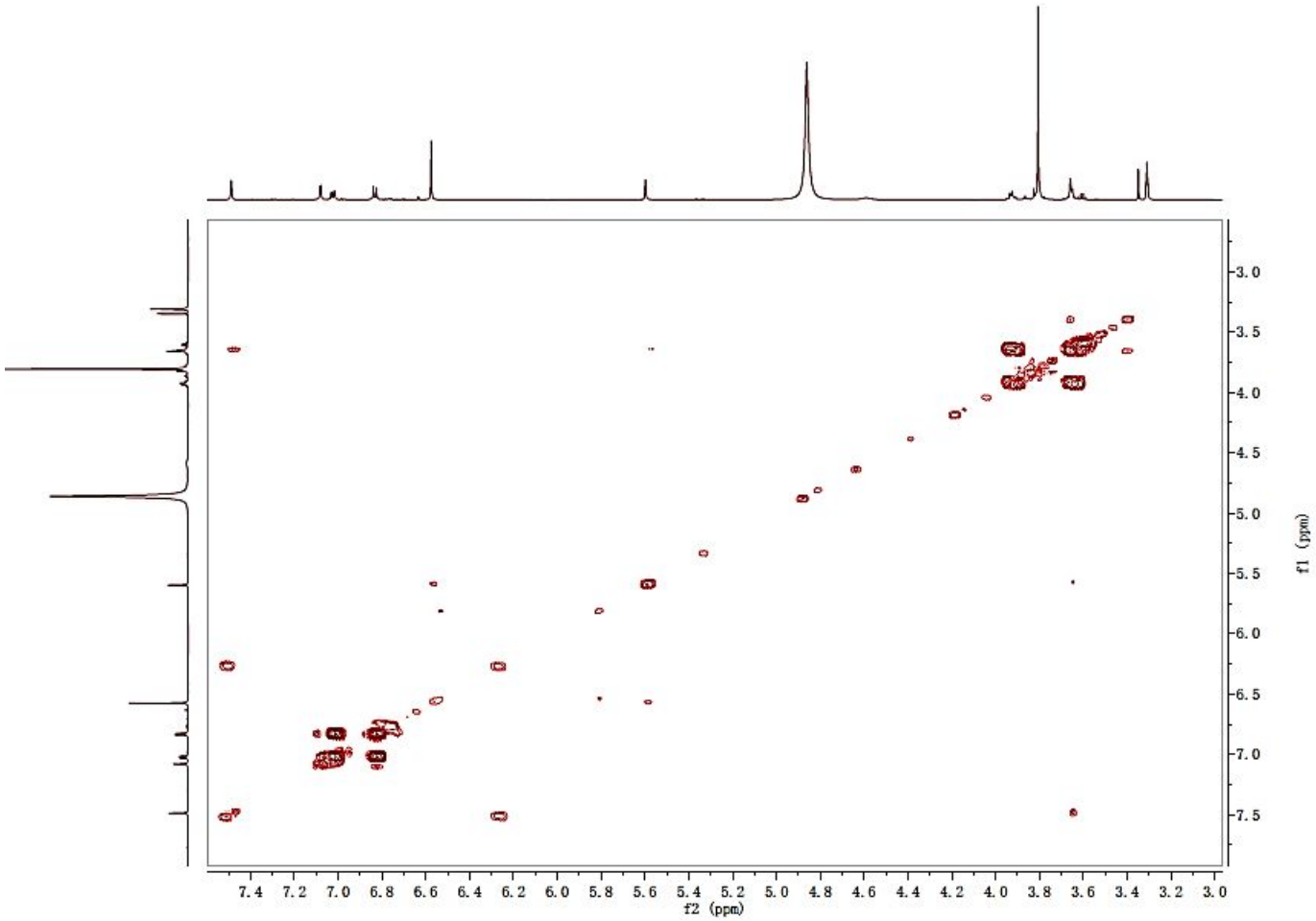

Figure 5S. $^{1}H–^{1}H$ COSY spectrum of compound 1 (1a/1b) in CD_3OD

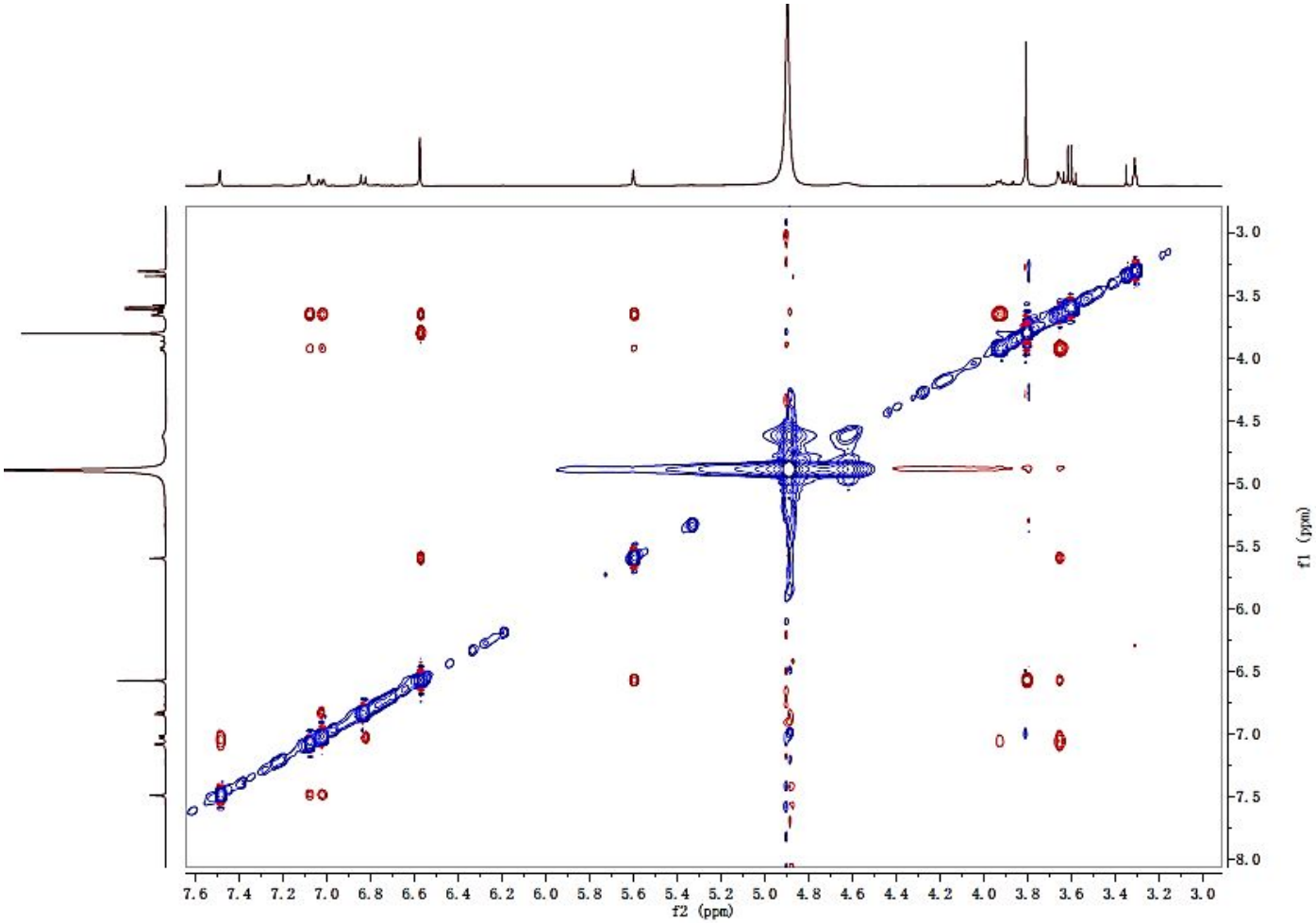

Figure 6S. ROESY spectrum of compound 1 (1a/1b) in CD_3OD

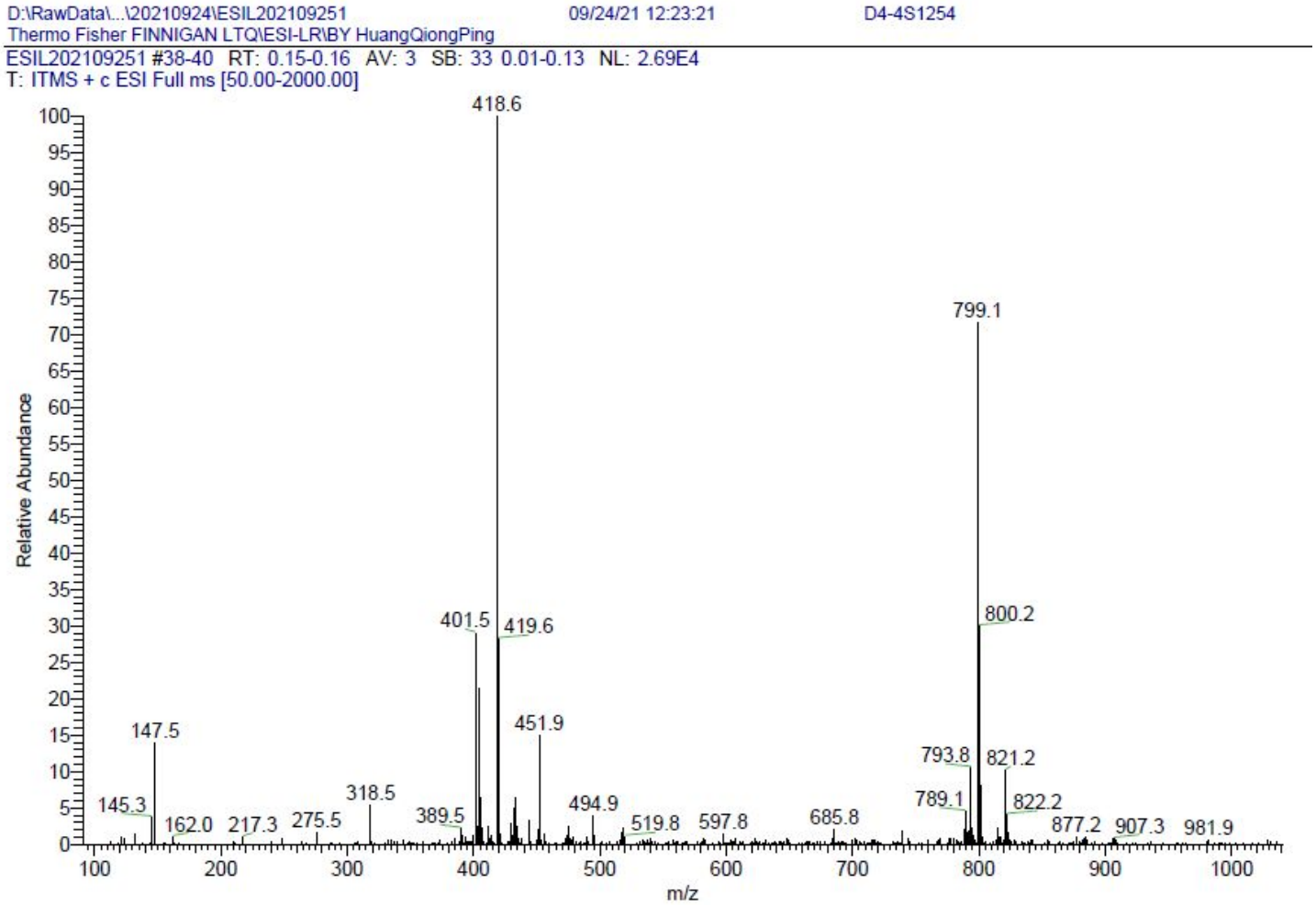

Figure 7S. (+)-ESIMS spectrum of compound 1 (1a/1b)

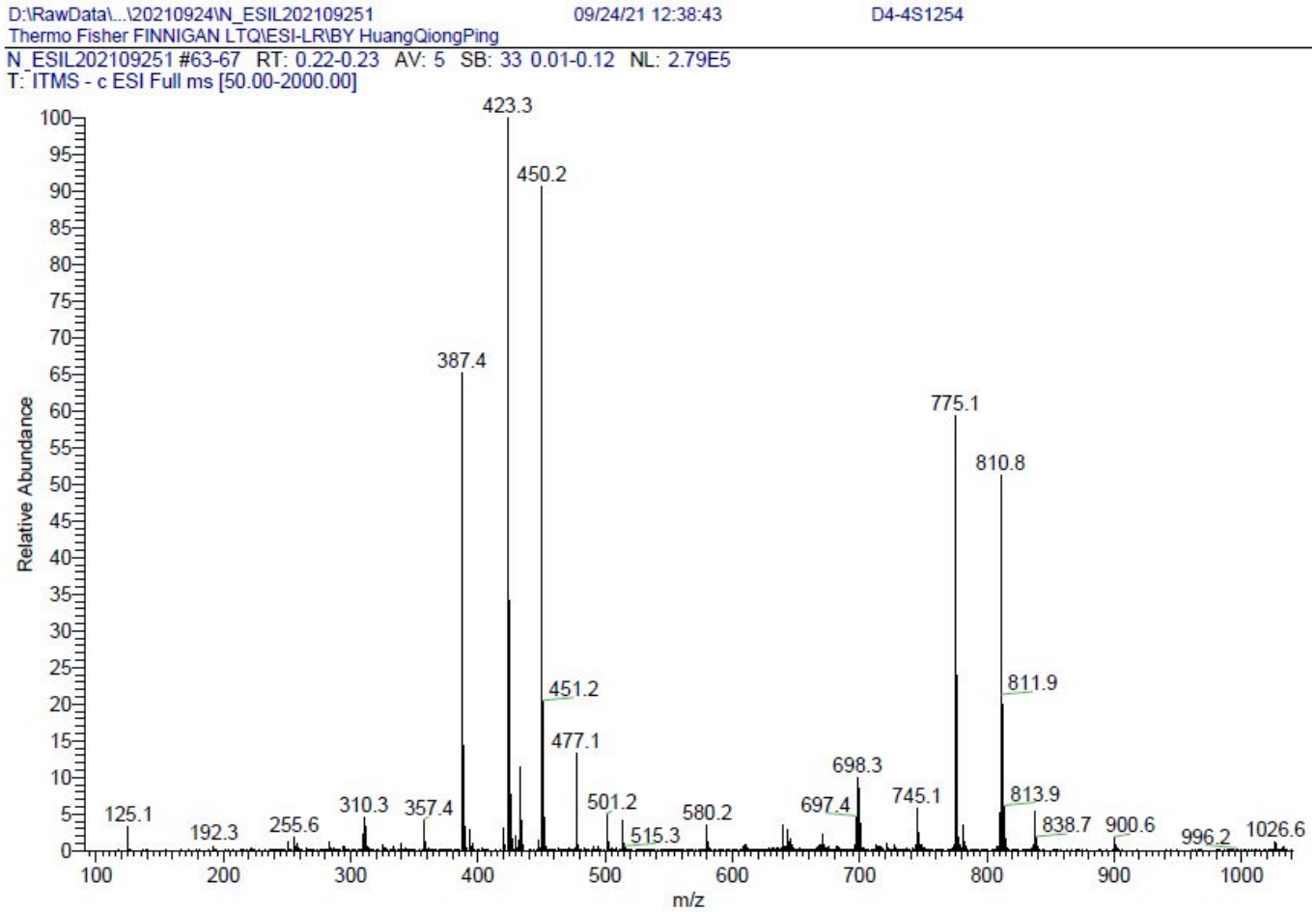

Figure 8S. (-)-ESIMS spectrum of compound 1 (1a/1b)

Qualitative Analysis Report

Data Filename	ESIH202104403.d	**Sample Name**	D4-4S1254
Sample ID		**Position**	P1-B2
Instrument Name	Agilent G6520 Q-TOF	**Acq Method**	20160322_MS_ESIH_POS_1min.m
Acquired Time	9/24/2021 19:23:56	**IRM Calibration Status**	Success
DA Method	small molecular data analysis method.m	**Comment**	ESIH by zhuzhenyun

User Spectra

Fragmentor Voltage	Collision Energy	Ionization Mode
175	0	ESI

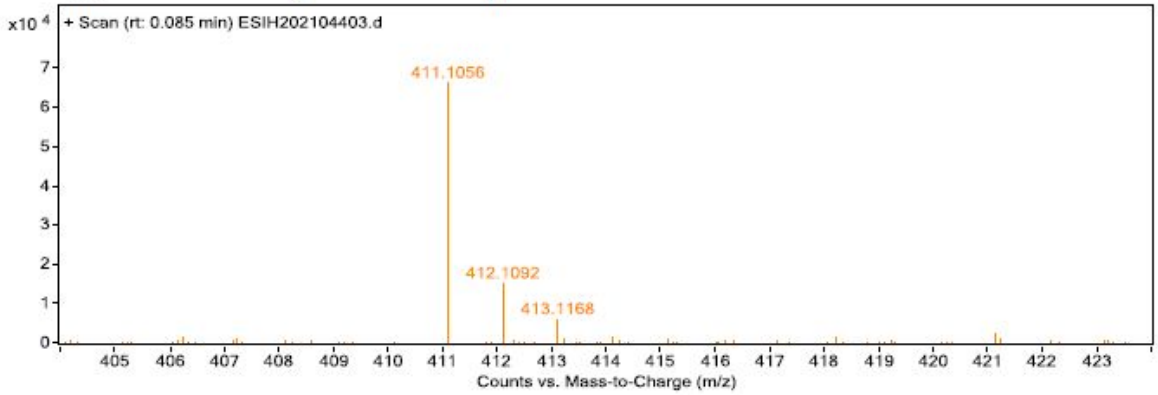

Formula Calculator Results

m/z	Calc m/z	Diff (mDa)	Diff (ppm)	Ion Formula	Ion
411.1056	411.105	-0.57	-1.39	C20 H20 Na O8	(M+Na)+

--- End Of Report ---

Agilent Technologies Page 1 of 1 Printed at: 19:26 on: 9/24/2021

Figure 9S. (+)-HRESIMS spectrum of compound 1 (1a/1b)

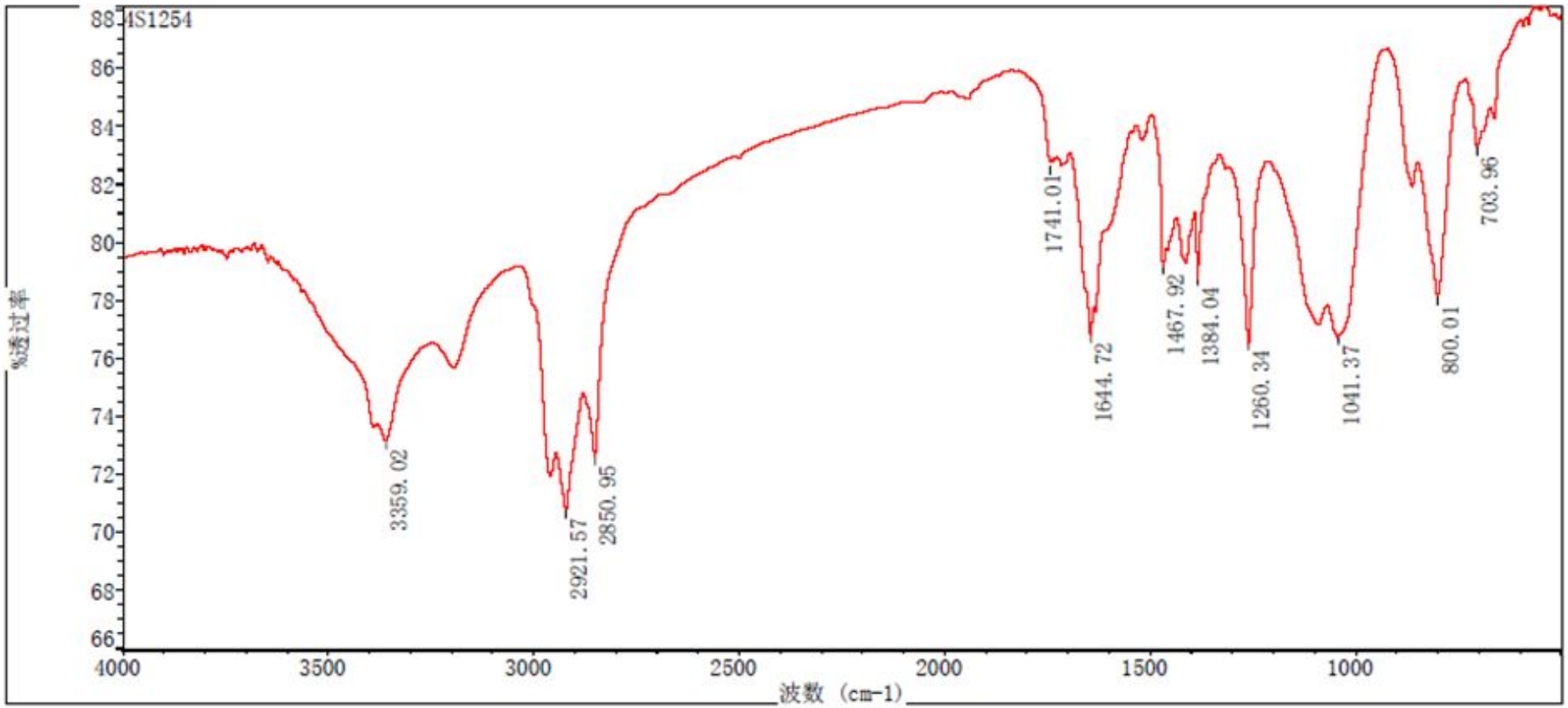

Figure 10S. IR spectrum of compound 1 (1a/1b)

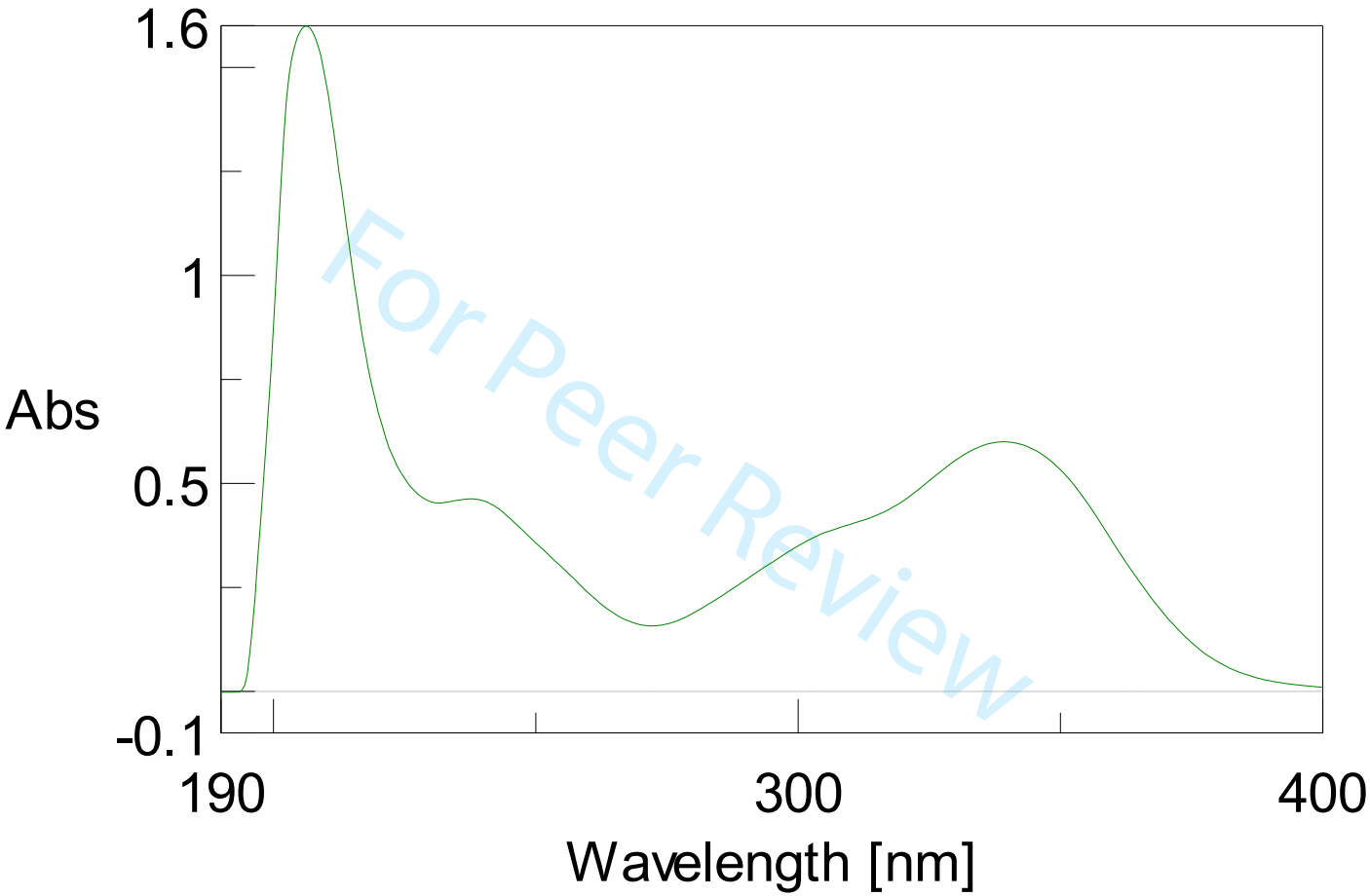

Figure 11S. UV spectrum of compound 1 (1a/1b)

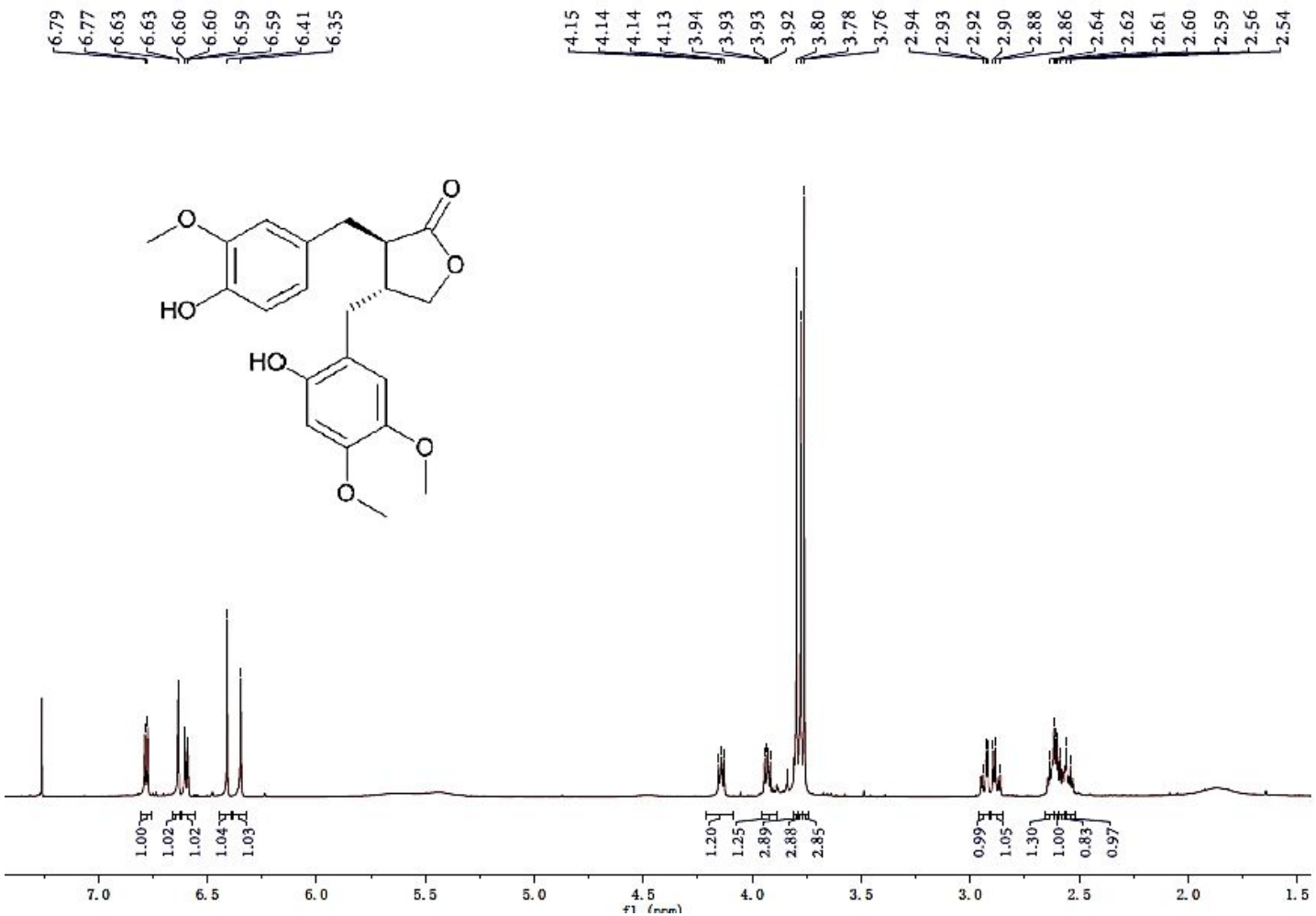

Figure 12S. ^{1}H NMR spectrum of compound 2 in $CDCl_3$

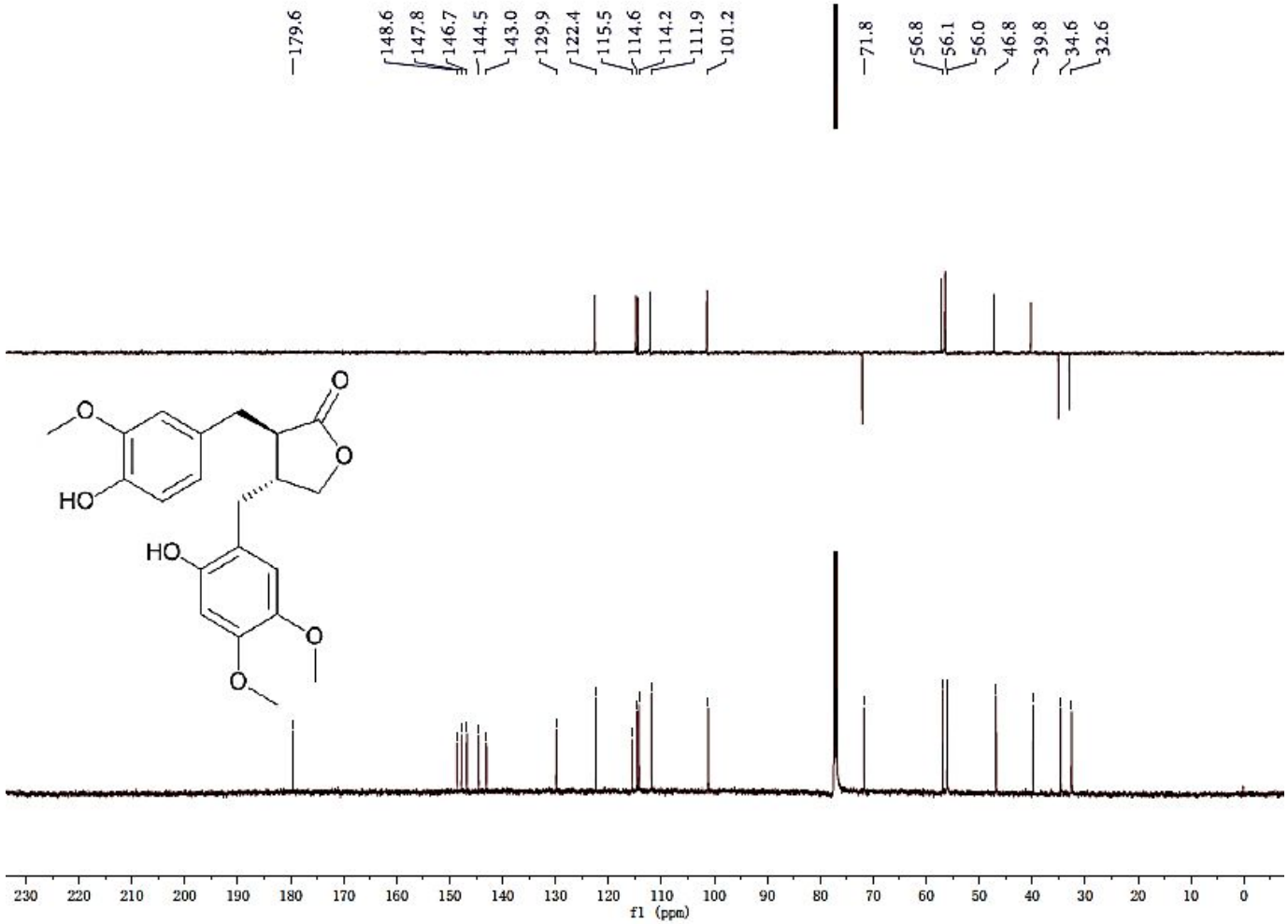

Figure 13S. ^{13}C NMR spectrum of compound 2 in $CDCl_3$

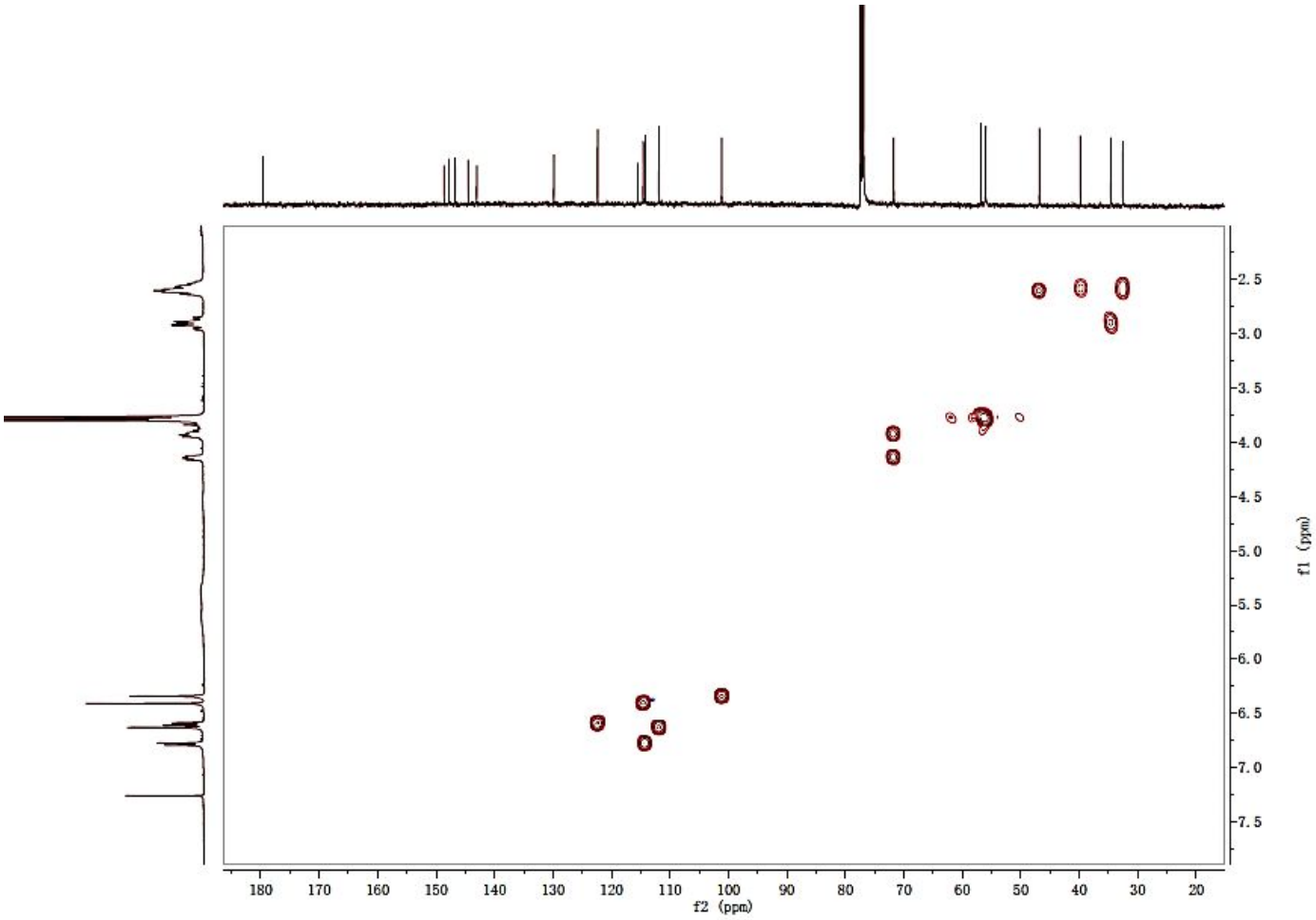

Figure 14S. HSQC spectrum of compound 2 in $CDCl_3$

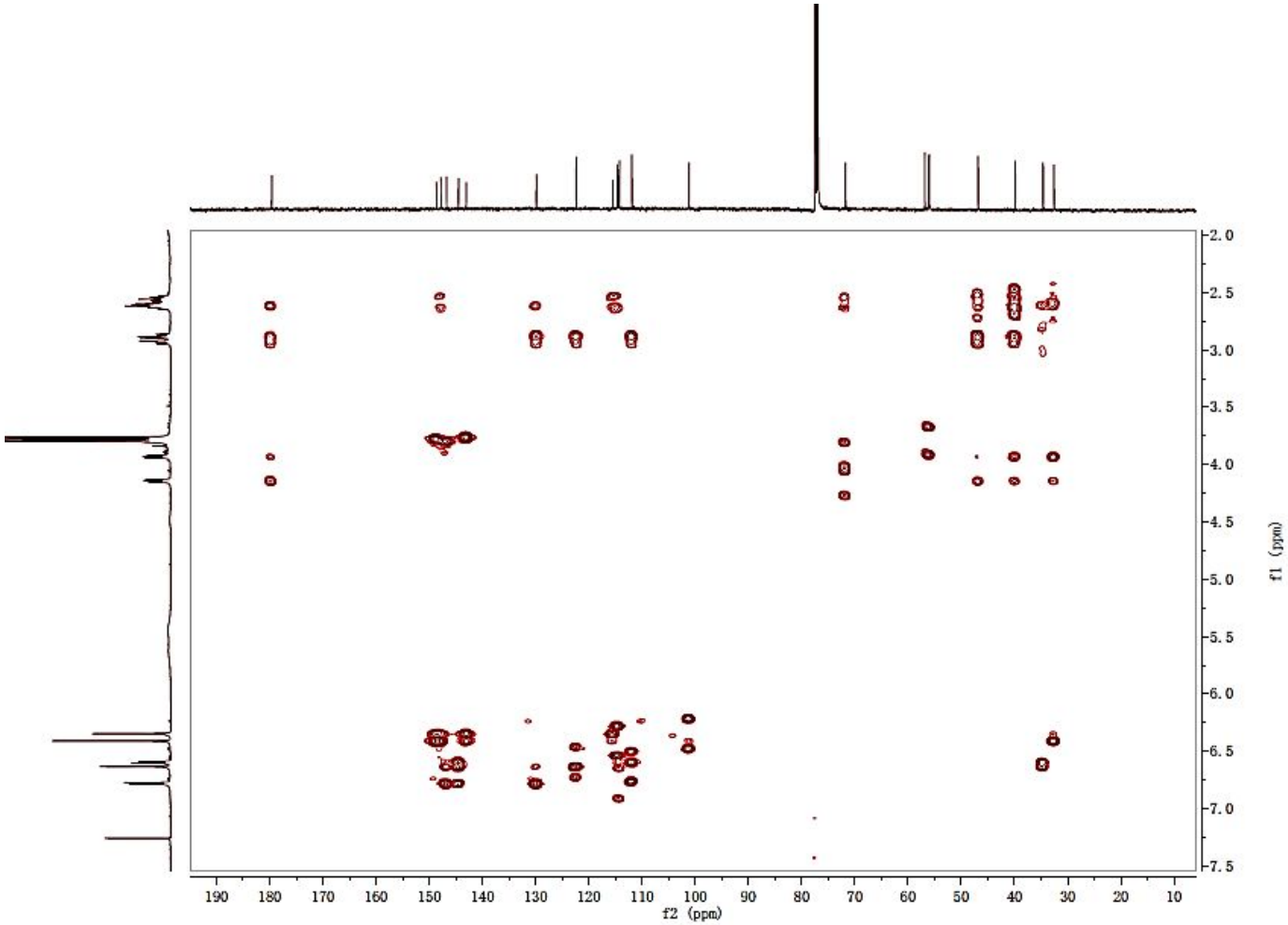

Figure 15S. HMBC spectrum of compound 2 in $CDCl_3$

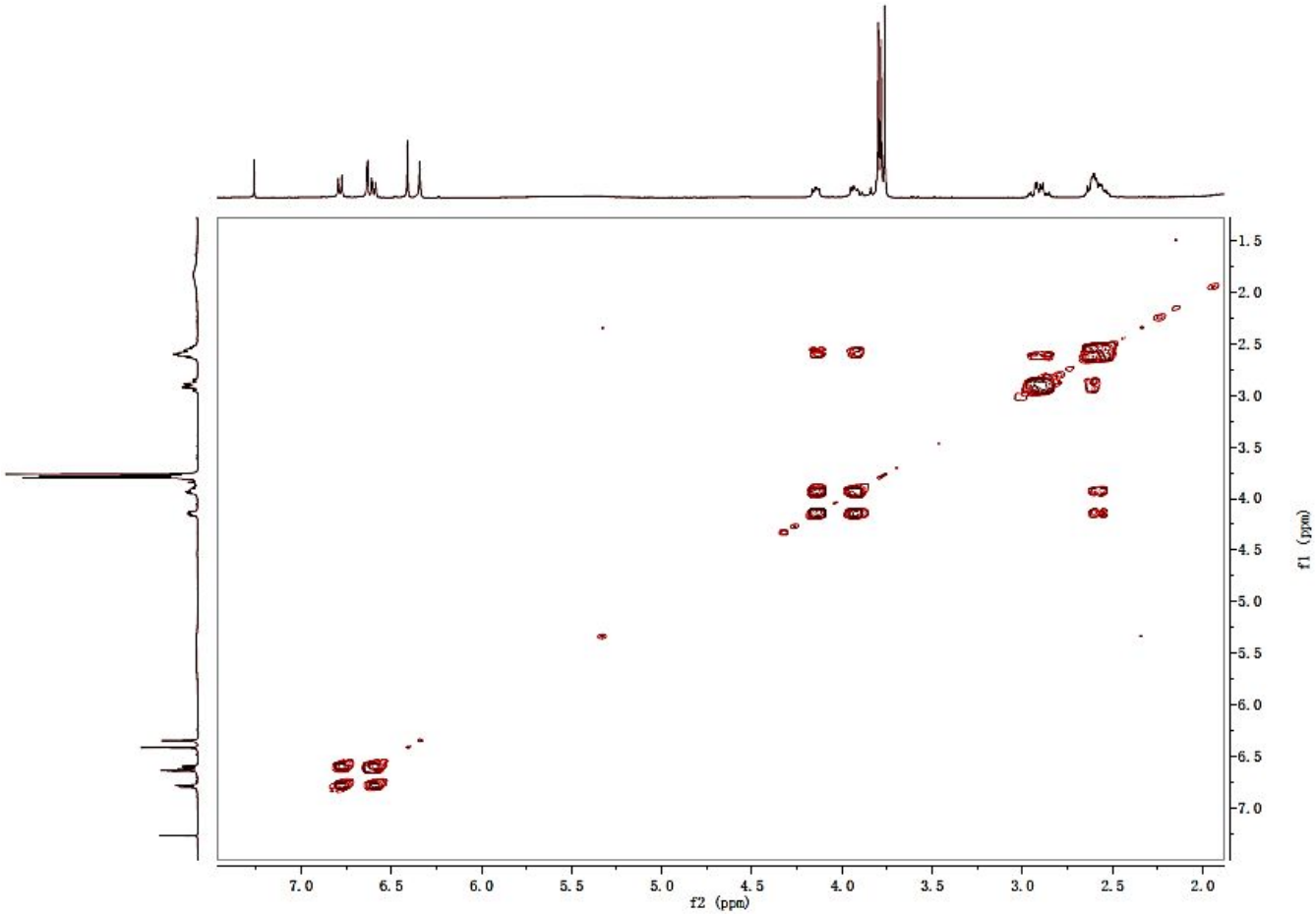

Figure 16S. $^{1}H–^{1}H$ COSY spectrum of compound 2 in $CDCl_3$

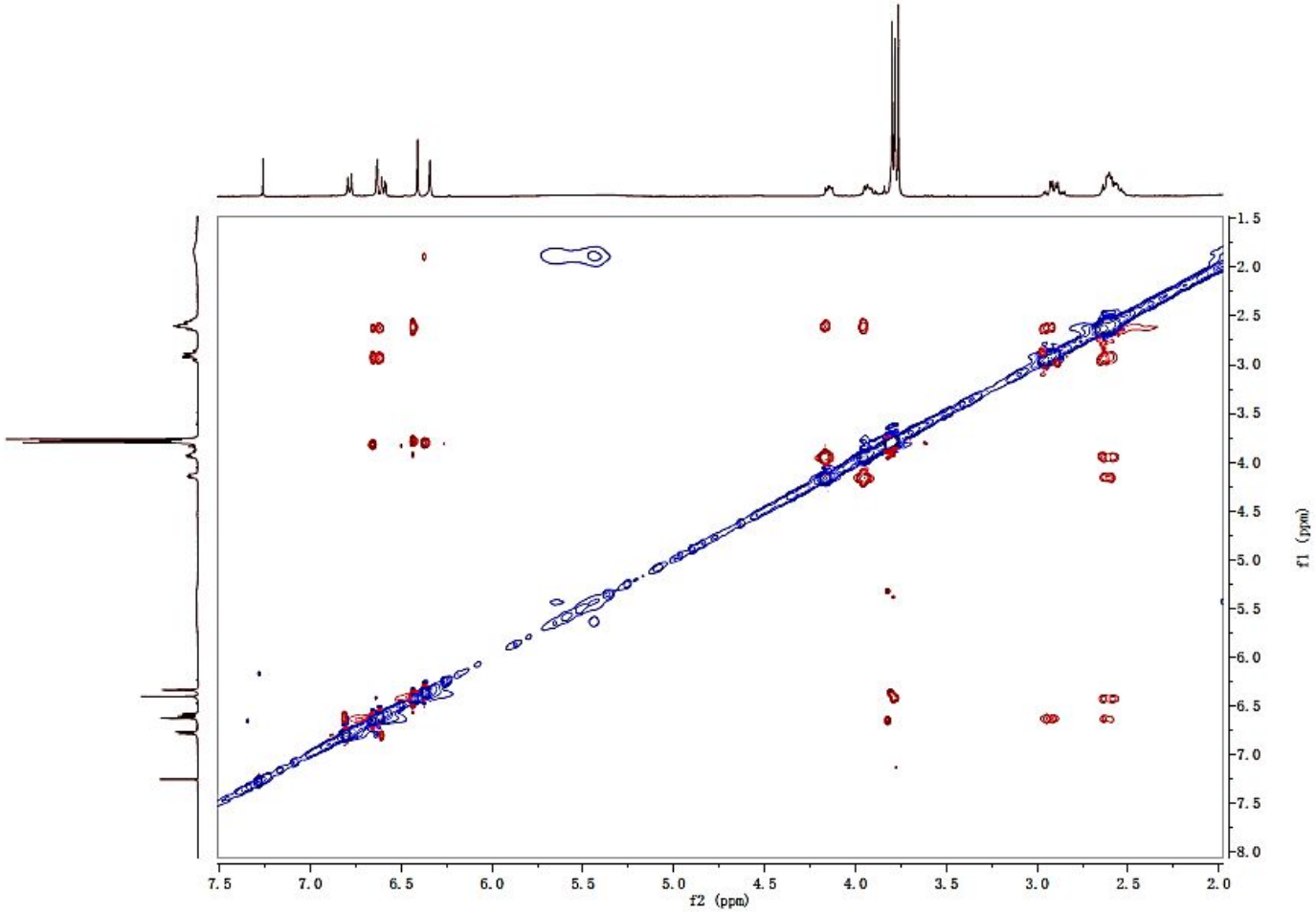

Figure 17S. ROESY spectrum of compound 2 in $CDCl_3$

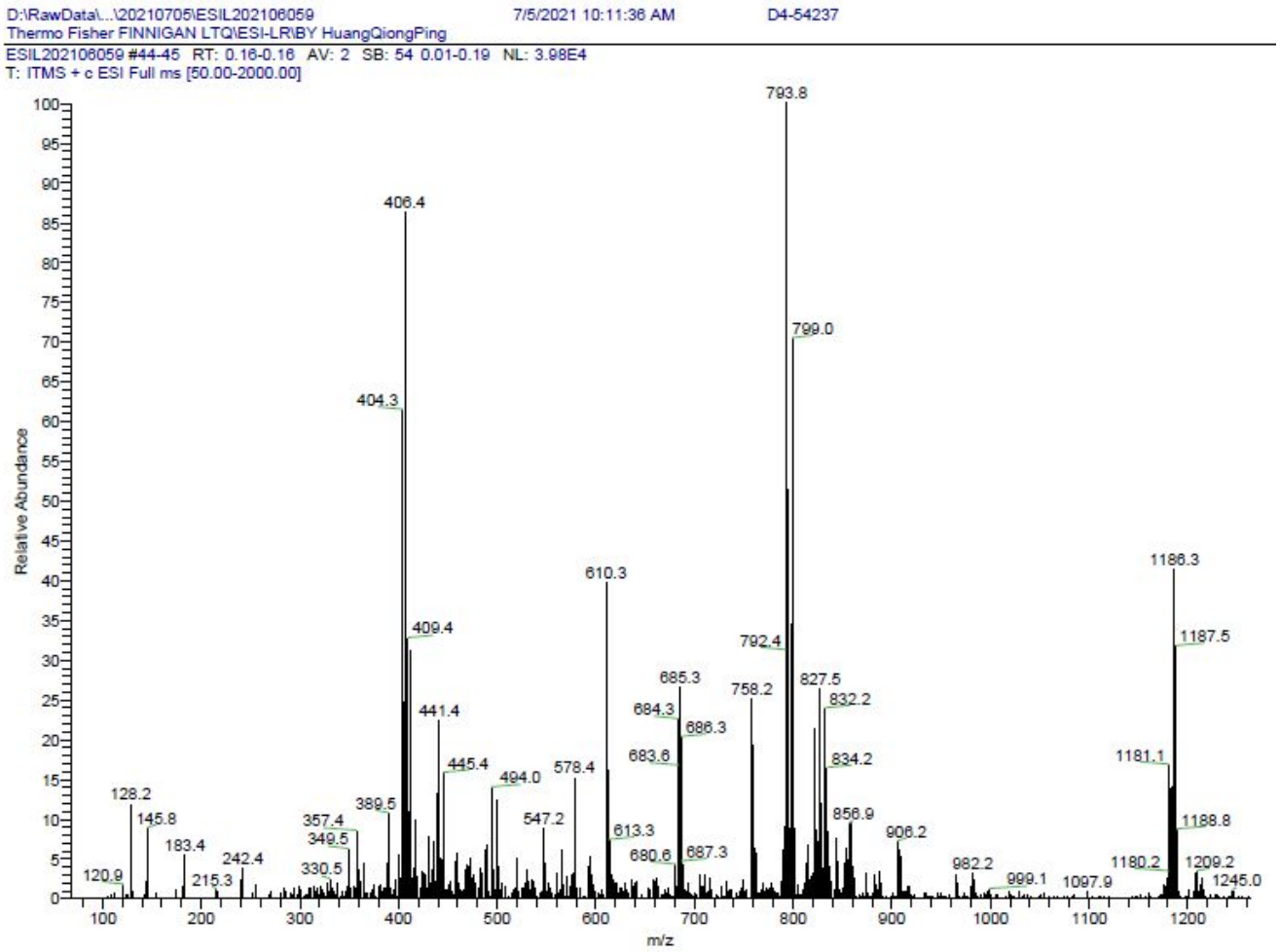

Figure 18S. (+)-ESIMS spectrum of compound 2

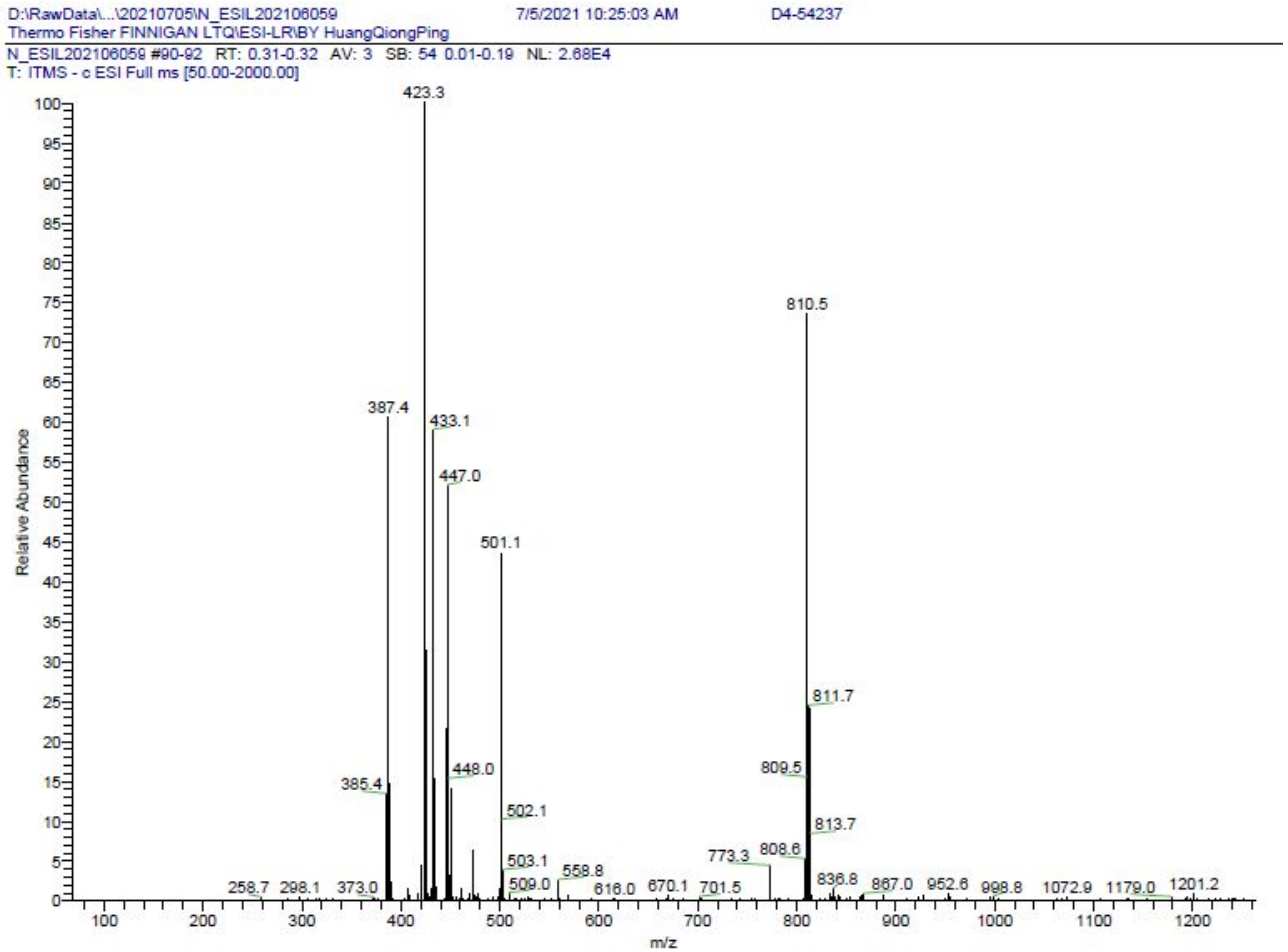

Figure 19S. (-)-ESIMS spectrum of compound 2

Qualitative Analysis Report

Data Filename	ESIH202103317.d	**Sample Name**	D4-54237
Sample ID		**Position**	P1-C6
Instrument Name	Agilent G6520 Q-TOF	**Acq Method**	20160322_MS_ESIH_POS_1min.m
Acquired Time	7/5/2021 20:50:58	**IRM Calibration Status**	Success
DA Method	small molecular data analysis method.m	**Comment**	ESIH by zhuzhenyun

User Spectra

Fragmentor Voltage	Collision Energy	Ionization Mode
135	0	ESI

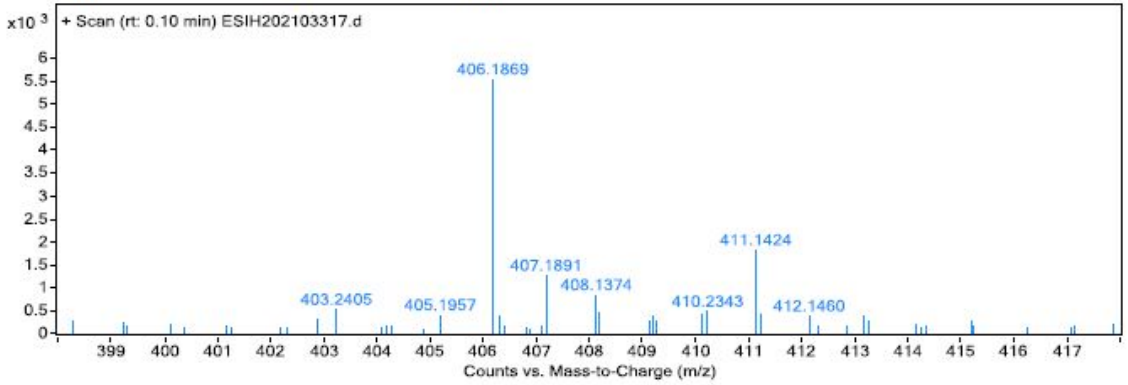

Formula Calculator Results

m/z	Calc m/z	Diff (mDa)	Diff (ppm)	Ion Formula	Ion
411.1424	411.1414	-1	-2.44	C21 H24 Na O7	(M+Na)+
406.1869	406.186	-0.84	-2.08	C21 H28 N O7	(M+NH4)+

--- End Of Report ---

Agilent Technologies Page 1 of 1 Printed at: 17:01 on: 7/6/2021

Figure 20S. (+)-HRESIMS spectrum of compound 2

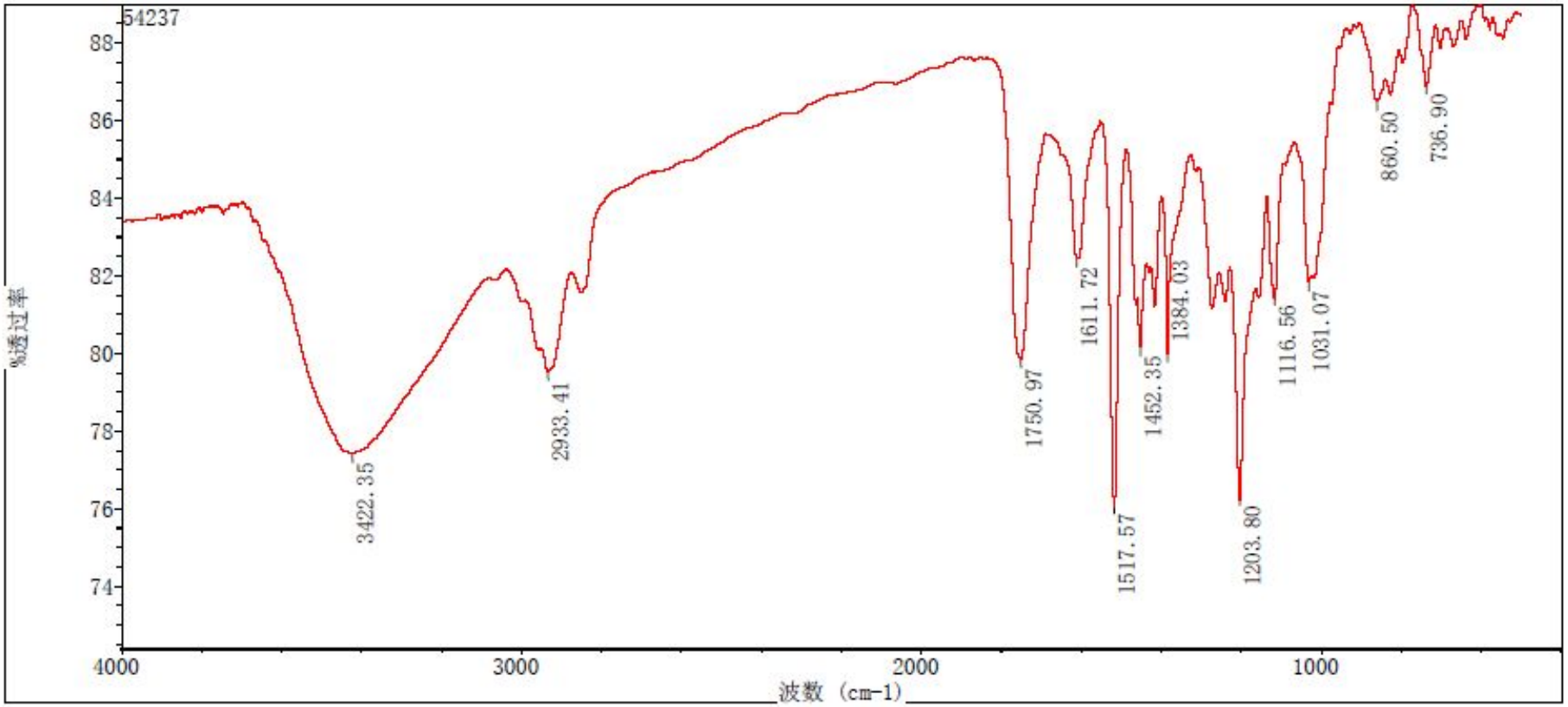

Figure 21S. IR spectrum of compound 2

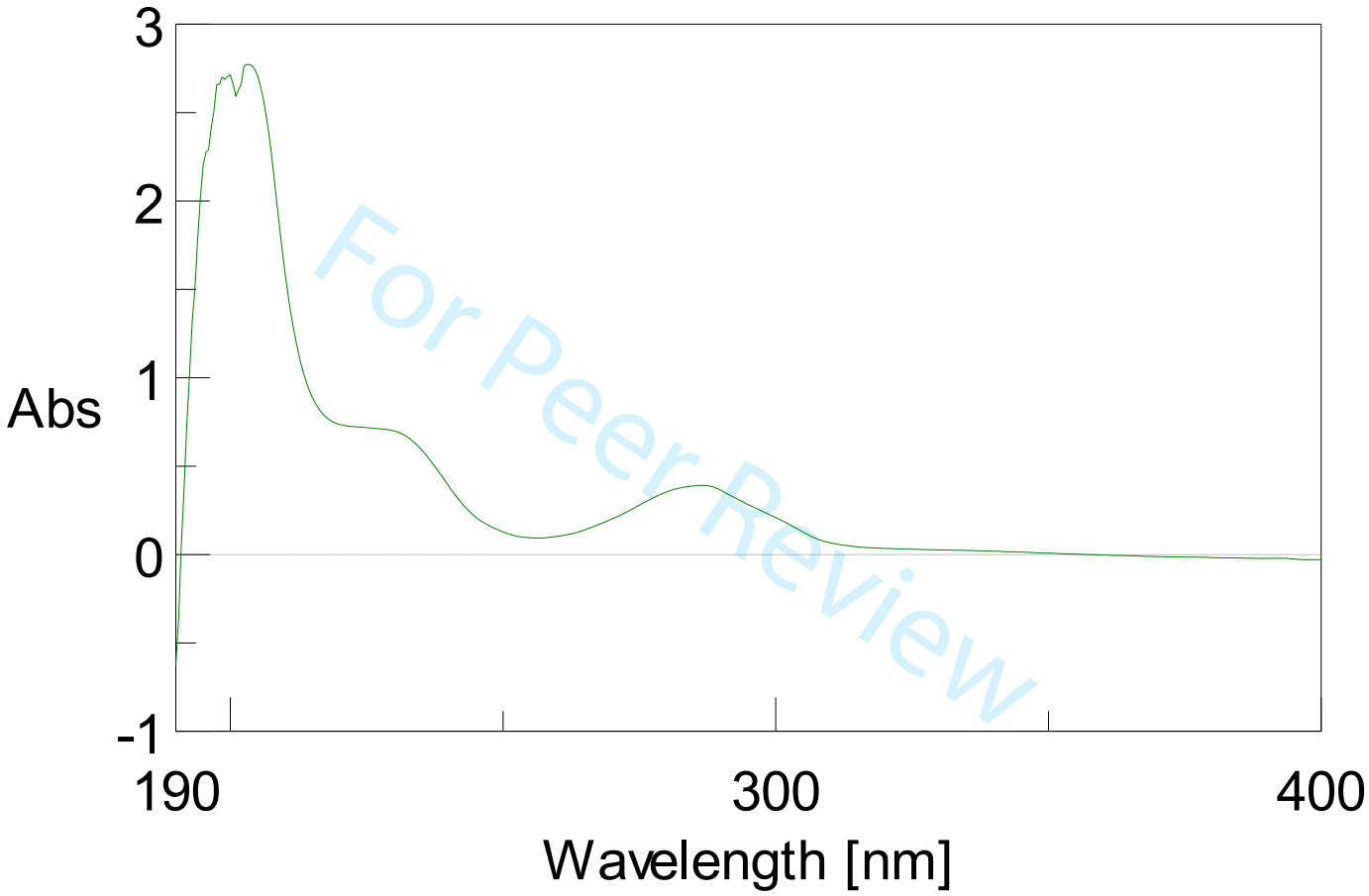

Figure 22S. UV spectrum of compound 2

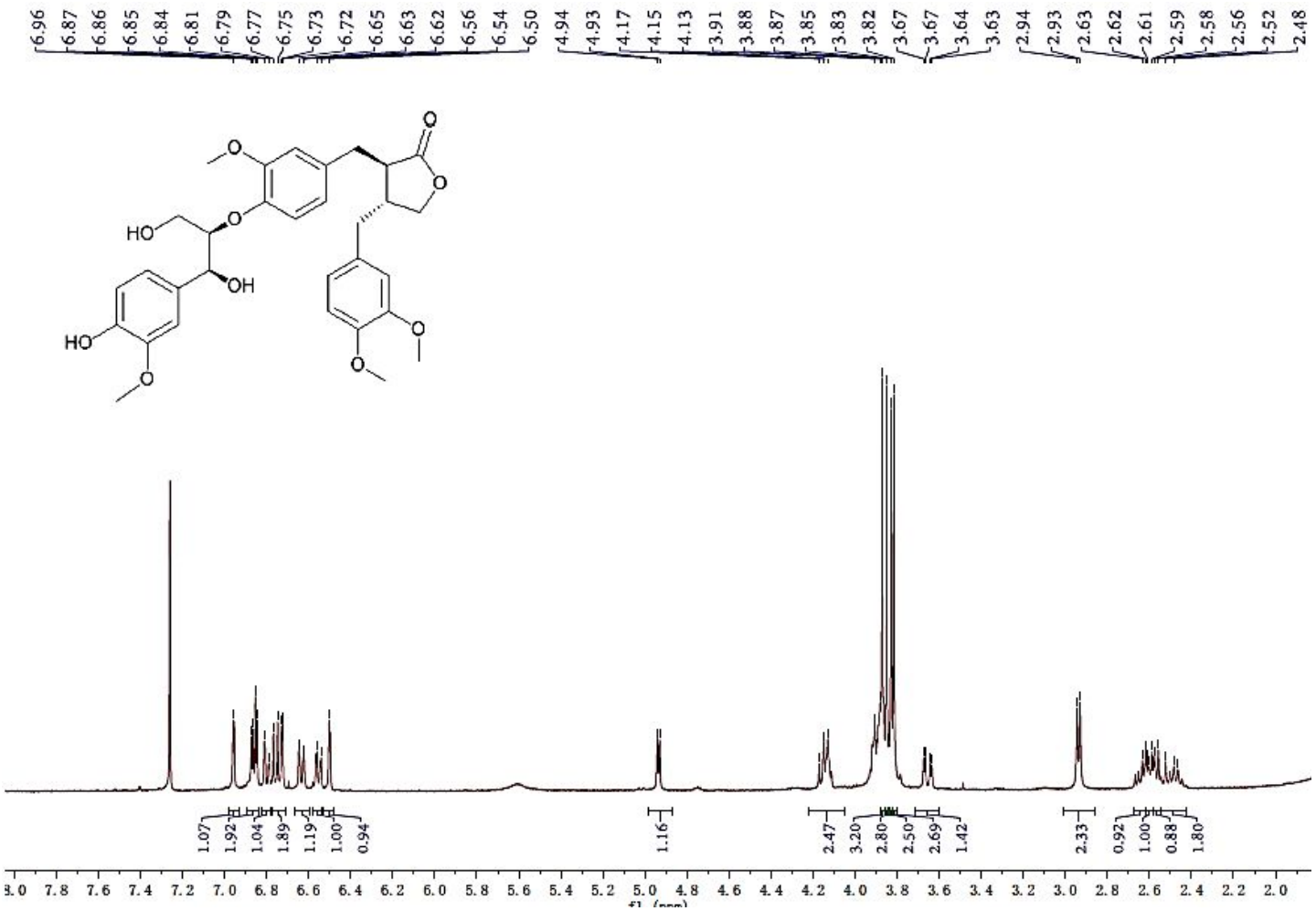

Figure 23S. ^{1}H NMR spectrum of compound 3 in $CDCl_3$

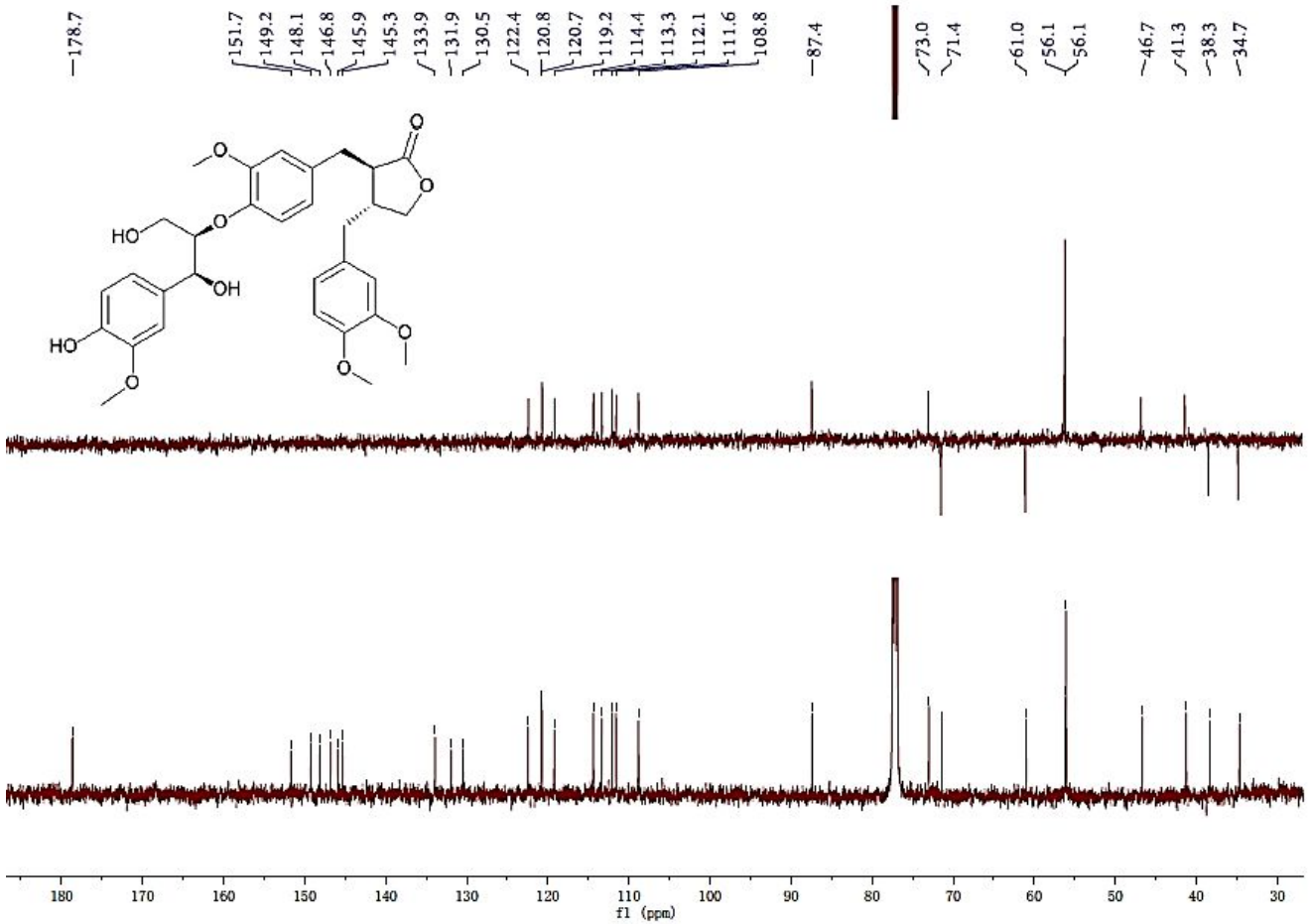

Figure 24S. ^{13}C NMR spectrum of compound 3 in $CDCl_3$

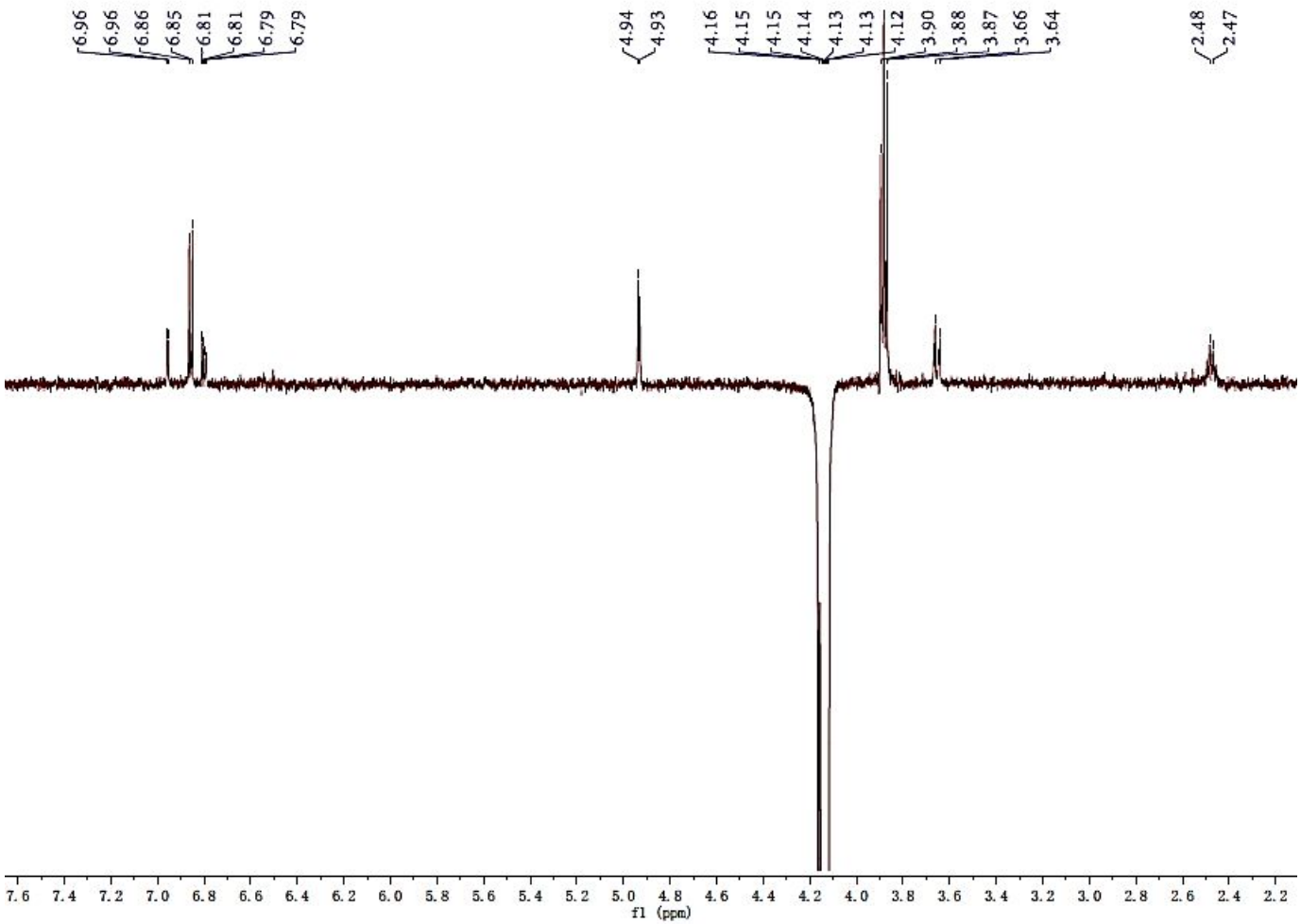

Figure 25S. NOE difference spectrum of compound 3 in $CDCl_3$

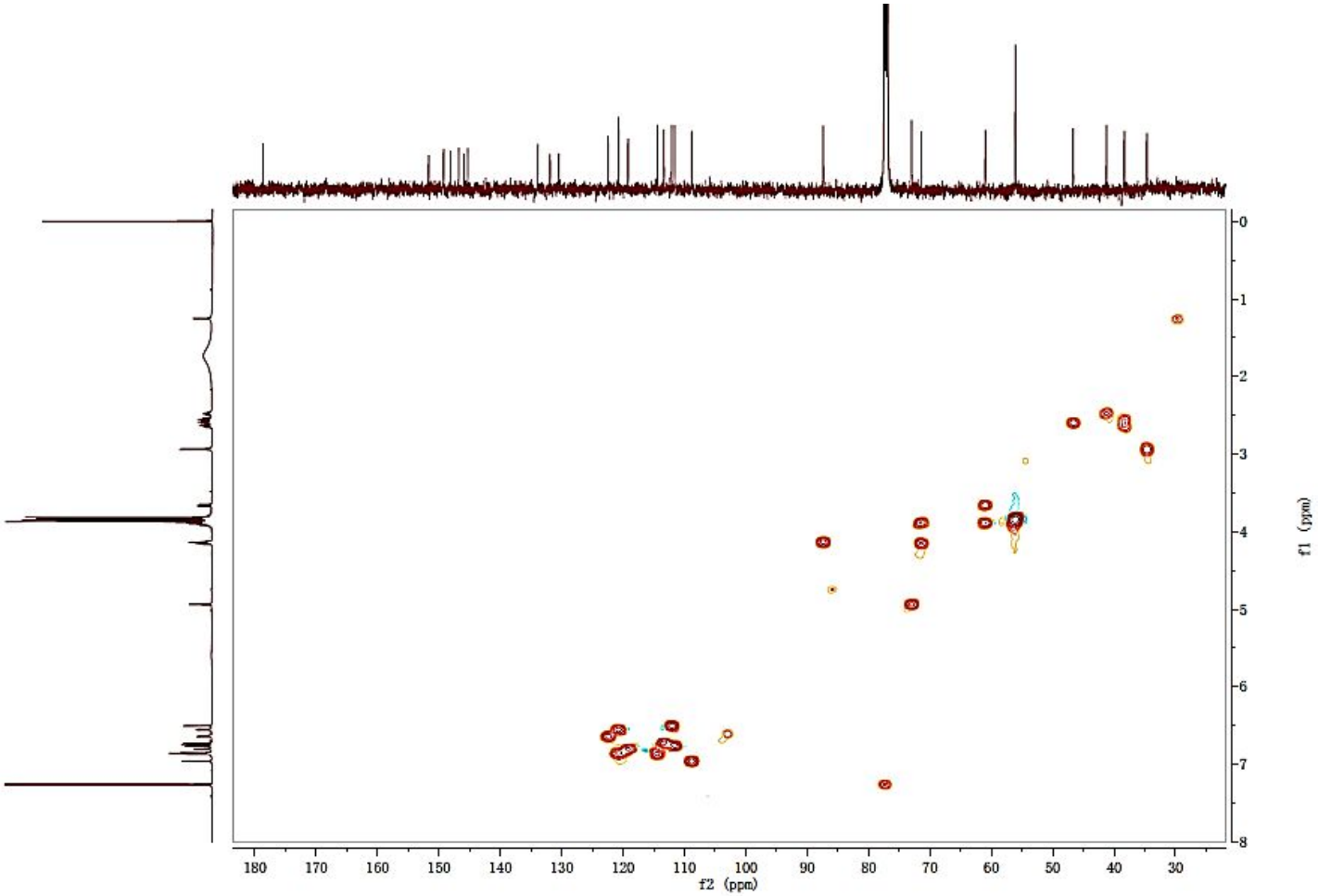

Figure 26S. HSQC spectrum of compound 3 in $CDCl_3$

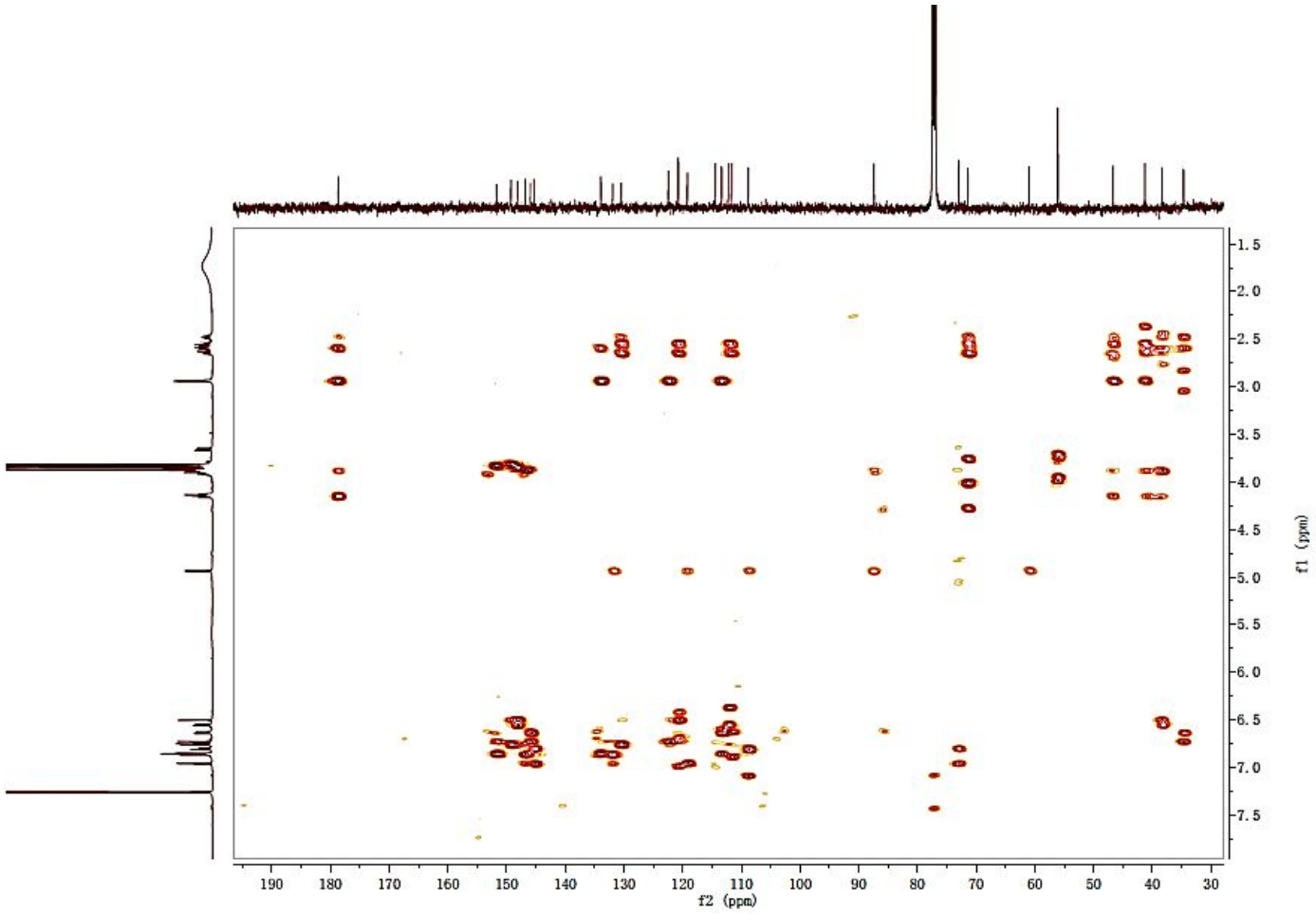

Figure 27S. HMBC spectrum of compound 3 in $CDCl_3$

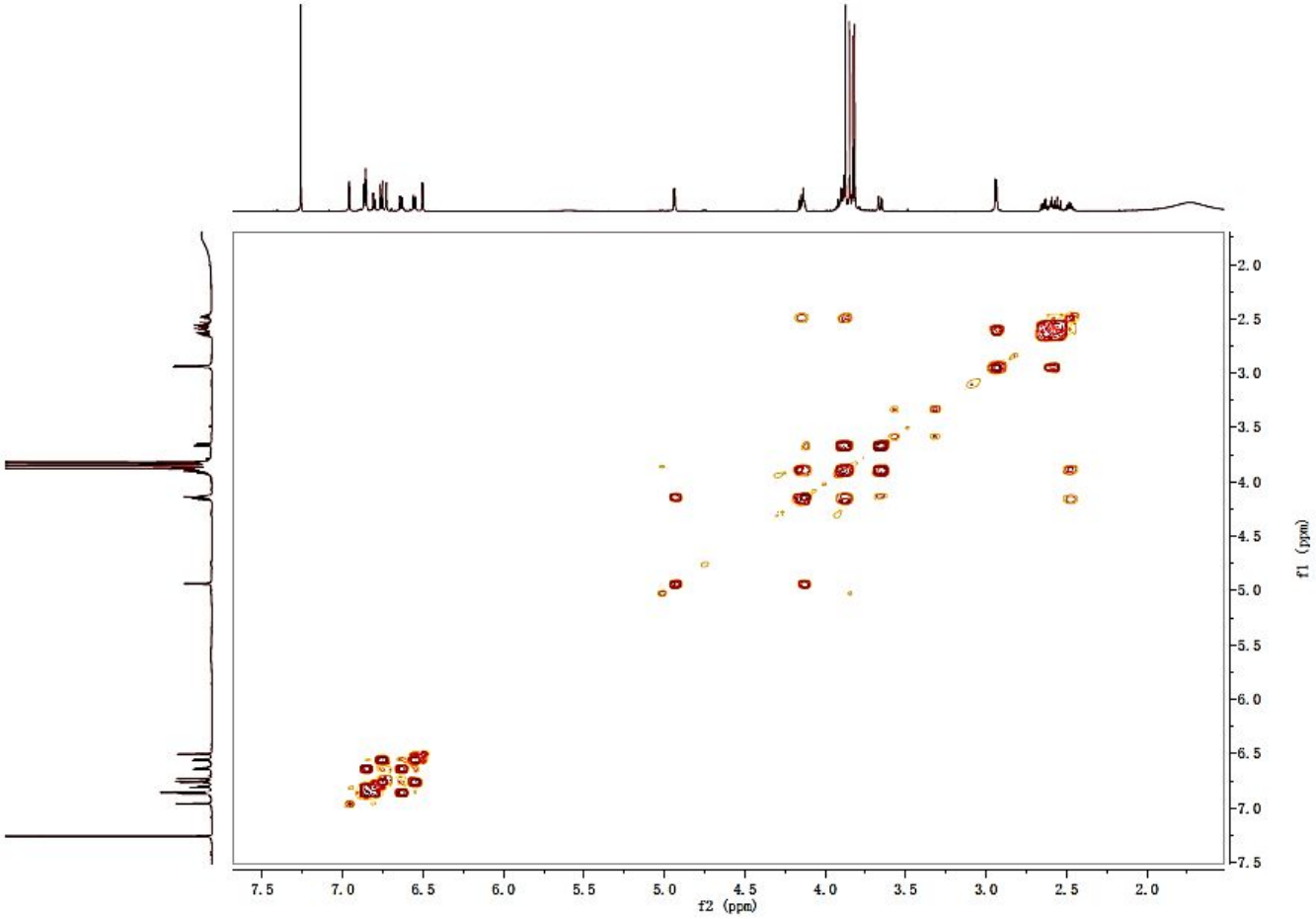

Figure 28S. $^{1}H–^{1}H$ COSY spectrum of compound 3 in $CDCl_3$

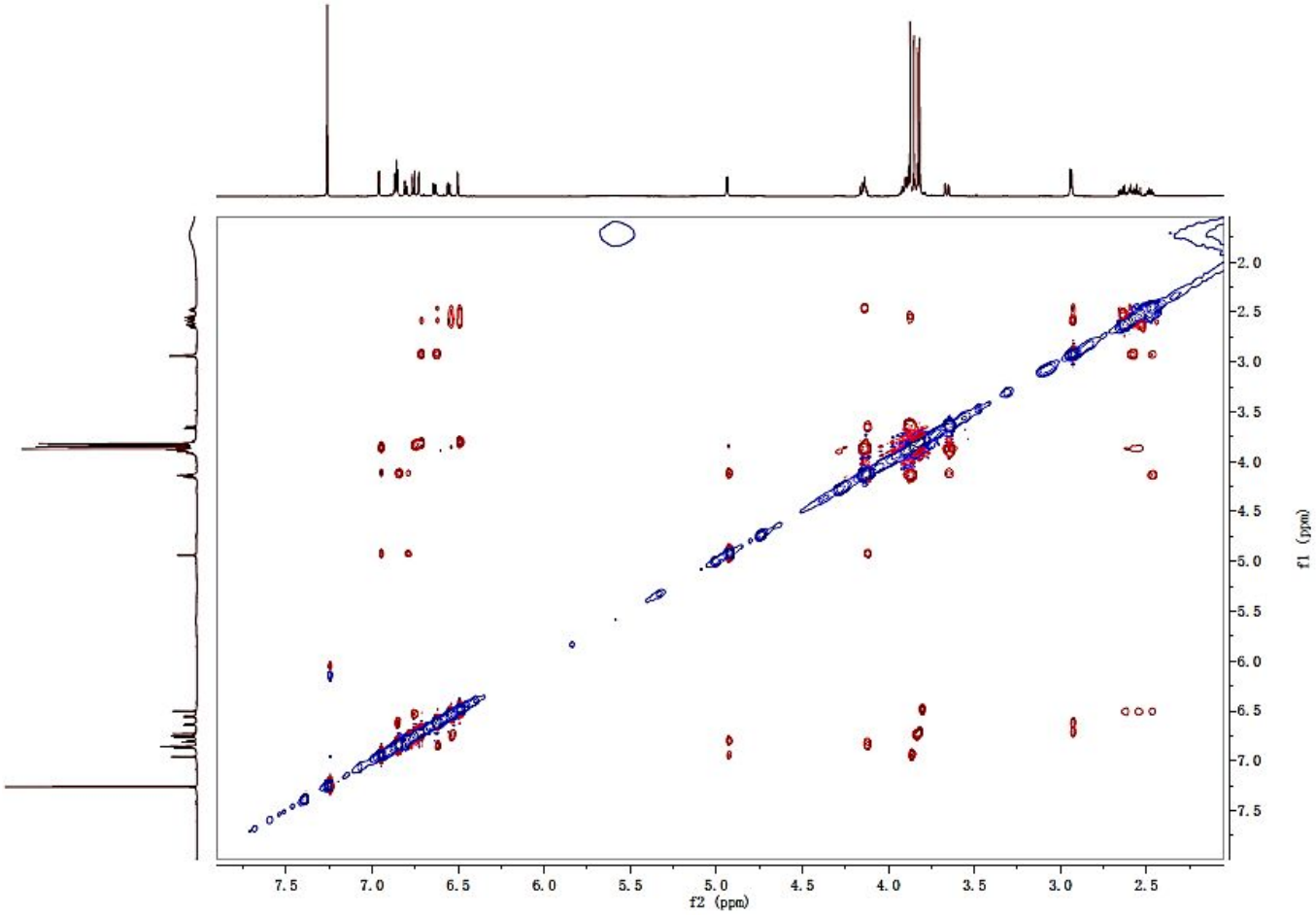

Figure 29S. ROESY spectrum of compound 3 in $CDCl_3$

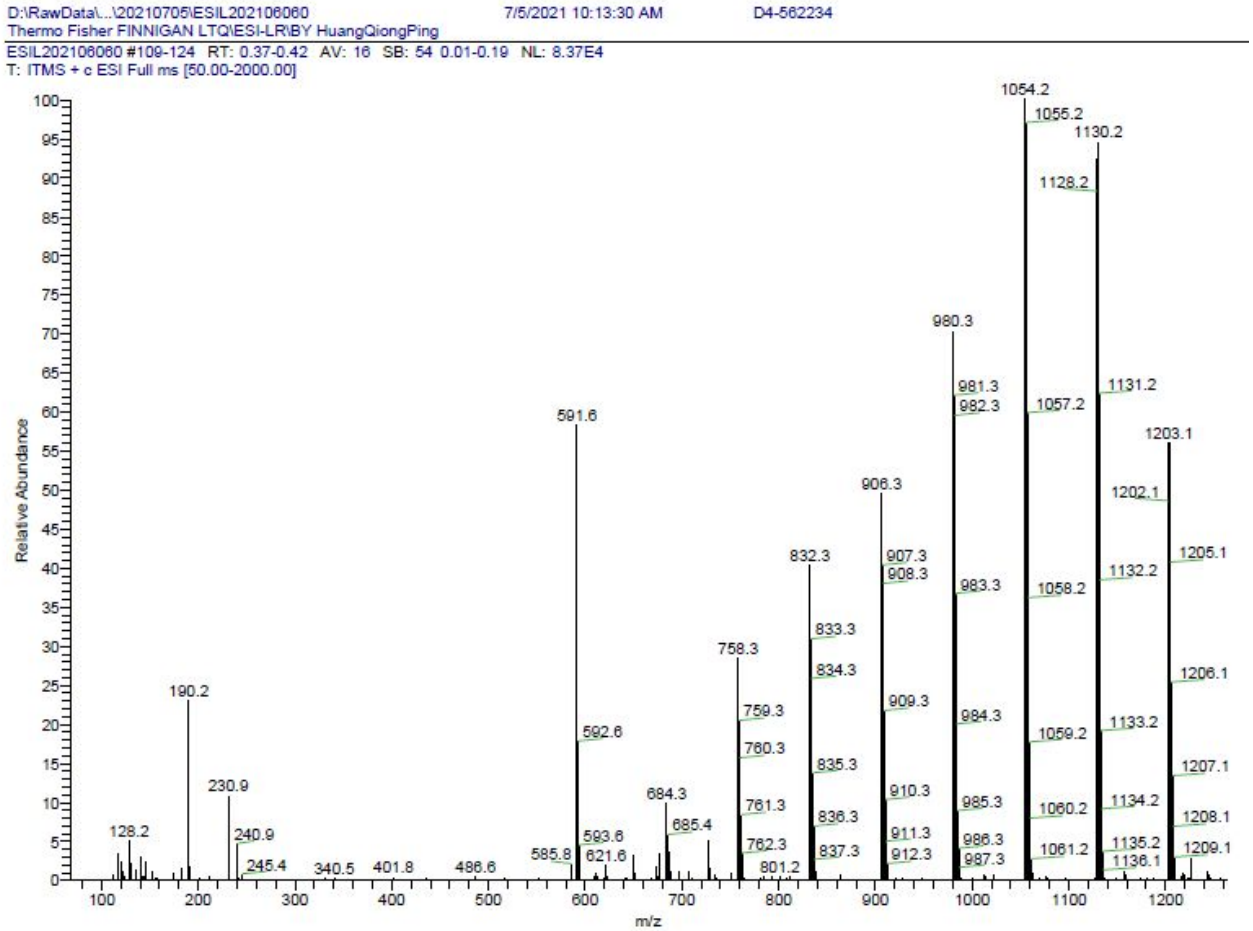

Figure 30S. (+)-ESIMS spectrum of compound 3

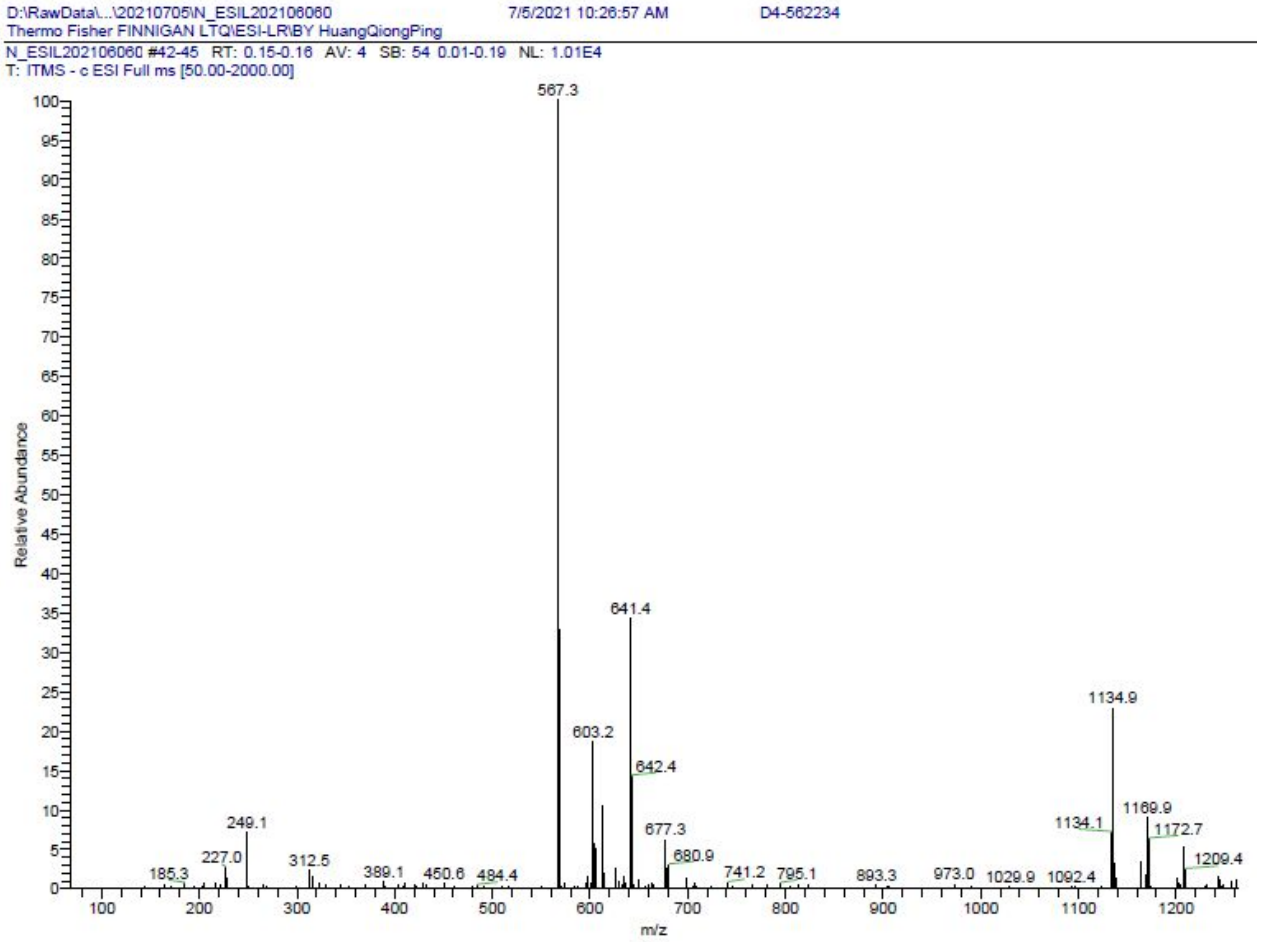

Figure 31S. (-)-ESIMS spectrum of compound 3

Qualitative Analysis Report

Data Filename	ESIH202103318.d	**Sample Name**	D4-562234
Sample ID		**Position**	P1-C7
Instrument Name	Agilent G6520 Q-TOF	**Acq Method**	20160322_MS_ESIH_POS_1min.m
Acquired Time	7/5/2021 20:52:15	**IRM Calibration Status**	Success
DA Method	small molecular data analysis method.m	**Comment**	ESIH by zhuzhenyun

User Spectra

Fragmentor Voltage	Collision Energy	Ionization Mode
135	0	ESI

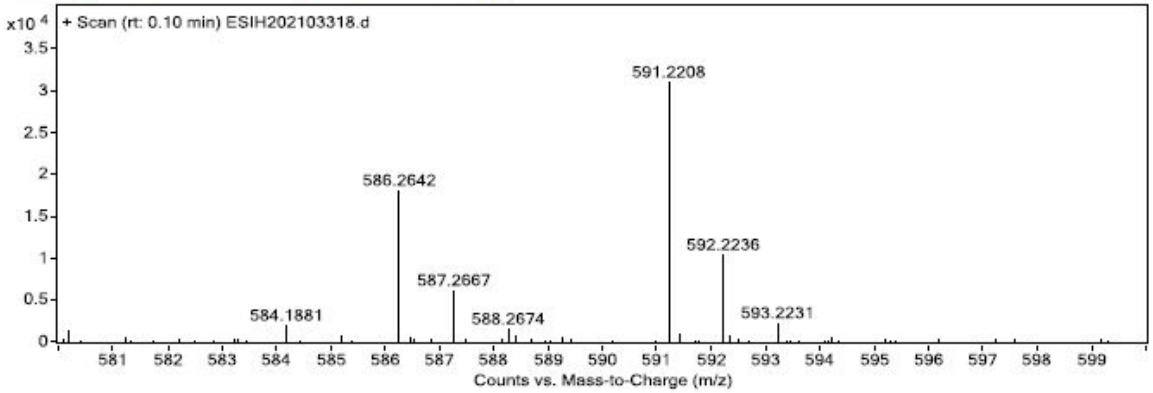

Formula Calculator Results

m/z	Calc m/z	Diff (mDa)	Diff (ppm)	Ion Formula	Ion
591.2208	591.2201	-0.75	-1.28	C31 H36 Na O10	(M+Na)+
586.2642	586.2647	0.48	0.81	C31 H40 N O10	(M+NH4)+

--- End Of Report ---

Agilent Technologies Page 1 of 1 Printed at: 17:02 on: 7/6/2021

Figure 32S. (+)-HRESIMS spectrum of compound 3

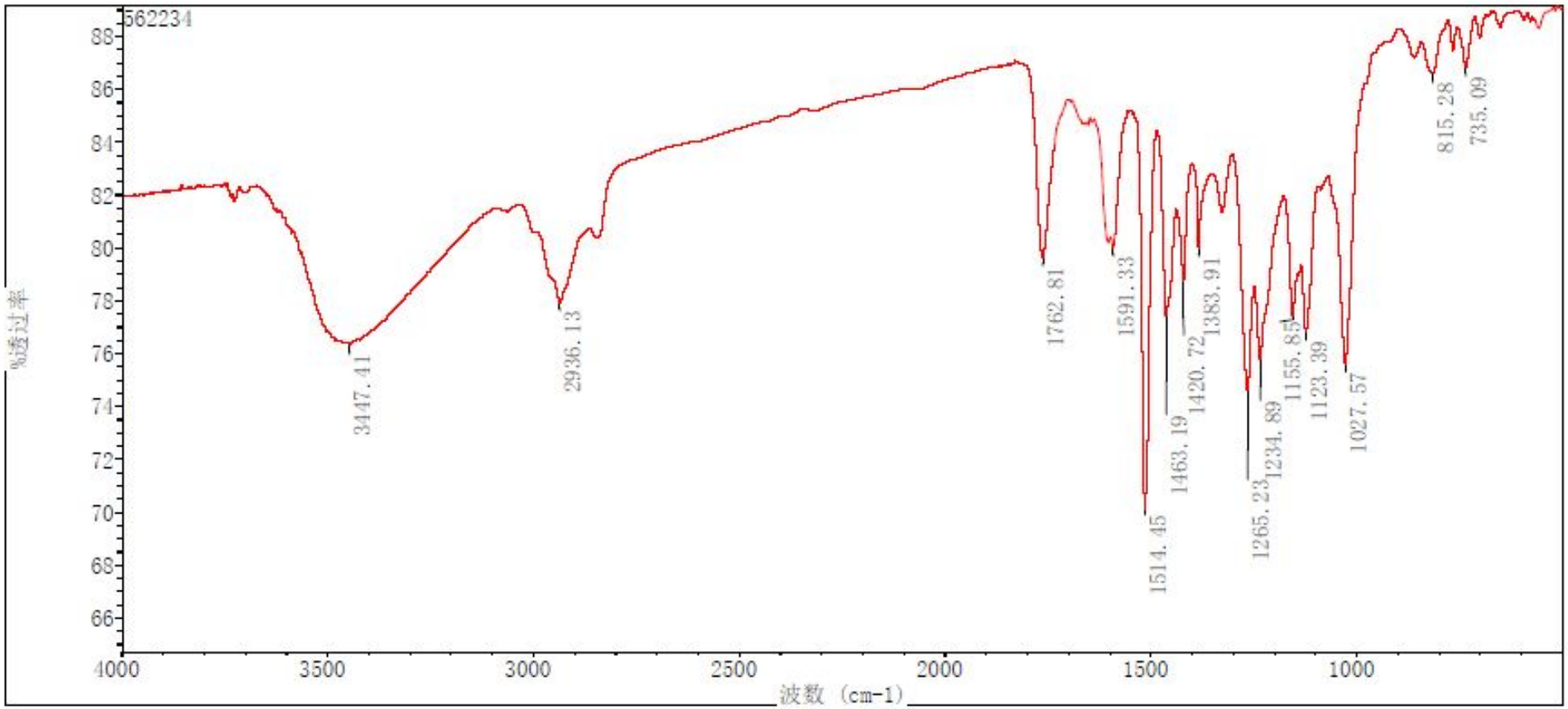

Figure 33S. IR spectrum of compound 3

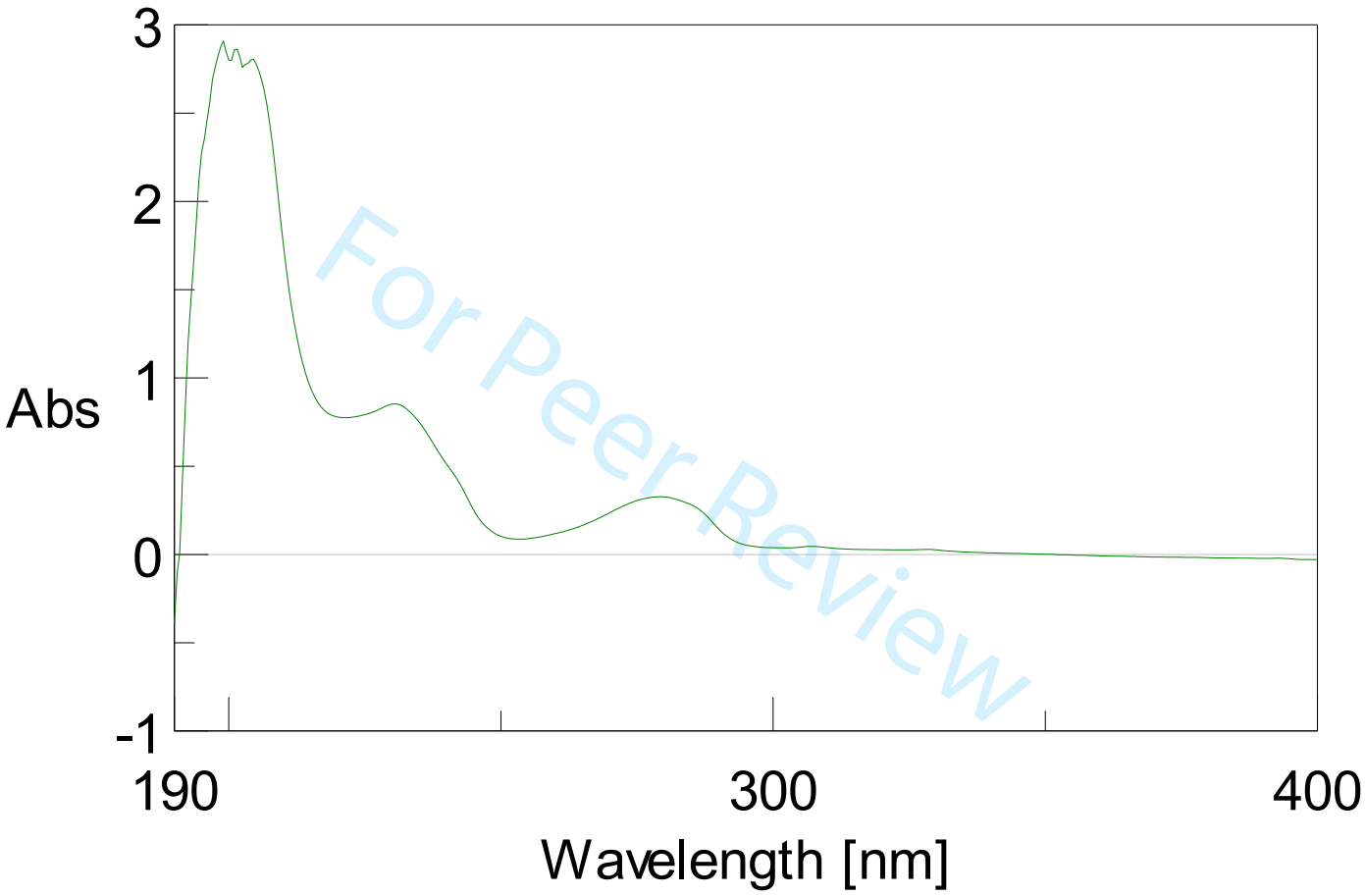

Figure 34S. UV spectrum of compound 3

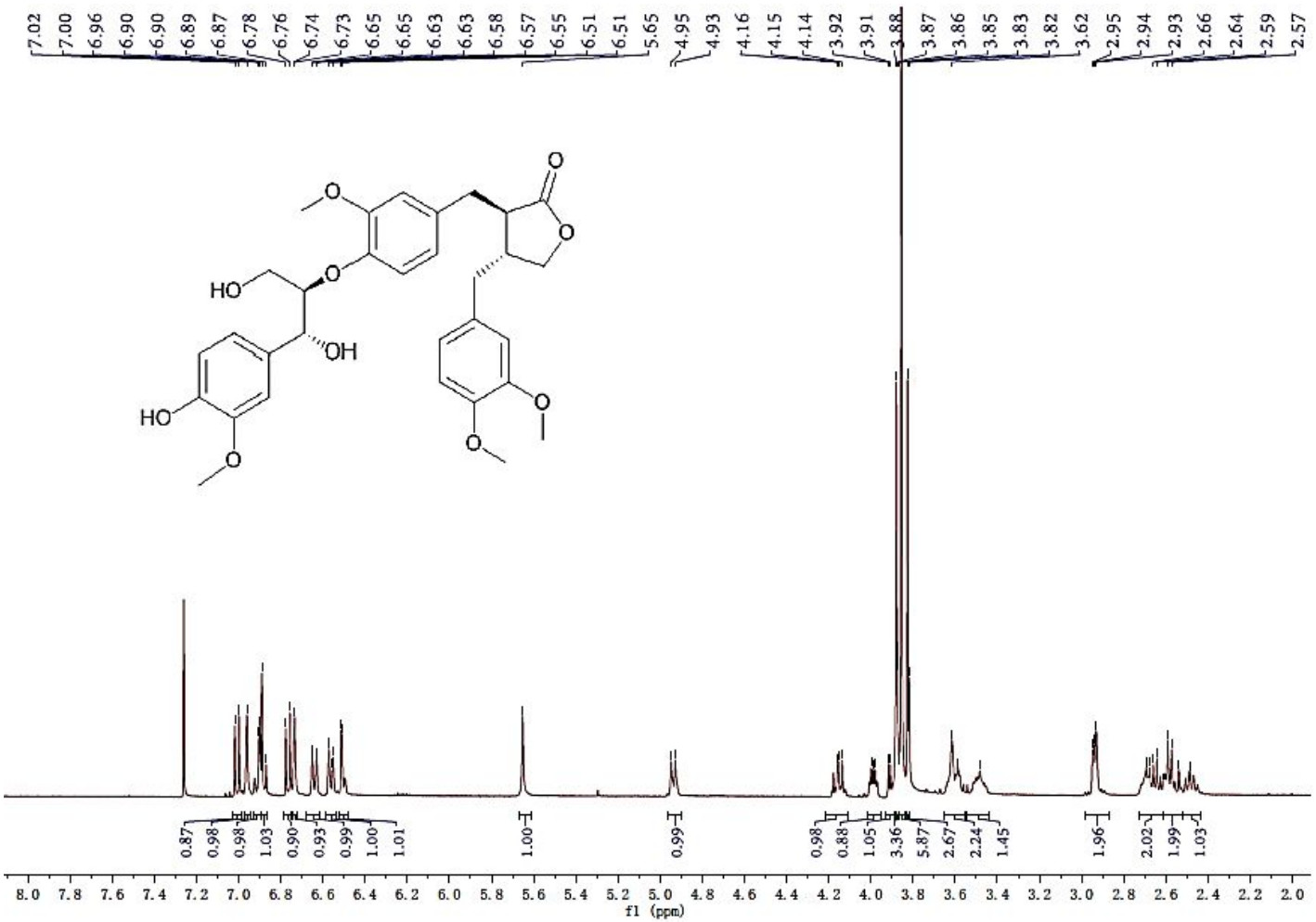

Figure 35S. ^{1}H NMR spectrum of compound 4 in $CDCl_3$

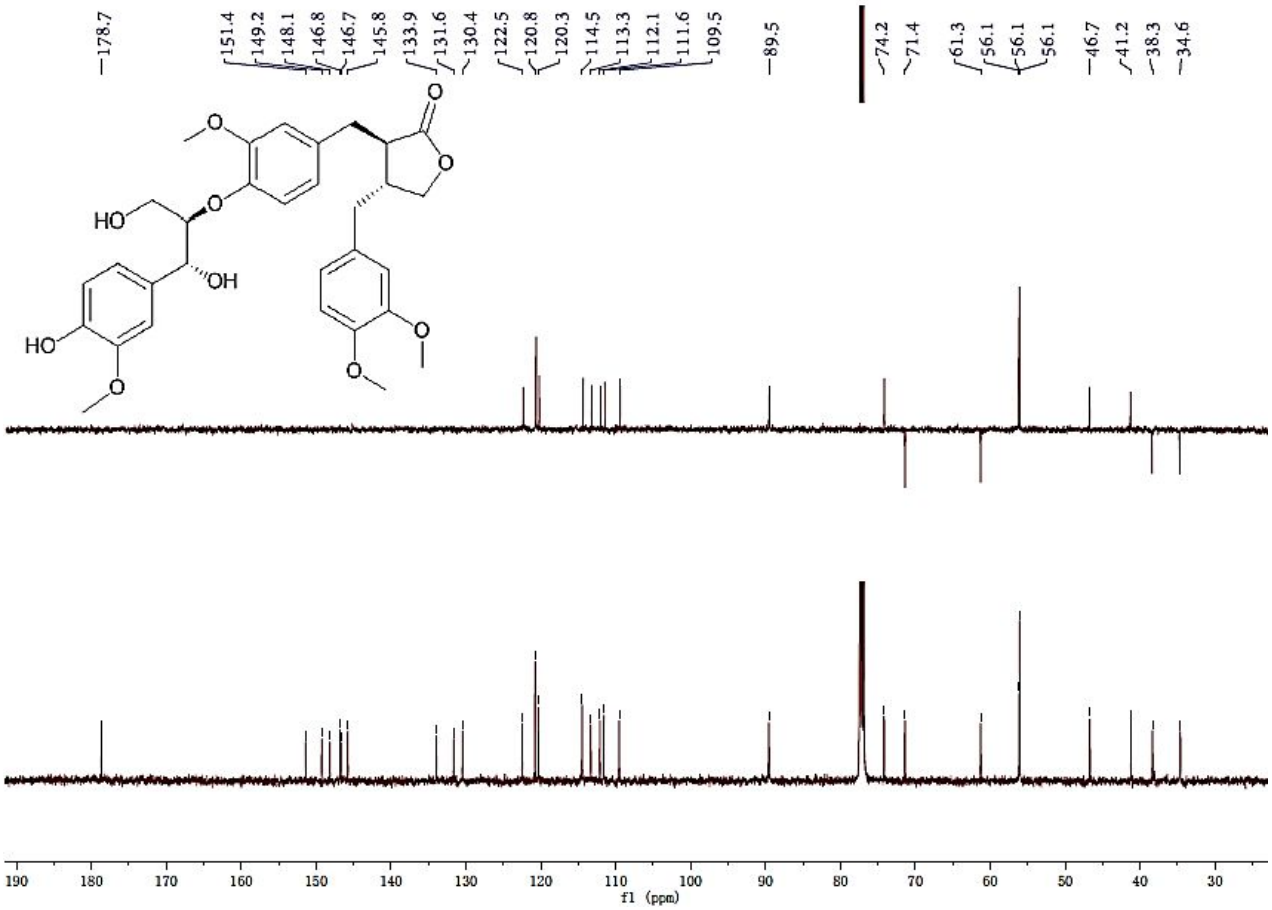

Figure 36S. ^{13}C NMR spectrum of compound 4 in $CDCl_3$

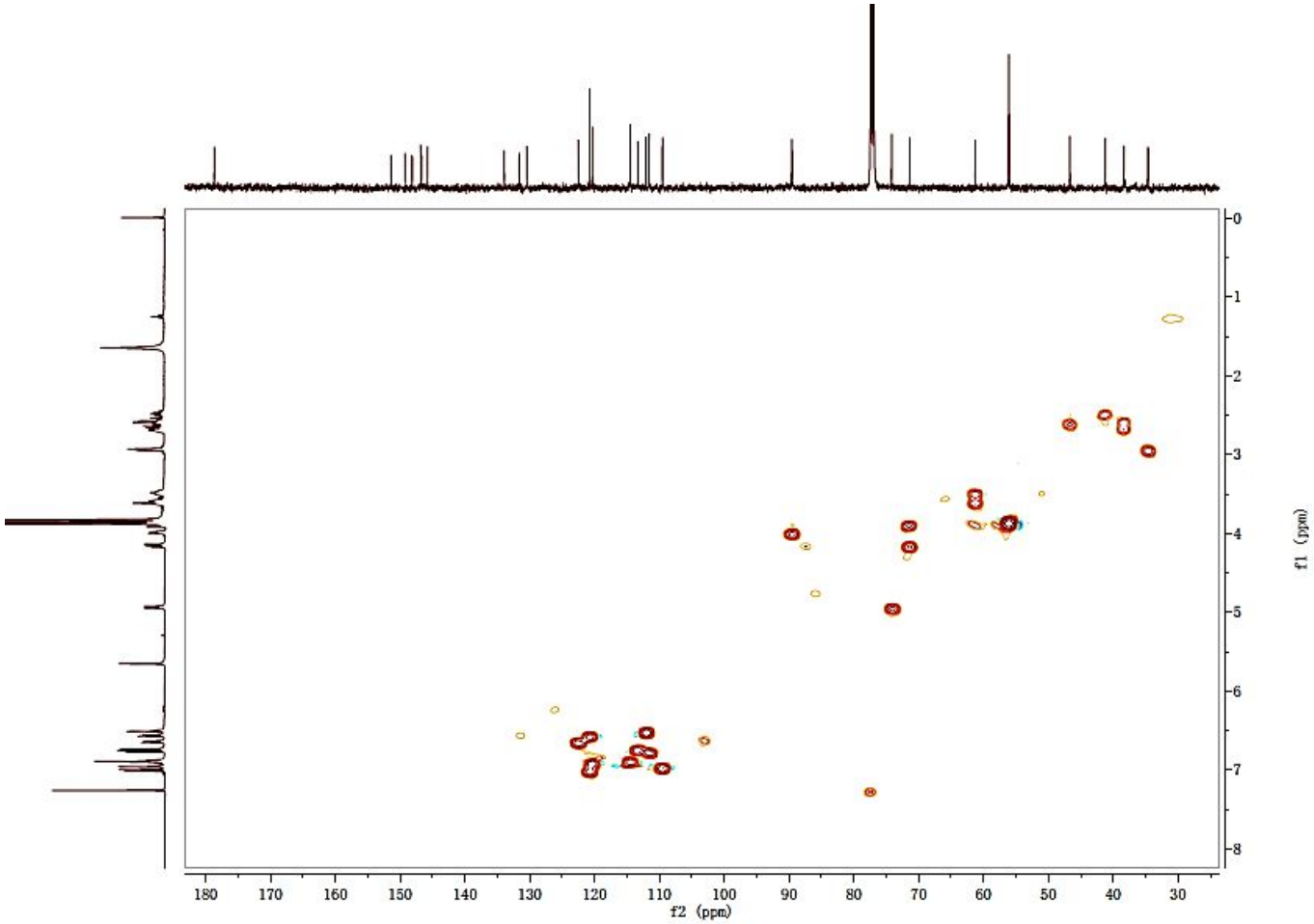

Figure 37S. HSQC spectrum of compound 4 in $CDCl_3$

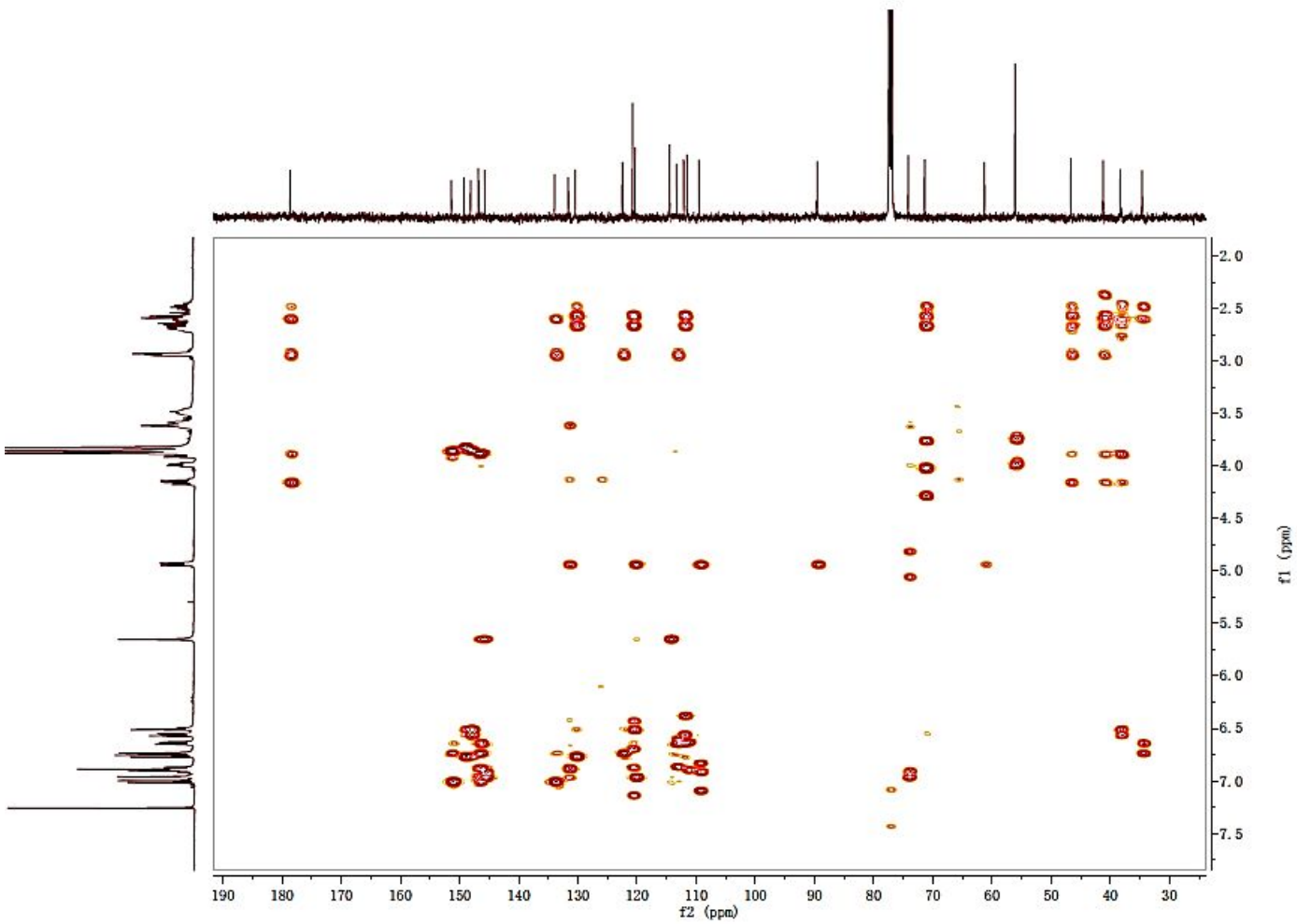

Figure 38S. HMBC spectrum of compound 4 in $CDCl_3$

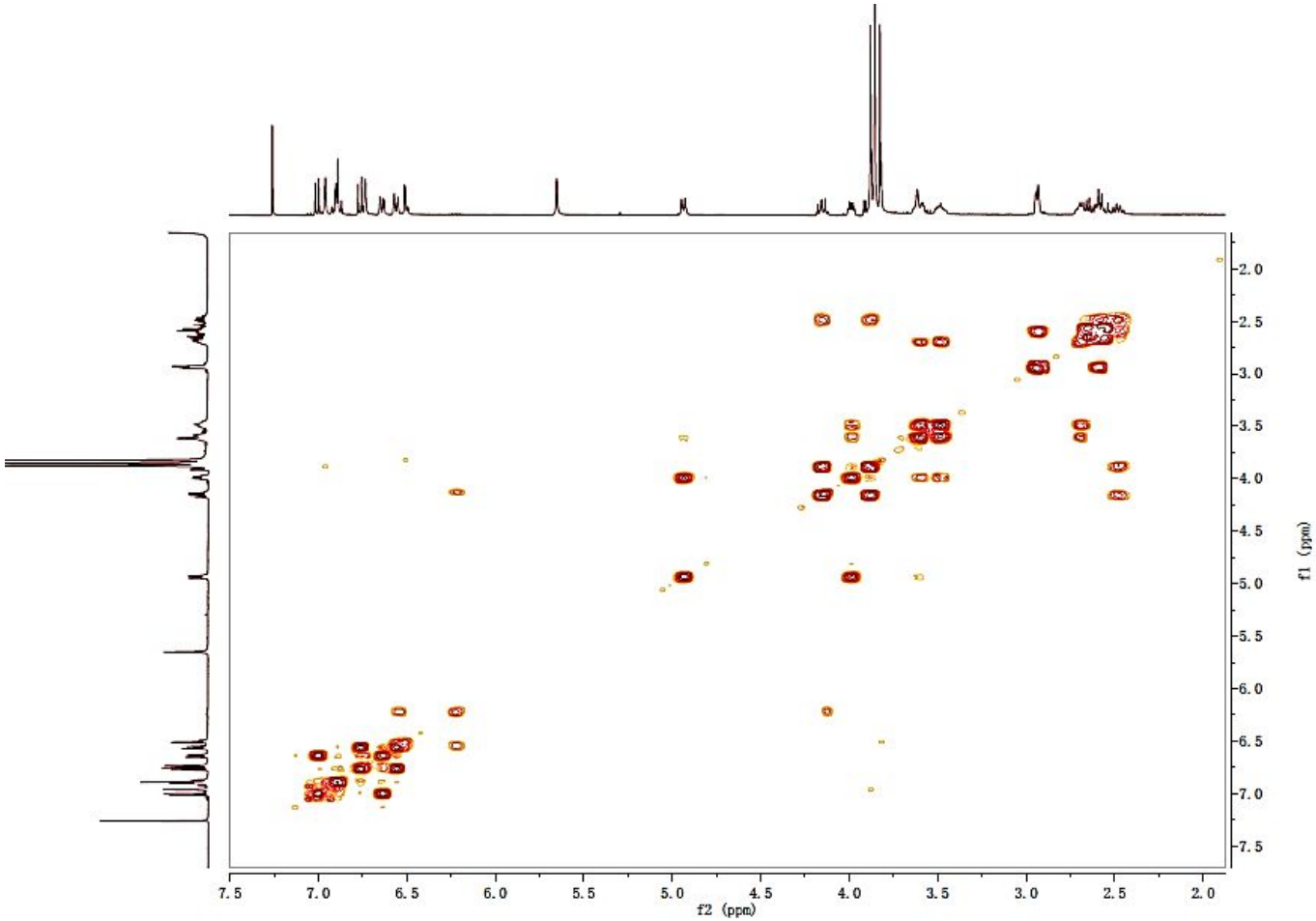

Figure 39S. $^{1}H–^{1}H$ COSY spectrum of compound 4 in $CDCl_3$

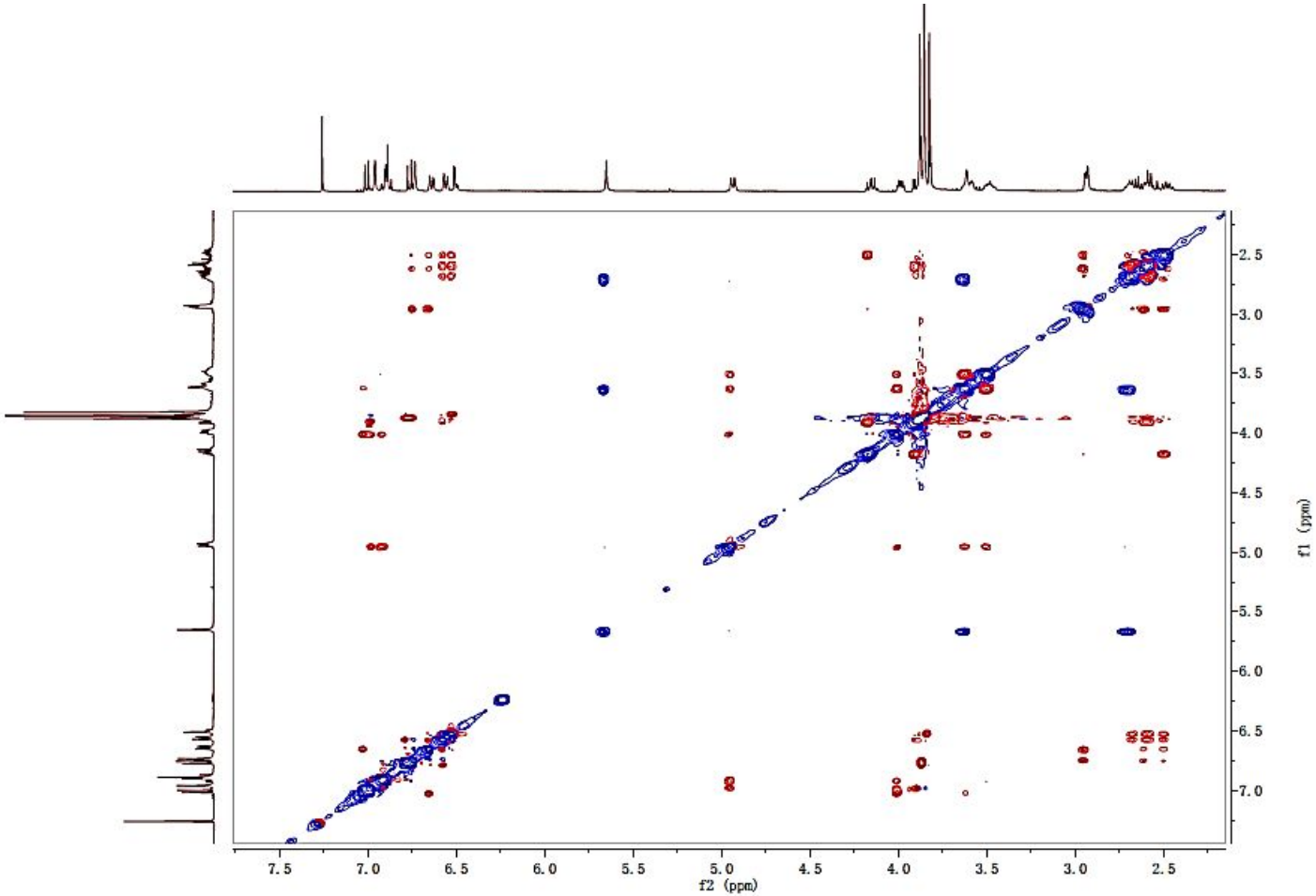

Figure 40S. ROESY spectrum of compound 4 in $CDCl_3$

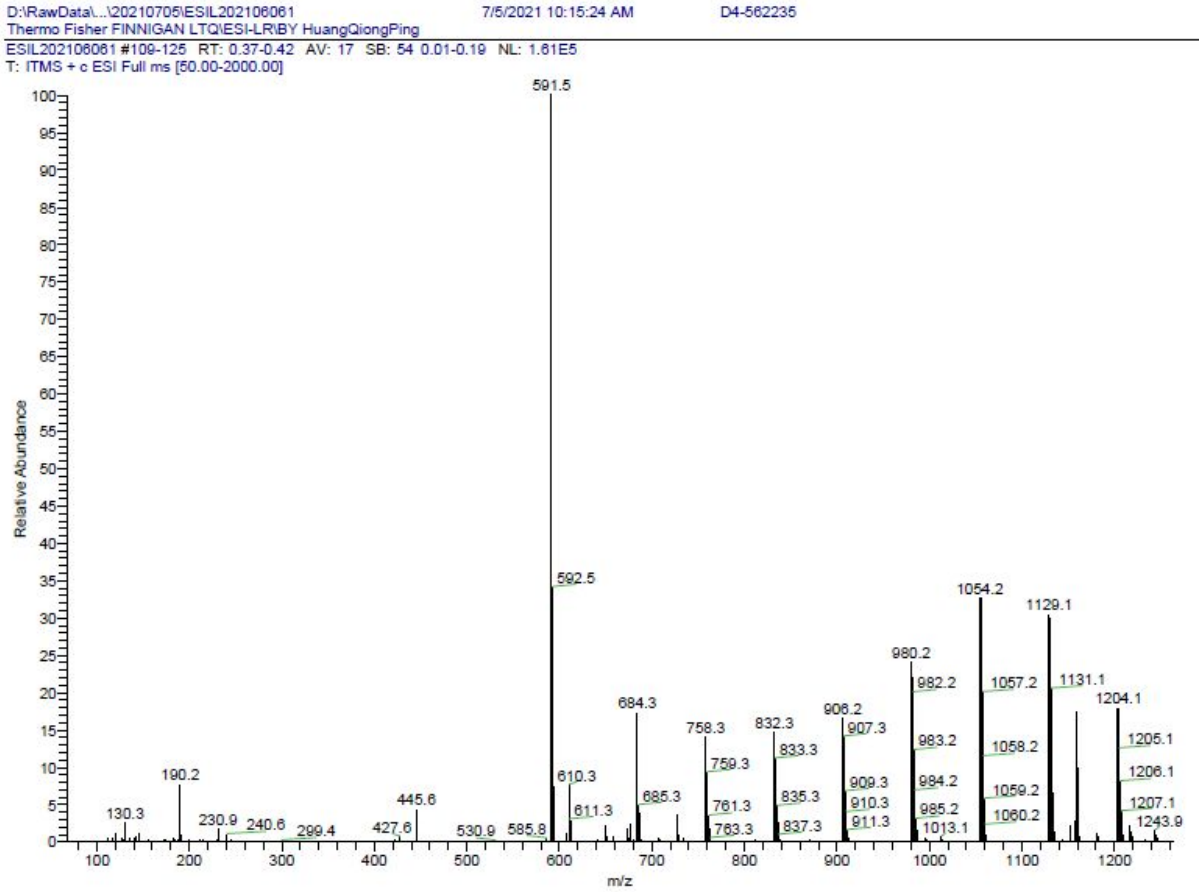

Figure 41S. (+)-ESIMS spectrum of compound 4

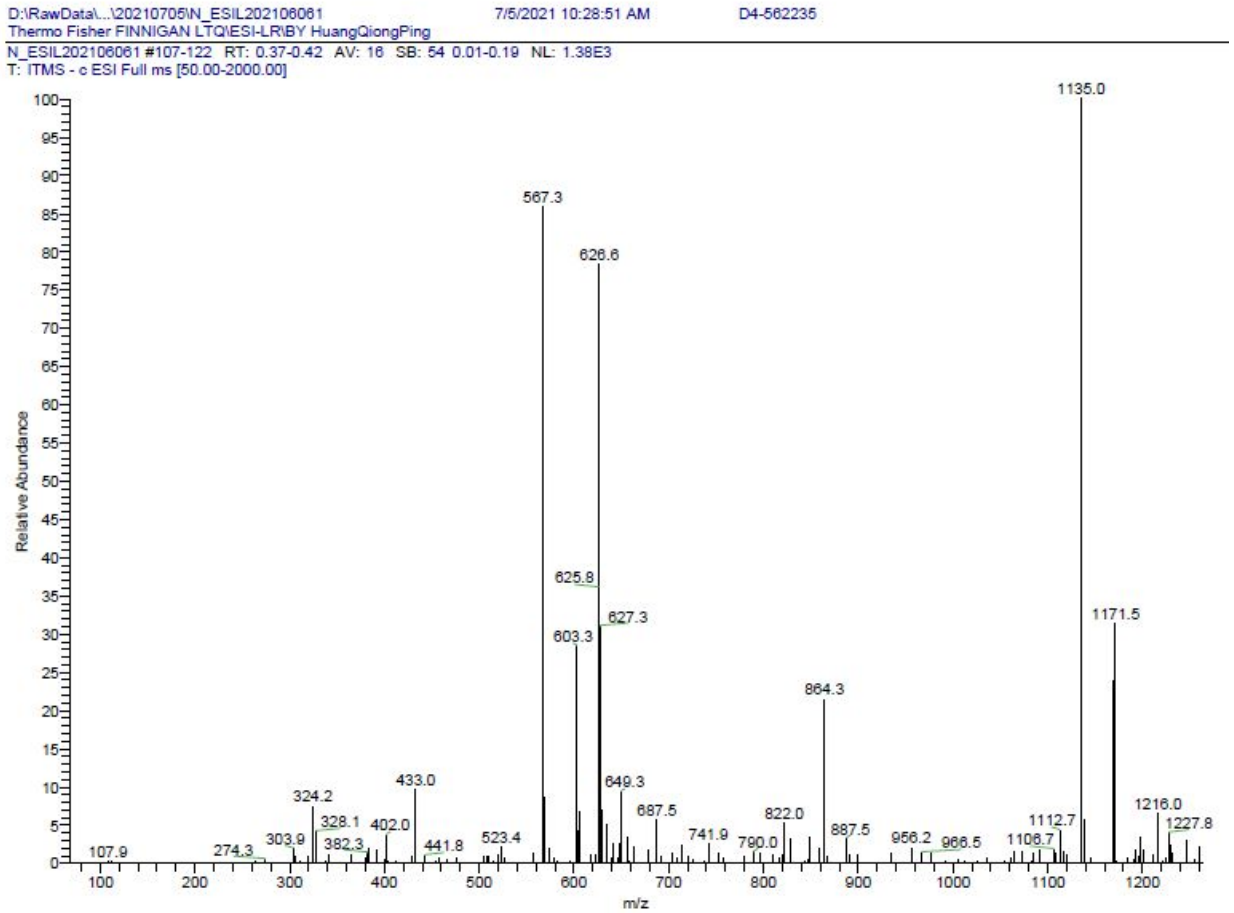

Figure 42S. (-)-ESIMS spectrum of compound 4

Qualitative Analysis Report

Data Filename	ESIH202103319.d	**Sample Name**	D4-562235
Sample ID		**Position**	P1-C8
Instrument Name	Agilent G6520 Q-TOF	**Acq Method**	20160322_MS_ESIH_POS_1min.m
Acquired Time	7/5/2021 20:53:33	**IRM Calibration Status**	Success
DA Method	small molecular data analysis method.m	**Comment**	ESIH by zhuzhenyun

User Spectra

Fragmentor Voltage	Collision Energy	Ionization Mode
135	0	ESI

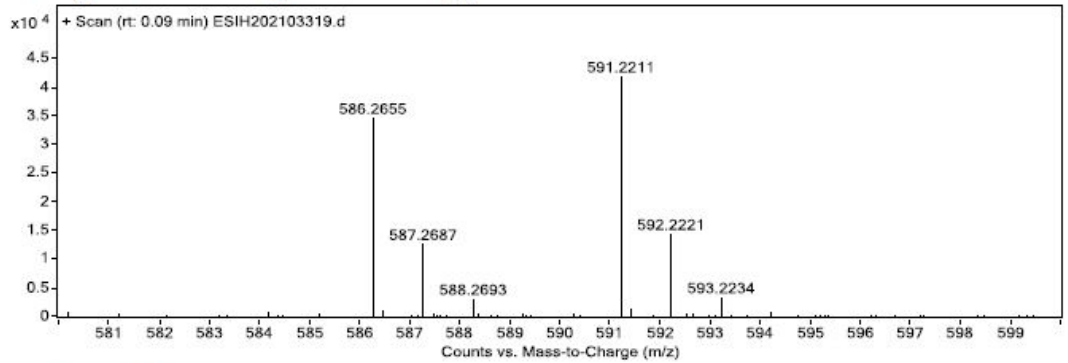

Formula Calculator Results

m/z	Calc m/z	Diff (mDa)	Diff (ppm)	Ion Formula	Ion
591.2211	591.2201	-1.05	-1.78	C31 H36 Na O10	(M+Na)+
586.2655	586.2647	-0.8	-1.37	C31 H40 N O10	(M+NH4)+

--- End Of Report ---

Agilent Technologies Page 1 of 1 Printed at: 17:02 on: 7/6/2021

Figure 43S. (+)-HRESIMS spectrum of compound 4

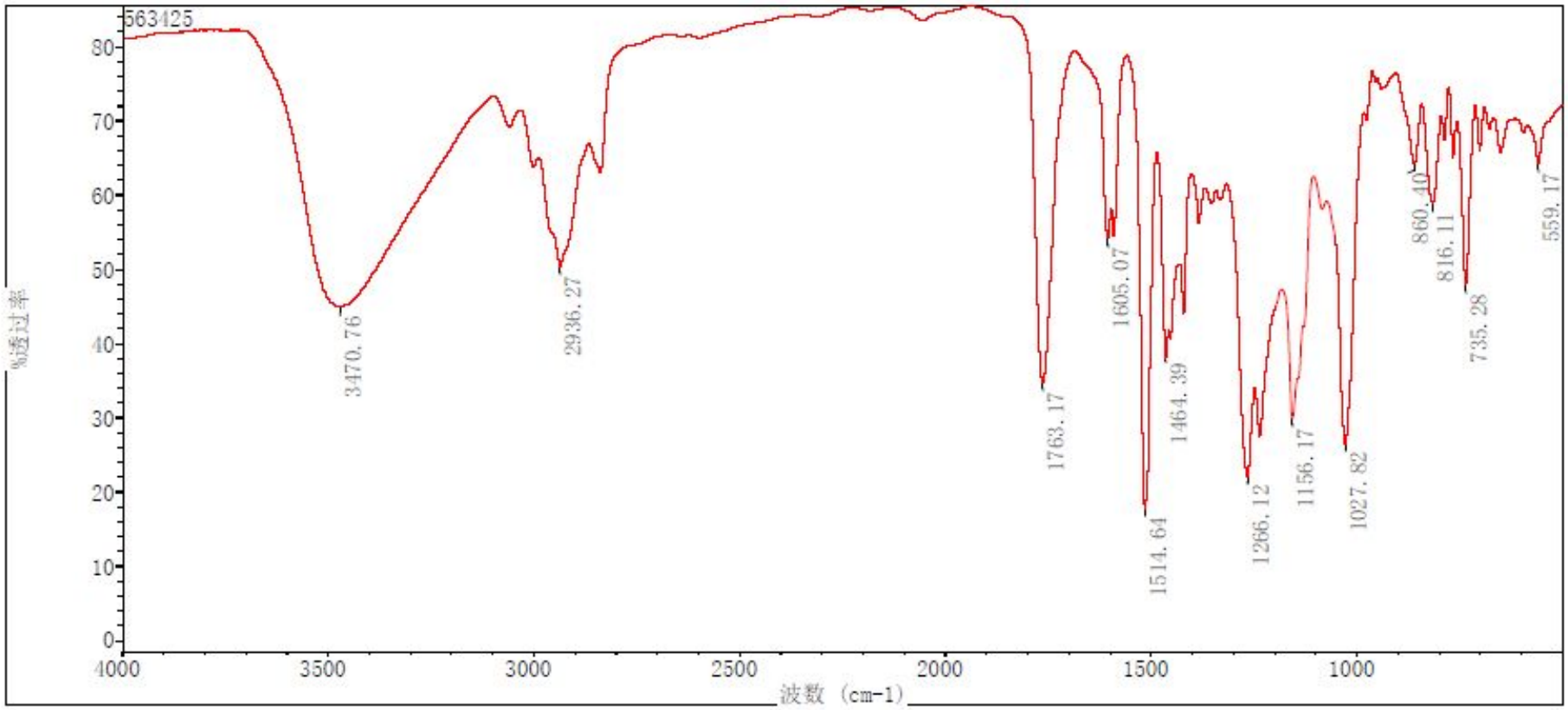

Figure 44S. IR spectrum of compound 4

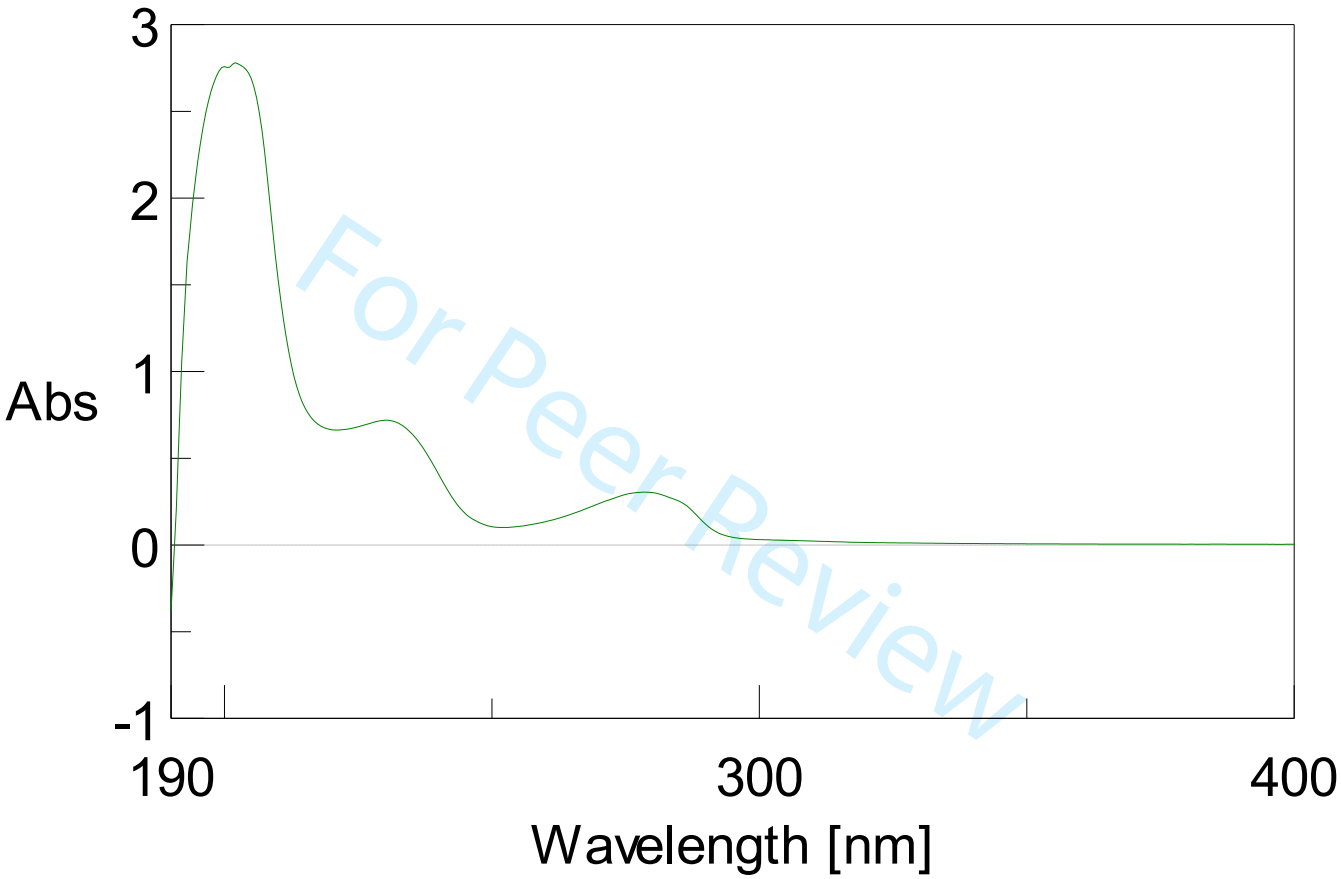

Figure 45S. UV spectrum of compound 4

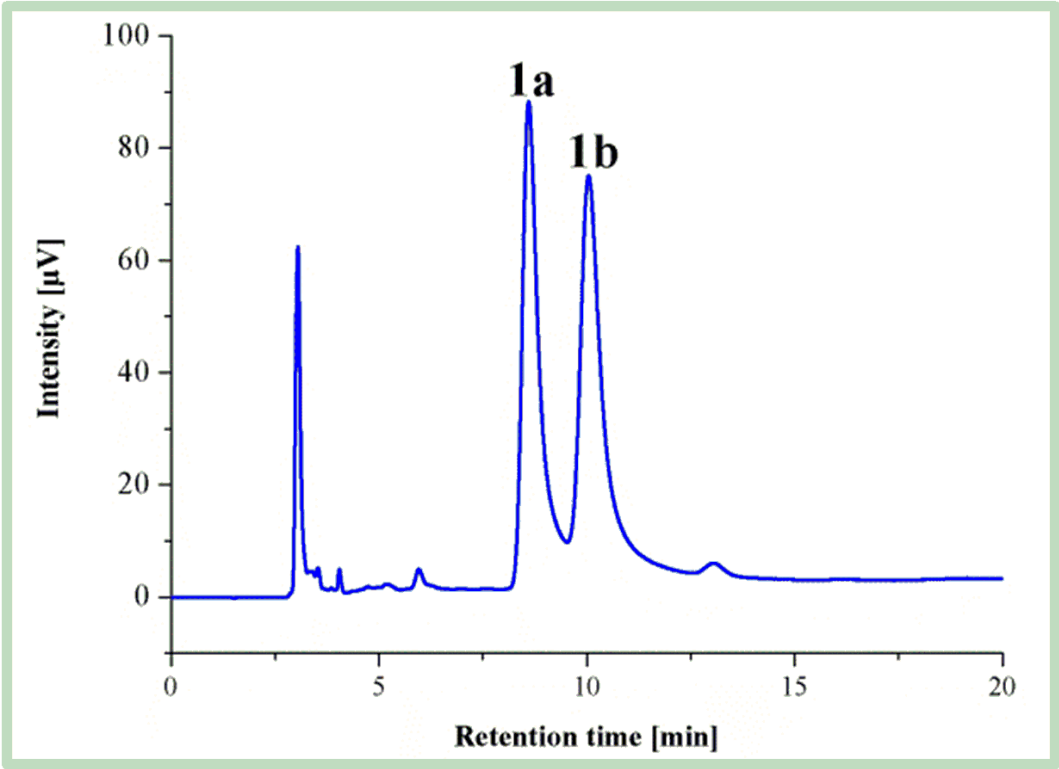

Figure 46S. Chiral HPLC separation profile of 1a/1b

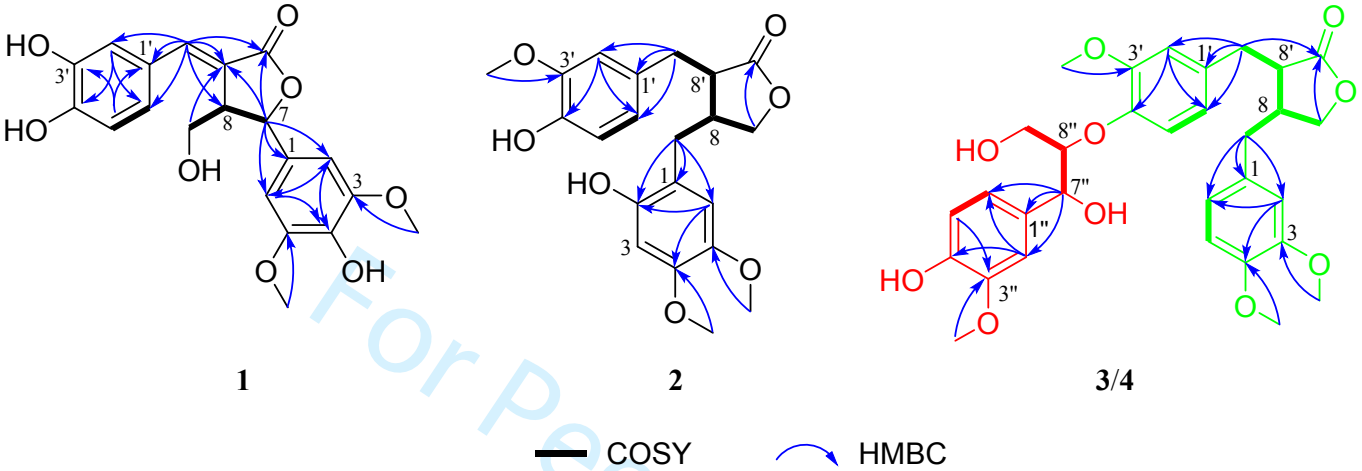

Figure 47S. ^{1}H-^{1}H COSY and key HMBC correlations of compounds 1–4.